Ion Assisted Deposition of Multicomponent Thin Films

by

Chen–Chung Li

Dissertation submitted to the Faculty of the

Virginia Polytechnic Institute and State University

in partial fulfillment of the requirements for the degree of

Doctor of Philosophy

in

Materials Engineering Science

APPROVED:

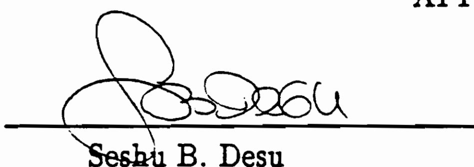

Seshu B. Desu

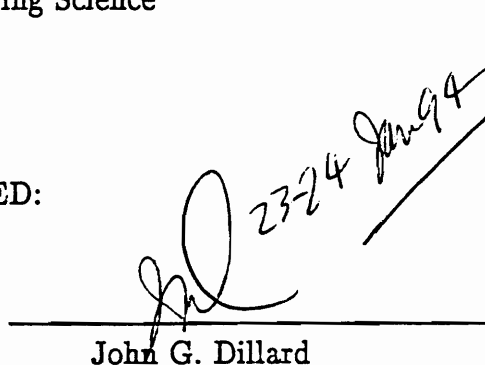

John G. Dillard

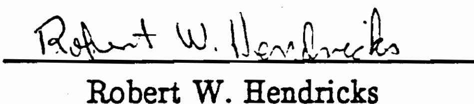

Robert W. Hendricks

David F. Cox

William T. Reynolds, Jr.

January, 1994

Blacksburg, Virginia

Ion Assisted Deposition of Multicomponent Thin Films

by

Chen–Chung Li

Committee chairman: Dr. Seshu B. Desu

ABSTRACT

A novel in–situ stress measurement technique to study the formation kinetics of multicomponent oxide thin films was developed and was applied to $PbTiO_3$. Single phase $PbTiO_3$ thin films were formed from the reaction between films in the deposited PbO/TiO_2 multilayer. The film stoichiometry was accurately controlled by depositing individual layers of the required thickness. Development of film stresses associated with the formation of the product layer at the PbO/TiO_2 interface of the multilayers was used to monitor growth rate of the $PbTiO_3$ layer. It was found that growth of the $PbTiO_3$ phase obeyed the parabolic law and the effective activation energy was estimated to be 108 kJ/mole. It is believed that the mechanism of this reaction was dominated by grain boundary diffusion of the participating cations.

Stress relaxation in $PbTiO_3$ films was also investigated by the in–situ stress measurement technique. A simple viscous flow model was successfully employed to interpret the kinetics and behavior of stress relaxation of $PbTiO_3$ thin films. The activation energy responsible for stress relaxation was estimated to be 190 kJ/mole,

which was accounted for by lattice diffusion of vacancies. A Nabarro–Herring creep model was successfully exploited to correlate the relationships among the viscosity, lattice diffusion coefficient and grain size of the $PbTiO_3$ films. The estimation of the lattice diffusion coefficient of vacancy motion during relaxation was obtained. Also, the observed time required for complete relaxation was found to be in accord with theoretical values. Hillock formation resulting from grain boundary sliding was believed to contribute to stress relaxation in its early stage. Thereafter, grain growth resulting from lattice diffusion played a major role in stress relaxation.

For the first time, the effects of ion bombardment on multicomponent oxides, such as $PbTiO_3$, and multilayer systems were extensively studied by the in–situ stress measurement technique. Energetic ion bombardment has been found to accelerate $PbTiO_3$ formation. Both annealing temperature and time needed for completion of reaction were reduced. Whereas, the apparent activation energy responsible for stress relaxation was 310 kJ/mole for IAD films, which is 120 kJ/mole higher than that for non–IAD films. This was attributed to stress reduction in $PbTiO_3$ thin films resulting from ion bombardment. In addition, effects of ion bombardment on the stress of as–deposited multilayers, on the stress development in multilayer during annealing, and on the structure–property–rocessing interrelationships were also investigated.

Stress change associated with the crystallization of amorphous $BaMgF_4$ films deposited on silicon wafers was studied by using the in–situ stress measurement technique.

Acknowledgement

The author would like to thank his advisor, Prof. Seshu B. Desu, for his advice and support throughout the course of the work. The author is indebted to Professor Desu for providing so much freedom and patience to learn and work independently and, at the same time, giving so many invaluable suggestions when needed.

Many thanks also go to his advisory committee members: Dr. John G. Dillard, Dr. Robert W. Hendricks, Dr. David F. Cox, and Dr. William T. Reynolds Jr. for their invaluable discussion and guidance in the completion of this work.

The author would also like to thank all his colleagues in Thin Film Laboratory and friends in the department of Materials Science and Engineering, Virginia Tech. It has been all his pleasure to have shared time with them throughout his graduate study. Special thanks to Mr. Harry Dudley and Mr. Steve McCartney, in MSE department and Mr. Frank Cromer in Chemistry department for helping solving instrumental problems and doing surface analysis and observation.

finally, the author would like to express his deepest love and appreciation to his family. Without their support and sacrifice, he could not have finished this work. This work is dedicated to his parents.

List of Figures

Chapter 1

Fig. 1 Schematic of an IAD system.

Fig. 2 Multilayer approach.

Chapter 2

Fig. 1 Schematic stress–time plot for $PbTiO_3$ thin film reaction.

Fig. 2 Configuration of the multilayer.

Fig. 3 Absorption edge of PbO and TiO_x films as a function of temperature.

Fig. 4 A typical film stress–temperature plot for a $PbTiO_3$ thin film.

Fig. 5 Interaction between PbO and TiO_x layers as a function of temperature.

Fig. 6 Stress–time plots for $PbTiO_3$ thin films

Fig. 7 XRD spectra of $PbTiO_3$ films.

Fig. 8 Implications in a stress–time plot

Fig. 9 Fractions of $PbTiO_3$ formation as a function of time.

Fig. 10 Time dependence of the thickness of $PbTiO_3$ films.

Fig. 11 The Arrhenius behavior of rate constants of $PbTiO_3$ formation.

Chapter 3

Fig. 1 The viscous flow model for stress relaxation.

Fig. 2 A modeled stress–time curve.

Fig. 3 Experimental stress–time plots for $PbTiO_3$ thin films.

Fig. 4 $Ln(|\sigma|)$ as a function of time.

Fig. 5 The Arrhenius behavior of viscosity of $PbTiO_3$ films.

Fig. 6 Schematic illustrations of possible paths along which atoms diffuse to relax stresses.

Fig. 7 The effects of both orientation and size of grains on film stresses.

Fig. 8 SEM microstructure of the $PbTiO_3$ films annealed at 625°C for 30 minutes.

Fig. 9 Hillock formation in the a $PbTiO_3$ film annealed at 600°C for 30 minutes.

Fig. 10 Grain boundary sliding by diffusion along grain boundary around the triple edge.

Chapter 4

Fig. 1 Schematic of IAD deposition.

Fig. 2 Sequence of multilayer deposition.

Fig. 3 Film stress of as–deposited multilayer as a function of ion flux density.

Fig. 4 Film stress of as–deposited multilayer as a function of normalized ion beam energy.

Fig. 5 Typical stress–temperature of the IAD–$PbTiO_3$ films annealed at 575 °C for 4 hours.

Fig. 6 Effect of ion bombardment on multilayer formation.

Fig. 7 Heating stage of the stress–temperature plots.

Fig. 8 Typical stress–time plots for $PbTiO_3$ films, (300 eV, 160 $\mu A/cm^2$).

Fig. 9 t_c as a function of normalized ion beam energy.

Fig. 10 t_c as a function of ion flux density.

Fig. 11 Film stress at t_c as a function of ion flux density.

Fig. 12 $Ln(|\sigma|)$ as a function of time

Fig. 13 The Arrhenius behavior of viscosity of $PbTiO_3$ films.

Fig. 14 The effects of both orientation and grain size on film stress.

Fig. 15 The effect of ion flux density on stress relaxation behavior.

Fig. 16 CTE as a function of (a) normalized ion beam energy and (b) ion flux density

Fig. 17 Film stress as a function of average grain size, (a) d and (b) $d^{-1/2}$.

Chapter 5

Fig. 1 Stress–temperature plot of the 123nm $BaMgF_4$ thin film.

Fig. 2 XRD spectra of $BaMgF_4$ thin films annealed at 375° C.

Fig. 3 XRD spectrum of BMF films annealed at 400° C for 5 minutes

Fig. 4 Surface morphology of $BaMgF_4$ thin films on Si(100) substrates.

List of Tables

Chapter 2

Table I: Kinetic Data of $PbTiO_3$ Formation

Chapter 3

Table I: The Time Required For Complete Stress Relaxation of $PbTiO_3$ films.

Table of content

Chapter 1 Introduction 1

1.1 Motivation 1

1.1.1 Ion Assisted Deposition 1

1.1.2 Approach 3

1.1.3 Issue of Film Stresses in Multilayers 5

1.1.4 Literature Review 8

1.2 Objective 9

1.3 Presentation of Results 9

1.4 References 11

Chapter 2 A Novel Technique For Investigating Multicomponent Oxide Films: I, Formation Kinetics 14

2.1 Abstract 14

2.2 Introduction 14

2.3 Methodology 16

2.4 Experimental Procedure 18

2.5 Results and Discussion 22

2.5.1 In–Situ Study of $PbTiO_3$ Formation by Stress Measurement 23

2.5.2 Formation Kinetics 31

2.5.3 Mechanism of $PbTiO_3$ Formation 34

2.6 Summary 38

2.7 References 40

Chapter 3 A Novel Technique For Investigating Multicomponent Oxide Films: II, Stress Relaxation 42

3.1 Abstract 42

3.2 Introduction 42

3.3 Analysis 44

3.4 Experiment Procedure 47

3.5 Results and Discussion 47

3.5.1 Mechanism of Stress Relaxation 52

3.5.2 Stress Relaxation by Diffusional Creep Mechanism 53

3.5.3 Estimation of Relaxation Time 56

3.5.4 Morphology Development During Stress Relaxation 59

3.5.5 Hillock Formation by Grain Boundary Sliding 61

3.6 Summary 65

3.7 References 67

Chapter 4 A Novel Technique for Investigating Multicomponent Oxide Films: III, Effects of Ion Bombardment 68

4.1 Abstract 68

4.2 Introduction 68

4.3 Basics of IAD 69

4.4 Experimental Procedure 72

4.4.1 System 72

4.4.2 Preparation 73

4.4.3 Characterization 73

4.5 Results and Discussion 75

4.5.1 Effect of Ion Bombardment on Stress of As–deposited Multilayers 75
4.5.2 Effect of Ion Bombardment on Stress Development in Multilayer 80
4.5.3 $PbTiO_3$ Formation 85
4.5.4 Stress Relaxation 92
4.5.5 Structure–Property–Processing Interrelationships 97
4.5.5.1 Property–Process Relations 97
4.5.5.2 Property–Structure Relations 100
4.6 Summary 102
4.7 References 104

Chapter 5 Crystallization–Induced Stress in $BaMgF_4$ Thin Films 106
5.1 Abstract 106
5.2 Introduction 106
5.3 Experimental Procedure 108
5.3.1 Sample Preparation and Characterization 108
5.3.2 Film Stress Measurement 108
5.4 Results and Discussion 109
5.4.1 Stress Development in $BaMgF_4$ Thin Films 109
5.4.2 Formation of $BaMgF_4$ Phase 112
5.4.3 The Mechanics of Stress in BMF Films 115
5.4.4 Morphology Development in BMF Films 116
5.5 Summary 118
5.6 Appendix 119

5.7 References 120

Chapter 6 Summary 121

Chapter 1 Introduction

1.1 Motivation

Thin films play a major part in many areas of technology, from electrically active layers in electronic devices through passive multilayers in precision optical coatings. The constraints placed upon the film depend on the specific application. For example, a high purity film is required in an electronic device whereas hardness is of prime importance for wear–resistant coatings on cutting tools. However there are properties required in thin films that are common to most applications such as adhesion, stability, reproducibility, structure, etc. There has been an increasing use of ion–based techniques in thin–film deposition to control such film properties. Among the processes that feature a strong ionization component are activated reactive evaporation, magnetron sputtering, arc evaporation, ion plating, ion–beam deposition, and ion assisted deposition. [1]

1.1.1 Ion Assisted Deposition

The term ion–assisted deposition (IAD) specifically relates to a deposition process in which a growing film produced from an evaporation source (usually electron beam) is bombarded by an ion beam produced by a low–energy (50 eV – 1 keV) ion source [2]. A schematic of a vacuum deposition system configured for IAD is shown in Fig. 1. As illustrated in Fig. 1, the gas is introduced through the ion source into the deposition chamber. IAD is inherently a low pressure process (10^{-5} to 10^{-4} Torr) that permits a great deal of flexibility in deposition configuration.

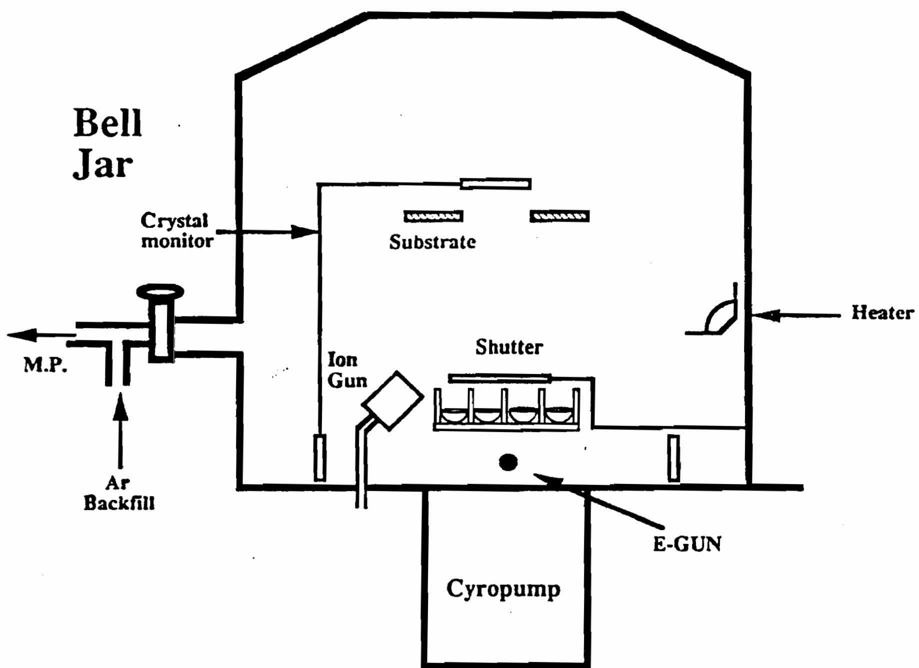

Fig.1 Schematic of an IAD system.

IAD offers independent control over the energy of the ions, flux of evaporated atoms, background gas pressure and composition, and if necessary the substrate temperature. Another direct advantage of IAD is that the technique is readily implemented with the addition of an ion source apparatus to an existing vacuum deposition system.

IAD has been employed in the fabrication of multilayer optical coatings, in the deposition of compound thin films at reduced substrate temperature and to modify film properties during deposition [3]. The properties of the films depend on the ion mass, its energy, and the ion–to–atom arrival rate. In addition, the substrate material and its temperature influence the growth of an ion–assisted film. Some of the ion–induced effects are acceleration of the nucleation stage [4], enhanced adhesion [5], high packing density [6], modification of crystal structure [7] and film stress [8], and in the case of compound deposition, stoichiometric changes.

The stoichiometry of thin films, especially multicomponent thin films, is always a prime concern when physical vaporization deposition (PVD) techniques such as evaporation and sputtering are employed, including IAD. IAD, combining the advantages of evaporation and sputtering, also fails to overcome this problem when compound source materials are utilized. Nevertheless, a multilayer approach, which is thoroughly described in the next section, is proposed to solve this problem.

1.1.2 Approach

It is well–known that the composition of the thin film plays a key role in

controlling the film properties [9]. For multicomponent oxide films such as $Pb(Zr,Ti)O_3$, (PZT), the film composition control is, in general, very difficult in the physical vapor deposition techniques [10]. This is a significant problem in the evaporation process if the source material is the compound itself. The compound source may decompose before evaporation or the sticking coefficients of different species on the substrate may be significantly different [10]. Hence, the film composition deviates from that of the source material. A way to alleviate this problem is to use a multi–electron gun evaporation process [11], where the different components in the film are co–evaporated using different guns. Since the vapor pressures of the components of the PZT (both for metals and oxides) are significantly different, this multi–electron gun evaporation process may not yield adequate film composition control.

Multi–component oxides can be fabricated with relative ease by depositing the individual components as multilayers. For example, PZT can be formed by heat treating either evaporated metallic multilayers (Ti/Pb/Zr/Ti/Pb/Zr/...) or evaporated oxide multilayers ($TiO_2/PbO/ZrO_2/TiO_2/PbO/ZrO_2/...$). This multilayer technique has been widely used for preparing electronic materials, such as silicides and selenides [12]. In this multilayer technique, the film composition can be accurately monitored and controlled by the use of thickness sensors. Furthermore, by decreasing the individual component layer thickness (i.e., increasing the number of layers in the multilayer for a given film thickness) the compound formation temperature can also be decreased. In addition, by bombarding the multilayers with low energy ions (as in IAD) during deposition the microstructure and properties of the films can be controlled.

The concept of the oxide multilayer deposition method is illustrated in Fig. 2. The example concentrates on the formation of a $PbTiO_3$ film of 300 nm thick on sapphire substrates. Lead titanate and its solid solutions (e.g. $Pb(Zr,Ti)O_3$) are well–known ferroelectrics having remarkable ferroelectric, pyroelectric, and piezoelectric properties [13]. Recently much attention has been paid to thin films of these ferroelectric materials for opto–electronic devices, sensors, transducers [14], and nonvolatile memory devices [15]. A variety of vapor deposition techniques has been applied to the fabrication of ferroelectric thin films [16].

It can be easily shown that the total thicknesses of the PbO and TiO_2 layers that are required to form 300 nm of $PbTiO_3$ are 200 nm and 100 nm, respectively. A 10 mol.% of excess PbO was included in the calculations to compensate the PbO loss during annealing. Four possible multilayer stacks were shown in Fig. 2 where the number of layers is increased progressively from 2 to 8 (Figs. 2a–2d). As the number of layers in the multilayer increased the thickness of individual layer decreases, and the diffusion distance also decreases.

Therefore, the temperature at which $PbTiO_3$ formation will be completed (T_f) can be expected to decrease with the decrease of individual component layer thickness. By directing a beam of Ar^+ ions to the substrate surface during deposition (Fig. 2e) T_f can be further lowered because the ion bombardment facilitates mixing and increases kinetic energy of adatoms on the substrate surface.

1.1.3 Issue of film stresses in multilayers

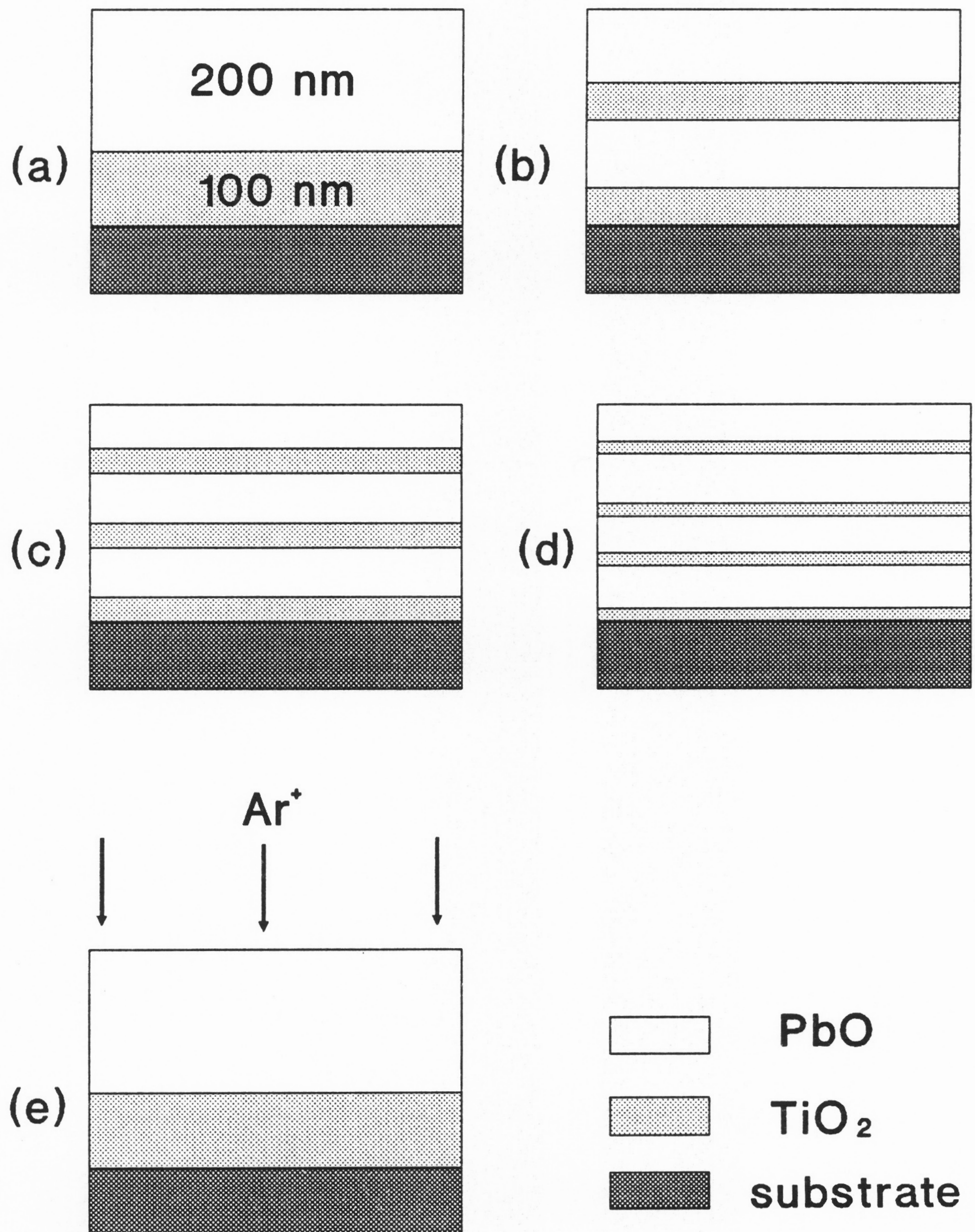

Fig. 2 Multilayer approach

Virtually all metallic and inorganic compound films are in a state of stress. This behavior is independent of the method of deposition and applies, for example, to evaporated films [17]. The total stress is composed of a thermal stress and a so–called intrinsic stress. The thermal stress is due to the difference in the thermal expansion coefficients of the coating and substrate materials. The intrinsic stress is due to the accumulating effect of the crystallographic flaws that are built into the coating during deposition.

The internal stresses in a thin film can give rise to seemingly unrelated behavior that can seriously influence the film's performance. In the multilayer, each layer not only serves as a coating but also servers as a substrate for the subsequent layer. Therefore, the accumulation of stress throughout the multilayer can be extremely high and complicated. The film–to–substrate bond must be capable of withstanding the force produced by the integrated stress throughout the multilayer. For this concern, the IAD technique can provide enhanced adhesion between film and substrate and prevent failure in the multilayer.

Since $PbTiO_3$ will be formed by annealing the oxide multilayer, the topic of stress formation as a result of solid state reactions between lead oxide and titanium dioxide becomes a major concern in the multilayer approach. It is of great importance to understand how the stress will be accumulated as the formation of $PbTiO_3$ proceeds and how the film stress relaxes during subsequent annealing. The state of the resultant stress during formation can dramatically affect the performance and microstructure of the films [18]. Excessive tensile stress can lead to film cracking and delamination, whereas excessive compressive stress can lead to

buckling in the film.

1.1.4 Literature Review

The topic of stress formation as a result of solid state reactions has been a matter of concern for a long time, e.g., with respect to metal oxidation [19], silicon oxidation [20,21] and metal–silicon reaction [22–26]. The examples quoted above all dealt with the reactions between film and substrate. The stresses determined after the reaction ($MoSi_2$, $TbSi_{1.7}$, $ErSi_{1.7}$) [22, 23] or more rarely in–situ ($PdSi_2$, $PtSi_2$, $CoSi_2$, and $TiSi_2$) [23–26] were all compressive. Buaud et al [25] used an in–situ double optical beam technique to study the evolution of the strain for the Pt–Si system before, during and after reaction. However they failed to quantitatively explain the kinetics and mechanisms of the reactions associated with stress evolution. Zhang and d'Heurle [27] proposed a simple model for the evolution of stresses during the formation of a reacted solid layer for silicides. Their model successfully modeled Buaud's data in the formation stage. However, the relaxation portion was modeled by assuming an exponential behavior in stress with respect to time. Although there was no well–established model of stress relaxation for silicide systems, Barnes et al [25] established a successful model for stress relaxation for oxide–metal systems.

Extensive efforts have been made to study the stress behavior associated with reactions between film and substrate. However, little [28] has been done for reactions in between films on a substrate, especially multicomponent oxide thin films on a substrate. In order to fabricate high quality and high performance thin

films, it is of vital importance to understand the structure–property (especially film stress) –processing interrelationships during thin film formation. Therefore, a new technique by which the formation and relaxation of thin films can be readily studied from the changes in film stress, is in great demand.

1.2 Objective

The objective of this study is to establish a novel technique, namely an **in–situ stress measurement technique**, to investigate the formation and stress relaxation of multicomponent thin films, $PbTiO_3$, and to propose theoretical models to explain the experimental results. In addition, the effects of ion bombardment on thin film stress were also elucidated using the same technique.

1.3 Presentation of Results

The in–situ technique was developed, and will be thoroughly described in chapter II, by in–situ monitoring the development of film stresses in oxide multilayers during thermal excursions. A simple model for the evolution of stresses during the formation of the $PbTiO_3$ layer is proposed.

In chapter III, a simple model is proposed to elucidate the kinetics and mechanisms of stress relaxation of the $PbTiO_3$ film after formation. It is based on the diffusional creep model proposed by Nabarro–Herring [29], and is correlated to its microstructural evolutions.

Using this technique, the effects of ion bombardment on film stresses in $PbTiO_3$ thin films fabricated by the IAD process were extensively studied and described in chapter IV. The effects of ion bombardment on film stresses before, during, and after $PbTiO_3$ formation were presented.

To further demonstrate the capability of in-situ stress measurement technique, the stress evolution associated with crystallization of $BaMgF_4$ thin films was reported in chapter V.

Chapter VI provides the overall summary of this work.

1.4 References

1. R.F.Bunshah, "Deposition Technologies for Films and Coatings", Noyes Publications, New Jersey, 1982, p. 115.

2. H.R. Kaufman, J.J. Cuomo and J.M.E. Harper, J. Vac. Sci. Technol., 21, 725, 1982.

3. K.K. Schuegraf, Handbook of Thin Film Deposition Process and Techniques, Noyes Publication, New Jersey, USA, 1988, p. 380,

4. M Marinov, Thin Solid Films, 46, 267, 1977.

5. J.E. Griffith, Y. Qiu, and T.A. Tombrello, Nucl. Instrum. Methods, 198, 607, 1982.

6. K.H. Muller, J. Appl. Phys., 59, 2803, 1986.

7. D. Dobrev, Thin Solid Films, 92, 41, 1982.

8. J.J. Cuomo, J.M.E. Harper, C.R. Guarnierei, D.S. Yee, L.J. Attanasio, J. Angilello, C.T. Wu, and R.H. Hammond, J. Vac. Sci. Technol., 20, 349, 1982.

9. J.R. McNeil, J.J. McNally, and P.D. Reader, in "Handbook of Thin-Film Deposition Processes and Techniques", edited by K.K. Schuegraf, Noyes Publications, New Jersey, 1988, p.201.

10. R.W. Berry, P.M. Hall, and M.T. Harris, "Thin Film Technology", Van Nostrand Reinhold, 1968, pp. 113–190.

11. R.F.Bunshah, "Deposition Technologies for Films and Coatings", Noyes Publications, New Jersey, 1982, p. 115.

12. S.P. Murarka, "Silicides for VLSI Applications", Academic Press, New York, 1982.

13. V.G. Gavrilyachenko, R.I. Spinko, M.A. Martynenko, and E.G. Fesenko, Soviet

Phys. Solid State, 12, 1203–04, 1970.

14. M. Okuyama, Y. Matsui, H. Hakano, T. Nakagawa, and Y.Hamakawa, Jpn. J. Appl. Phys., 18, 1633–34, 1979.

15. J.C. Crawford and F.L. English, IEEE Trans. Electron. Devices, ED–16, 525–32, 1969.

16. E.R. Myers and A.I. Kingon, "Ferroelectric Thin Films", Materials Research Society Symposium Proceedings, Vol. 200, Materials Research Society, Pittsburgh, PA, 1990.

17. D.S. Campbell, in Handbook of Thin Film Technology, edited by L. Maissel and R. Glang, McGraw–Hill, New York, 1970, p. 22.

18. W. D. Nix, Metall. Trans. A, 20A, 2217, 1989.

19. J.J. Barnes, J.G. Goedjen, and D.A. Shores, Oxid. Met., 32, 449, 1989.

20. E. Kobeda and E.A. Irene, J. Vac. Sci. Technol. B, 7, 163, 1989.

21. G. Ghibaudo, Philos. Mag. B, 55, 147, 1987.

22. S. Yanagisawa and T. Fukuyami, J. Electrochem. Soc., 127, 1150, 1980.

23. J. J. Angilello, J.E. Baglin, F. M. d'Heurle, C.S. Petersson and A. Segmuller, in J.E. Baglin and J. Poate (eds.) Thin Film Interfaces and Interactions, Electrochemical Society, Pennington, NJ, 1980, p. 370.

24. P. Buaud and E.A. Irene, unpublished. 1991.

25. P. Buaud, F.M. d'Heurle, E.A. Irene, B.K. Patnaik and N.R. Parikh, J. Vac. Sci. Technol. B, 9, 2356, 1991.

26. L. Van den Hove, Ph.D. Thesis, Katholieke Universiteit Leuven. 1988.

27. S.L. Zhang and F.M. d'Heurle, Thin Solid Films, 213, 34, 1992.

28. C.A. Apblett and P.J. Ficalora, Materials Research Society Symposium Proceedings, Vol. 239, p.99, 1992.

29. F.M. d'Heurle, Int. Mater. Rev., 34, 53, 1989.

Chapter 2

A NOVEL TECHNIQUE FOR INVESTIGATING MULTICOMPONENT OXIDE FILMS: I, FORMATION KINETICS

2.1 Abstract

A novel in–situ stress measurement technique to study the formation kinetics of multicomponent oxide thin films was developed and was applied to $PbTiO_3$ growth. Single phase $PbTiO_3$ thin films were formed from the reaction between films in the deposited PbO/TiO_2 multilayer. The film stoichiometry was accurately controlled by depositing individual layers of the required thickness. Development of film stresses associated with the formation of the product layer at the PbO/TiO_2 interface of the multilayers was used to monitor growth rate of the $PbTiO_3$ layer. The growth of the $PbTiO_3$ phase obeyed the parabolic law and the apparent activation energy was estimated to be 108 kJ/mole. It is believed that the mechanism of this reaction was dominated by grain boundary diffusion of the participating cations.

2.2 Introduction

Thin films of multicomponent oxides such as $PbTiO_3$ have been extensively studied due to their remarkable ferroelectric, pyroelectric, and piezoelectric properties. The applications of these thin films include opto–electroonic devices,

sensors, transducers, and non–volatile memory devices [1]. A variety of vapor deposition techniques has been applied to the fabrication of these thin films. Physical vapor deposition techniques such as sputtering and evaporation often encounter a problem of controlling film stoichiometry. One way to overcome this problem is the use of multilayer approach [2], in which the composition of the films is accurately controlled by depositing required thicknesses of individual layers (e.g. A + B $\longrightarrow$ AB). For $PbTiO_3$ system, either metallic,

$$Pb + Ti \xrightarrow{O_2} PbTiO_3, \qquad (1)$$

or oxide multilayers,

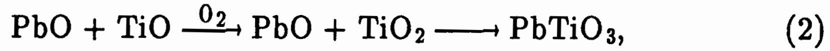

$$PbO + TiO \xrightarrow{O_2} PbO + TiO_2 \longrightarrow PbTiO_3, \qquad (2)$$

can be used to obtain the compound.

In order to optimize the process of thin film fabrication, it is of great importance to understand the formation kinetics. When a thin film, A, is deposited on a substrate, the total film stress of film A can be a function of temperature, time, substrate and film thickness [3]. If a second film, B, is deposited on top of A, the total film stress of this bilayer can be influenced not only by the aforementioned factors but also by interaction between them. Assume that film stresses of the individual layers are constant at a given temperature, and a product layer of AB is formed at the interface between A and B, then the total stress of the multilayer will be influenced by the thickness of the AB film. Since the extent of reaction is

time–dependent at a given temperature, the total stress of the multilayer is also time–dependent. Therefore, the formation kinetics of multicomponent thin films can be studied by using the in–situ stress measurement technique.

In–situ stress measurement technique was applied by Apblett and Ficalora on the Cu/Ti multilayer alloy system [4]. In their study, the origin of these stresses was attributed to the formation of compounds such as TiCu and $TiCu_3$. TiCu formed during the compressive stage and $TiCu_3$ formed during the tensile stage. However, neither semi–quantitative nor quantitative relations between total stress and reaction kinetics have been documented. In addition, the unavoidable phenomena of stress relaxation in thin films was not discussed either.

In this chapter it is demonstrated the use of the in–situ stress measurement technique for studying the formation kinetics of $PbTiO_3$ from PbO/TiO_2 multilayers. The kinetic data matched very well with the reported data obtained for the PbO and TiO_2 powder mixtures. Using this technique, the grain boundary diffusion coefficient was deduced. In the next chapter, the phenomena of stress relaxation in $PbTiO_3$ thin films will be reported.

2.3 Methodology

Formation of $PbTiO_3$ thin films takes place via the reaction between PbO and TiO_2 films. The reaction product separates the reactants from one another, and the reaction proceeds by diffusion of the participating components through the reaction

product. For very low solubilities of the reactants in the reaction product (i.e. for a product with a very low range of homogeneity, as shown in the $PbO-TiO_2$ phase diagram [5]) the particle fluxes are locally constant, and as long as local thermodynamic equilibrium is maintained at the phase boundary, a planar growth mode is made possible and a parabolic growth law results.

When sequentially deposited films are all very thin compared with the substrate, each film imposes a separate bending moment and a separate curvature (R). Since moments are additive so are the curvatures.

$$1/R_1 + 1/R_2 + \cdots = \frac{1-\nu_s}{E_s}\frac{6}{{d_s}^2}(\sigma_1 d_1 + \sigma_2 d_2 + \cdots) \quad (3)$$

where E_s and ν_s are the Young's modulus and Poisson's ratio of the substrate.

$$\sigma d = \sum_{i=1}^{n} \sigma_i d_i, \quad (4)$$

where σ and d denote total film stress and thickness, respectively.

For a PbO/TiO_2 multilayer on a sapphire substrate, the total film stress can be expressed as:

$$\sigma d = \sigma_a d_a + \sigma_b d_b, \quad (5)$$

where (σ_a, d_a) and (σ_b, d_b) denote the stress and thickness of PbO and TiO_2 layers.

Assume that, (i), stresses of the PbO, TiO_2 and $PbTiO_3$ layers (σ_a, σ_b, and σ_{ab}) are constant during formation, (ii), the total thickness (d) of the multilayer is constant, and (iii), initial stress is defined as $\sigma_i = (\sigma_a d_a + \sigma_b d_b)/d$, where $d_a/d_b \simeq 2/1$, this ratio is close to the ratio of density of the participating materials. Accordingly, the consumption of the PbO layer should be twice as fast as that of the TiO_2 layer. The value of σ_i is obtained from the stress–temperature plot where the temperature is 500° C, which will be explained in the later sections.

At a certain fraction of reaction where a layer of $PbTiO_3$ (d_{ab}) is formed, the total film stress becomes

$$\sigma = \frac{1}{d}[\sigma_a(d_a - \frac{2}{3}d_{ab}) + \sigma_b(d_b - \frac{1}{3}d_{ab}) + \sigma_{ab}d_{ab}]$$

$$= \frac{1}{d}[(\sigma_a d_a + \sigma_b d_b) + d_{ab}(\sigma_{ab} - \frac{2\sigma_a + \sigma_b}{3})]$$

$$= (\frac{\sigma_a d_a + \sigma_b d_b}{d}) + (\sigma_{ab} - \frac{2\sigma_a + \sigma_b}{3})(\frac{d_{ab}}{d})$$

$$= \sigma_i + (\sigma_{ab} - \sigma_i)(\frac{d_{ab}}{d}) \qquad (6)$$

Therefore, $\frac{d_{ab}}{d} = \frac{\sigma - \sigma_i}{\sigma_{ab} - \sigma_i} = f(\text{Temp, time}).$ (7)

From equation (6) and parabolic law, the film stress–time relationship can be plotted as shown in Fig. 1.

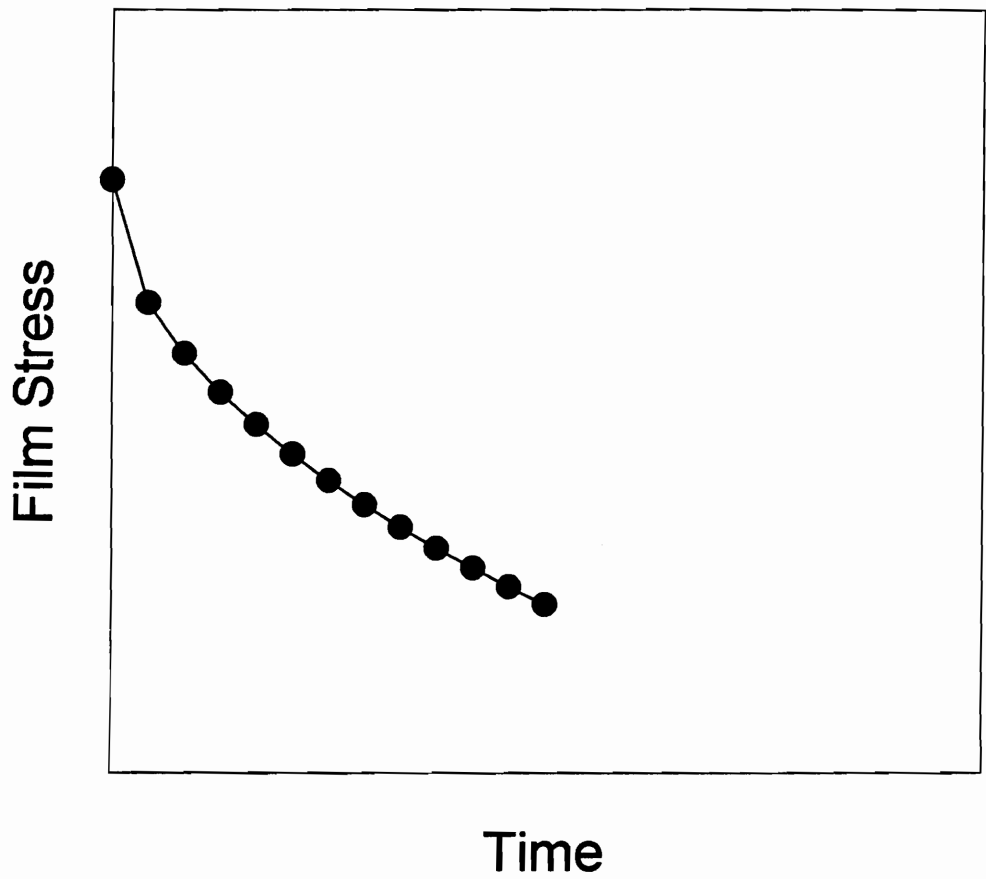

Fig. 1 Schematic stress-time plot for $PbTiO_3$ thin film reaction.

2.4 Eeperimental Procedure

The film deposition system was a conventional cryopumped electron beam evaporator. The 2–in. sapphire substrates were mounted 34 cm above the electron beam evaporation source. Before deposition, the system was pumped down to 4×10^{-8} torr, rising to $2–3 \times 10^{-7}$ torr during deposition. All the depositions were performed at ambient temperature with a deposition rate of 0.2–0.5 nm/s. Total film thickness was kept constant at 300nm.

High purity, vapor deposition grade oxides (PbO and TiO) were used as the evaporation sources. TiO_2 was not used due to its decomposition during deposition. Based on theoretical calculations and taking into account the loss of Pb (10 mol.% of PbO was added), the thicknesses of the PbO and TiO layers were approximately 200nm and 100nm, respectively. The configuration of the multilayer is shown in Fig. 2. The substrates were cleaned by a series of organic solutions and deionized water followed by drying in N_2 gas.

Film stress measurements as a function of temperature and time were performed for the PbO/TiO oxide multilayers, on 2–inch diameter sapphire substrates in air. The heating rate was 5°C/min. The sample curvature was calculated from the change in position of a reflected laser beam. The position was measured by a position sensitive detector while the beam was scanned across the sample. The total film stresses were calculated by comparing the substrate curvature before and after film deposition using Stoney's equation [6], which yields the biaxial stress in the thin films parallel to the substrate:

200nm PbO
100nm TiO
Sapphire

Fig. 2 Configuration of the multilayer.

$$\sigma = \frac{E_S}{6(1-\nu_S)} \frac{t_S^2}{t_f} \frac{1}{R} \quad (8)$$

where E_S, ν_S, and t_S are Young's modulus, Poisson's ratio, and thickness of the substrate, respectively, and t_f is the film thickness. R is an effective radius of curvature of the substrate determined by $R = 1/(1/R_2 - 1/R_1)$, where R_1 and R_2 are the substrate radii of curvature before and after film deposition. This formula is applicable when t_f is far smaller than t_S and the central wafer deflection is much smaller than the diameter of the wafer. Both conditions are met in the present work.

Based on this technique, stress–temperature and stress–time plots of the PbO/TiO/sapphire specimens were obtained. In order to quantify the extent of the reaction and the morphological change associated with film stresses development, separate tests were carried out, such as x–ray diffraction analysis for phase determination and scanning electron microscopy for morphology observation.

2.5 Results and Discussion

ESCA analysis of as–deposited individual PbO and TiO layers indicated that Pb:O and Ti:O ratios to be near unity (1.03 for PbO and 1.0 for TiO). Similar analysis was also carried out for the films subjected to annealing at temperatures lower than 500°C. The Pb:O ratio quickly became 1:1 upon heating, whereas Ti:O ratio gradually reached 1:2 in the temperature range from 400° to 500°C. No $PbTiO_3$ formation was found from x–ray diffraction analysis in this temperature

range.

Since ESCA can only analyze the film composition of the surface layers, a transmittance method is used to detect oxidation of the bulk films. Here the absorption edges of both PbO and TiO layers were used as the indication of the extent of oxidation. An independent experiment was conducted to study the oxidation of both 200nm PbO and 100nm TiO layers on sapphire substrates as a function of temperature. Both films were subjected to transmittance vs. wavelength measurement. It was found that, as shown in Fig. 3, the absorption edge for both oxide layers was temperature–dependent. For the PbO layer, since it was nearly stoichiometric, its oxidation completed upon heating. Therefore its absorption edge stayed constant throughout the temperature range examined. For the TiO layer, incorporation of oxygen was slow at temperatures less than 450°C and became active above 450°C. The TiO layer completely transformed into TiO_2 when the temperature reached 500°C.

It was reported [7] that reaction between lead oxide and titanium oxide could not take place below 400°C and was very slow at $\leq$ 500°C. In accordance with earlier reports the current data also showed that when the temperature reached 500°C, the PbO/TiO multilayer would become PbO/TiO_2 multilayer, and the extent of reaction between PbO and TiO_2 could be neglected. This will be confirmed in the latter section of the paper. The formation of $PbTiO_3$ from the PbO/TiO_2 multilayers was then activated at $\geq$ 500°C.

2.5.1 In–Situ Study of $PbTiO_3$ Formation by Stress Measurement

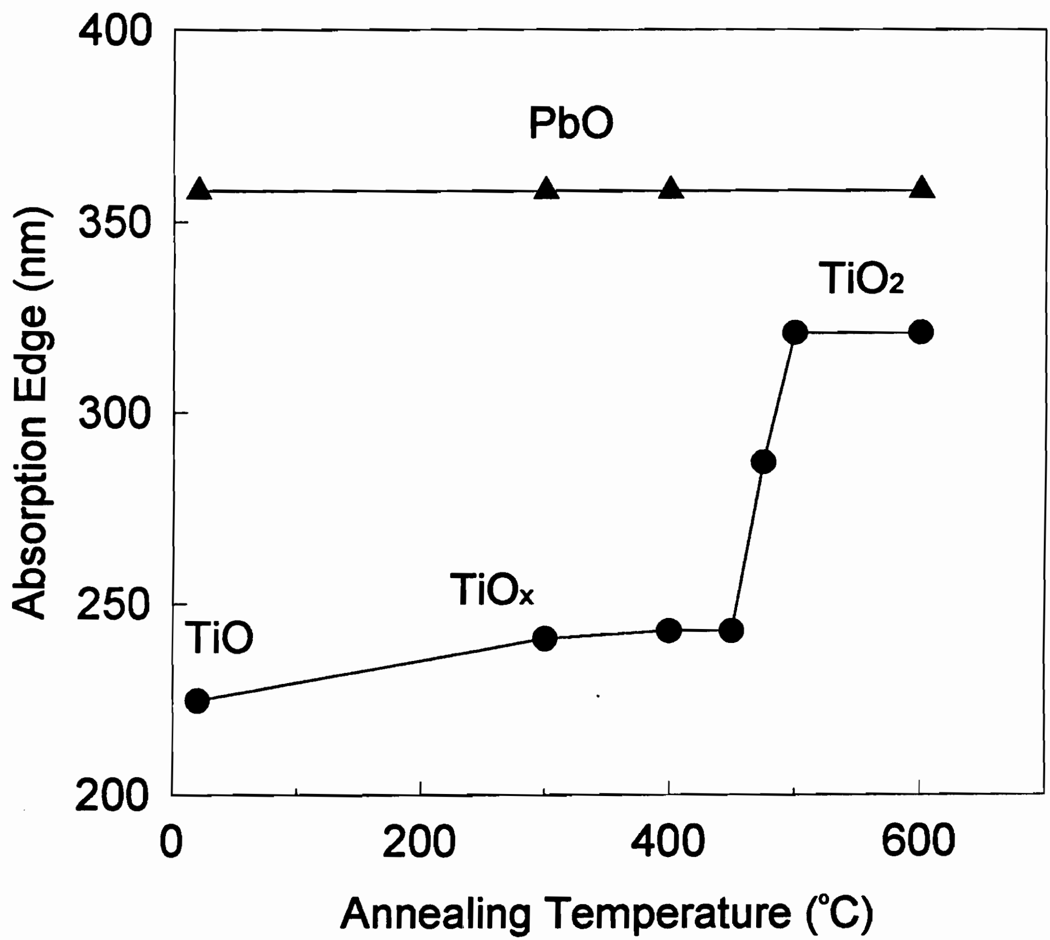

Fig. 3 Absorption edge of PbO and TiO_x films as a function of temperature.

Fig. 4 depicts a typical stress–temperature plot for the PbO/TiO multilayer on sapphire substrate which was subjected to annealing in air at 575° C for 4 hours with a heating rate of 5° C/min. The as–deposited multilayer is under tension with a film stress of approximately 100 MPa. It was found that the as–deposited film stress was very sensitive to deposition rate. For a better understanding, Fig. 4 was divided into three regions. As the temperature was increased, film stress did not change much, as shown in region I. Compressive film stress started building up while the curve entered region II at around 300° C and reached a local minimum at around 400° C, then increased slightly and decreased to a state where the film was nearly stress free at 500° C. The stress development in region II was attributed to the oxidation of TiO to TiO_2. This was confirmed by a separate study which showed that stress of an individual PbO layer remained constant throughout the temperature range examined. The uptake of oxygen into the films could result in increased film volume, generating compressive stresses. A reasonable explanation for the local stress surge at around 450° C is due to the crystallization in the titanium oxide layer which generates tensile stress. In region III, the stress–temperature curve entirely fell into the compressive state. Compressive stress continued developing in the films when the temperature was above 500° C and reached a local minimum in the isothermal region, and then tensile stress started building up. This region of the curve was attributed to the formation of the $PbTiO_3$ phase in the film and stress relaxation.

Film stresses during cooling showed very good linearity vs temperature only. Therefore thermal stress (σ_{th}) could be calculated as:

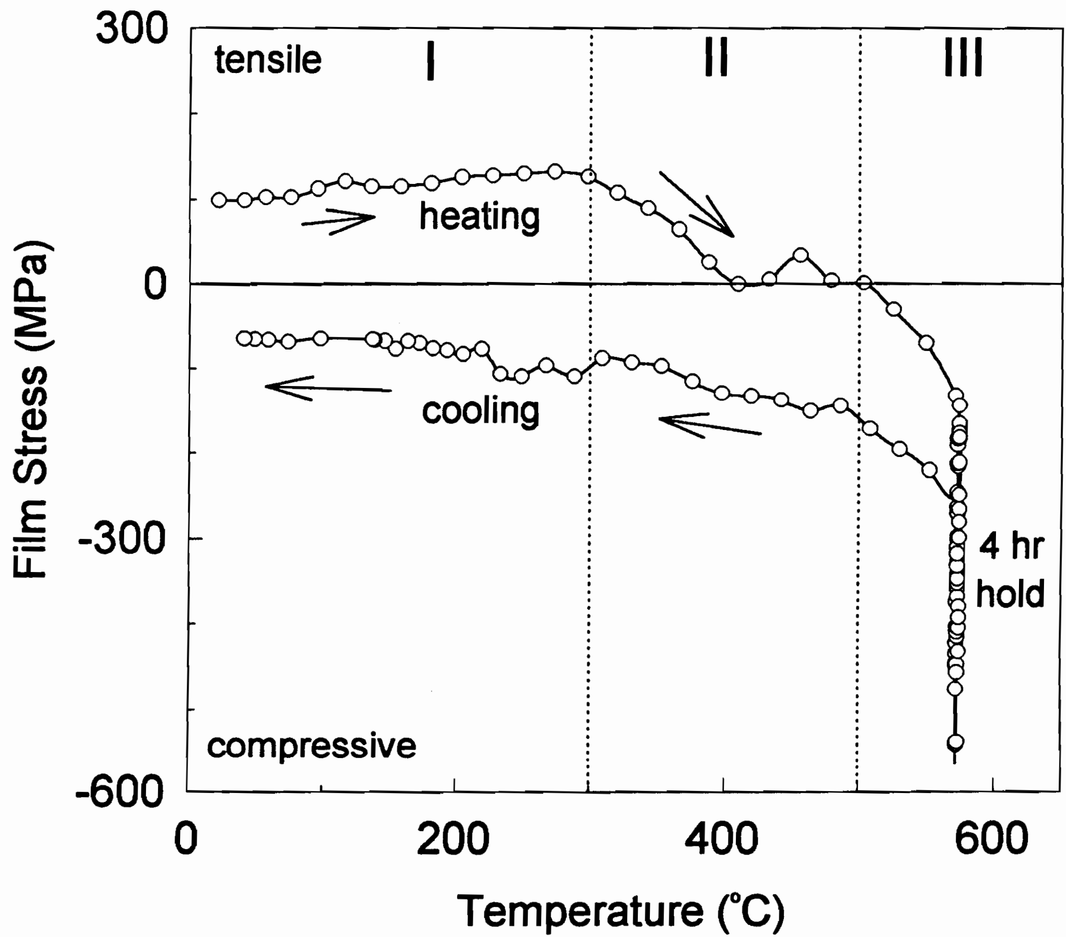

Fig. 4 A typical film stress-temperature plot for a $PbTiO_3$ thin film.

$$\sigma_{th} = \frac{E_f}{(1 - \nu_f)}(\alpha_f - \alpha_s)(T_a - T) \quad (9)$$

where T_a is the annealing temperature, $E_f/(1-\nu_f)$ is the biaxial modulus of the $PbTiO_3$ film, and α_f and α_s are thermal expansion coefficients of film and substrate. Take α_s of sapphire as 8.8×10^{-6} 1/°C [8], the thermal expansion coefficient of the $PbTiO_3$ film was calculated as 10.6×10^{-6} 1/°C. This value was found to be higher than that of 7.1×10^{-6} 1/°C for $PbTiO_3$ ceramics [9], which is consider to be stress free, in the temperature range below Curie point.

With increasing temperature, the interaction between lead oxide and titanium oxide layers can be schematically depicted in Fig. 5. In region III, stress developments involve two kinetic processes, $PbTiO_3$ formation and stress relaxation. In this paper, the authors try to establish a basic understanding of the kinetics of $PbTiO_3$ formation **only** using the in–situ stress measurement technique.

This study, hereafter, concentrates on the temperature regime from 550°C to 625°C.

The isothermal region for several different annealing temperatures was replotted in Fig. 6. The development of compressive stress in the early stage of the stress–time plots can be attributed to the growth of the $PbTiO_3$ layer. During the growth process, absorption of vacancies from a free surface by the product layer can bring about a compressive stress because of "swelling" of the deposit. As the growth process is completed, film stress reached an extreme, that is the local minima in the plots as shown in Fig. 6. This is also confirmed by x–ray diffraction analysis as

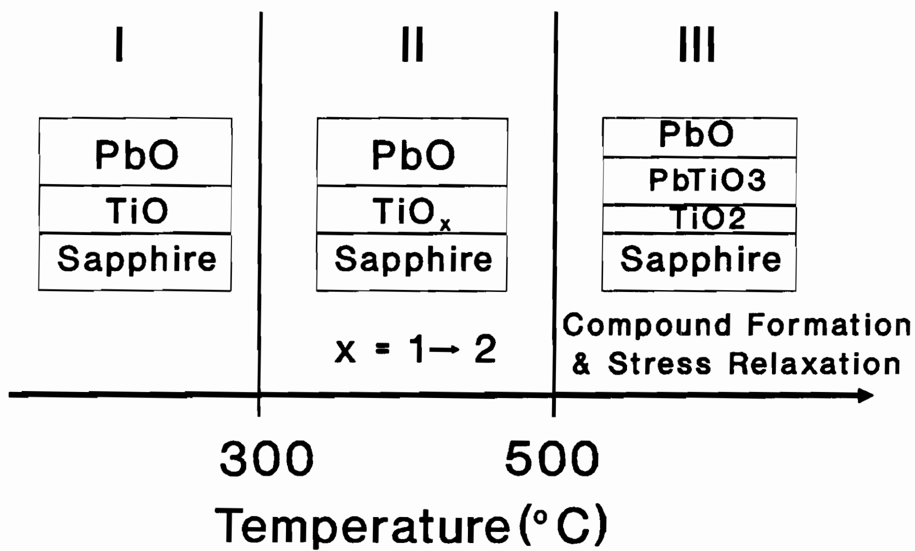

Fig. 5 Interaction between PbO and TiO_x layers as a function of temperature.

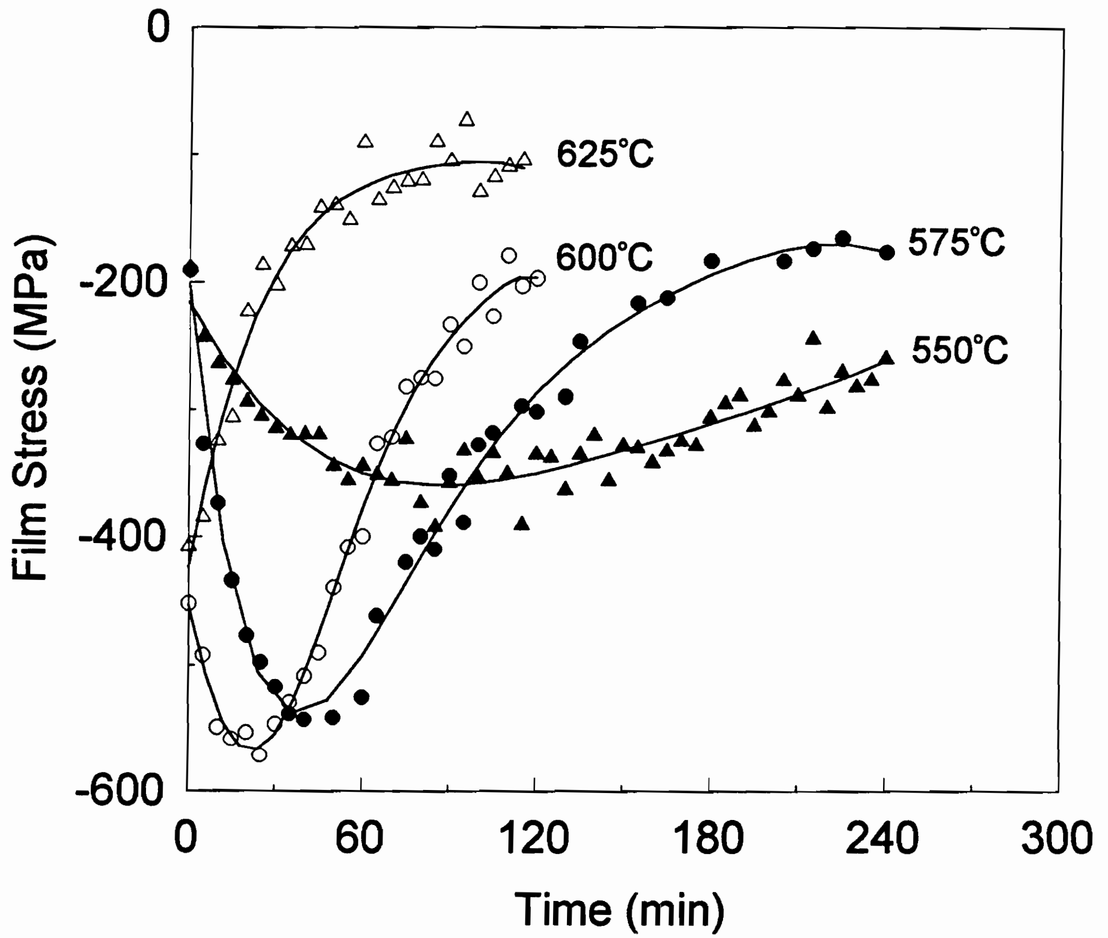

Fig. 6 Stress-time plots for $PbTiO_3$ thin films.

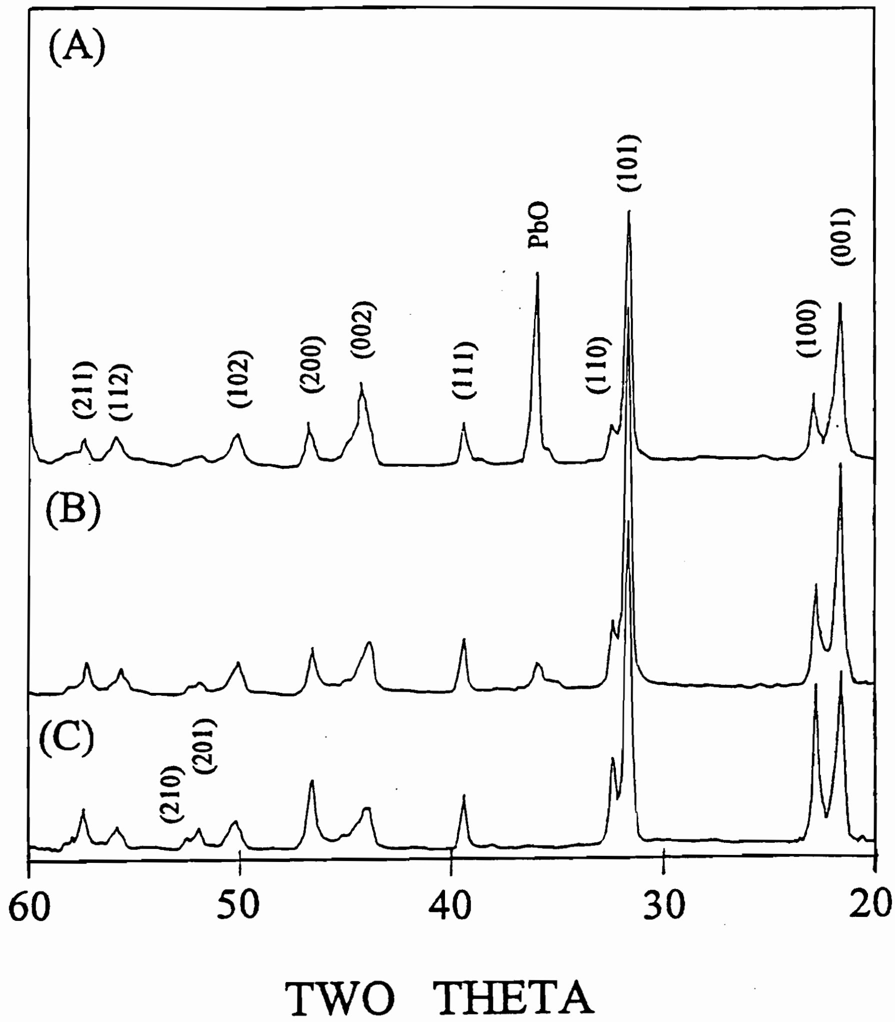

Fig. 7 XRD spectra of $PbTiO_3$ films.

shown in Fig. 7.

Using this in–situ stress measurement technique, one can monitor the kinetics of compound formation step by step even if the reaction is reasonably fast. For instance, the minimum was found at around 40 minutes for 575° C. Lowering the annealing temperature increased the time to achieve a minimum, e.g. around 100 minutes for 550° C. Conversely, raising the annealing temperature decreased the time to achieve a minimum e.g. around 20 minutes for 600° C. By annealing at 625° C, the minimum occurred too fast to appear on the plot.

Intuitively, the stress plots (Fig. 6) can be divided into two different region as shown in Fig. 8. The asymmetry of the curve implied two different mechanisms for the two distinct regions. During the region of formation, a large amount of vacancies and grain boundaries were generated. Accordingly, the strain energy stored in vacancies and grain boundaries needed to be released. Tensile stresses were generated by the elimination of vacancies and grain boundaries, and, therefore, film stress relaxed.

2.5.2 Formation Kinetics

Fig. 9 shows the fraction of the $PbTiO_3$ formation as a function of annealing time for the temperatures ranging from 550° C to 600° C. From Fig. 9 the thickness of the $PbTiO_3$ layer formed can be deduced from

$$d_{ab} = d \cdot f. \qquad (10)$$

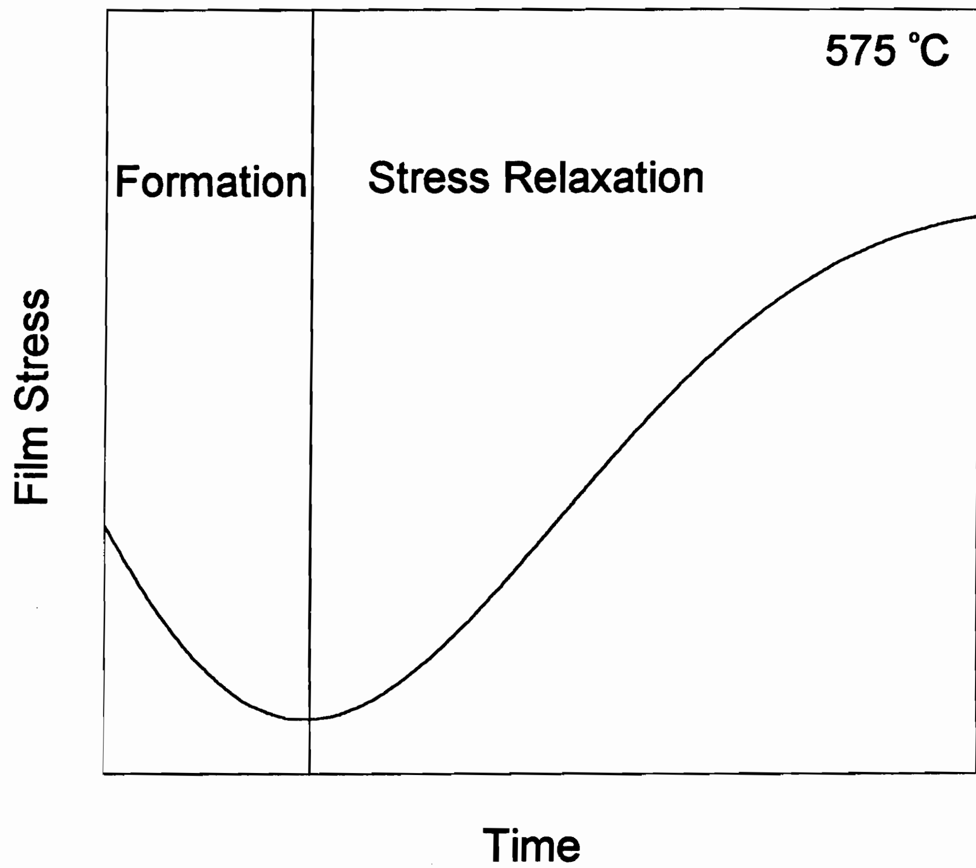

Fig. 8 Implications in a stress-time plot.

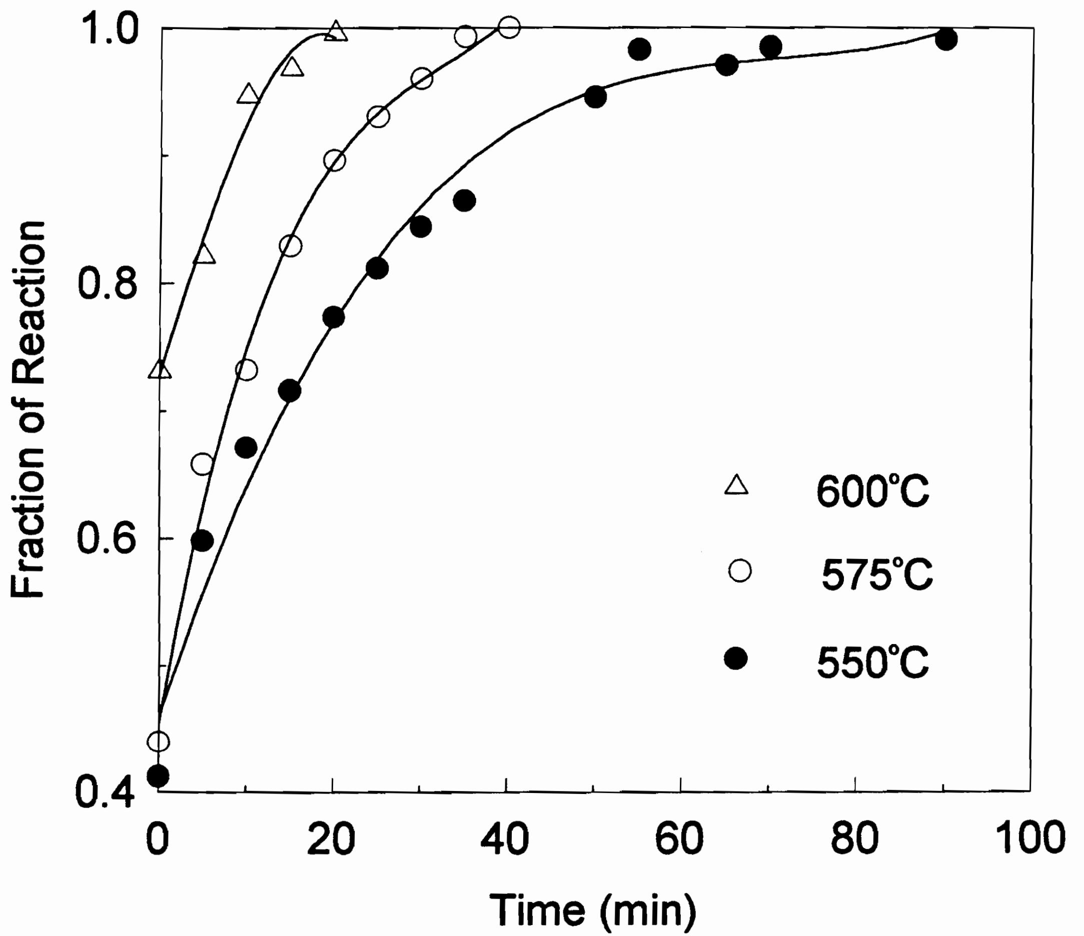

Fig. 9 Fraction of $PbTiO_3$ formation as a function of time.

The growth of the $PbTiO_3$ layer is governed by the parabolic law, i.e.,

$$(d_{ab})^2 = kt, \quad (11)$$

where k is the rate constant. Fig. 10 illustrates the kinetics of $PbTiO_3$ growth for three different temperatures. Since the data of Fig. 9 represents a diffusion–controlled growth process the chemical interdiffusion coefficient (D) can be determined from the rate constant, k = 4D. The rate constant, k, has an Arrhenius behavior as shown in Fig. 11. The straight line fit points to a thermally activated growth of $PbTiO_3$ on sapphire. The activation was estimated to be 108 kJ/mole. This value is in excellent agreement with the literature values as shown in Table I.

2.5.3 Mechanism of $PbTiO_3$ Formation

From PbO and TiO_2 layers, a polycrystalline $PbTiO_3$ phase is formed. During reaction, the fluxes of the components in the product layer, which are responsible for the advancement of the reaction, are the moving ions. Therefore, in order to preserve local electrical neutrality, the fluxes of the different ions must always be coupled with each other. Consequently, the following combinations are possible: either oppositely charged ions flow in the same direction, or ions with like charges flow in opposite directions through the reaction product. These simple considerations give the possible limiting cases of a solid state reaction between ionic crystals. For the formation of ionic crystals such as $PbTiO_3$ it is the slower partner that essentially determines the reaction rate. From the rate constants, the chemical diffusion constant of $PbTiO_3$ formation in this work could be calculated as 6.8×10^{-14}

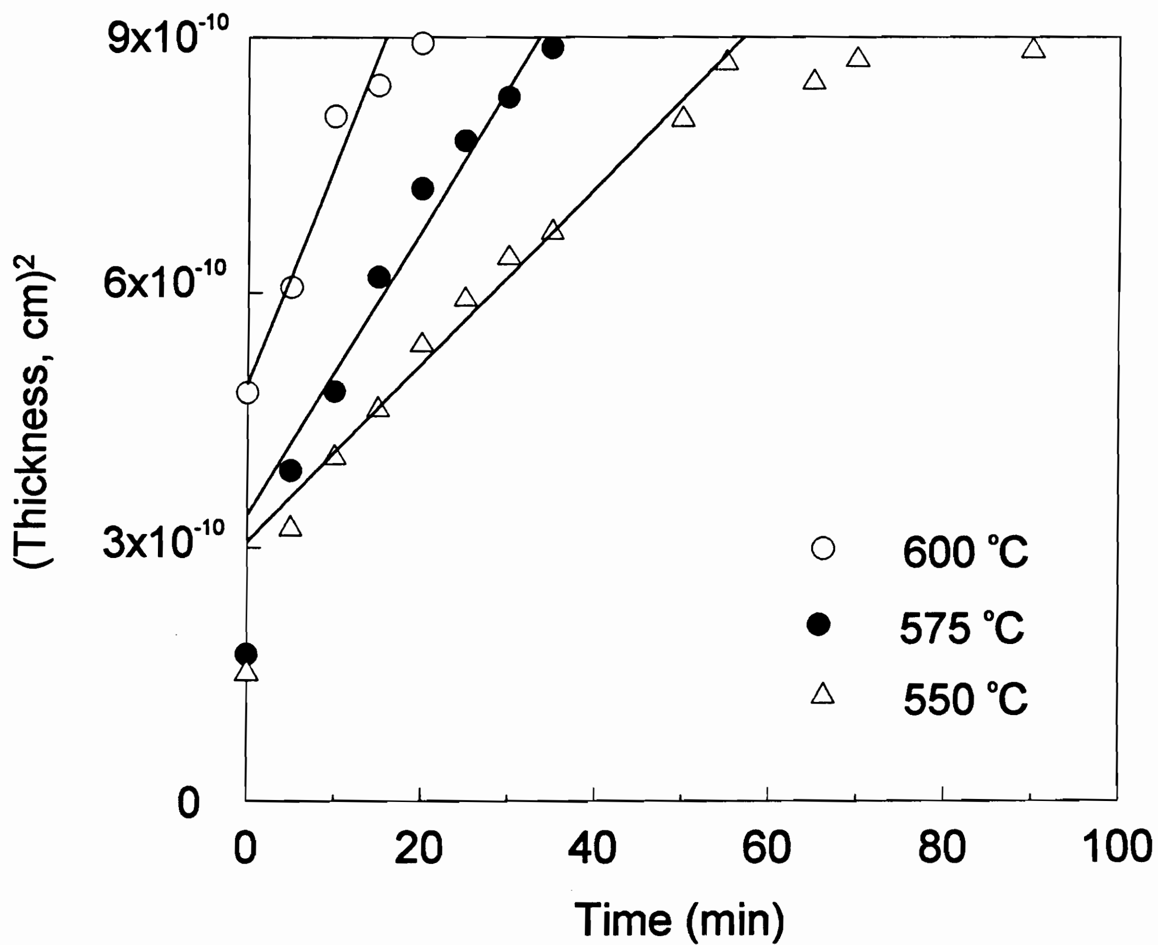

Fig. 10 Time dependent of the thickness of $PbTiO_3$ films.

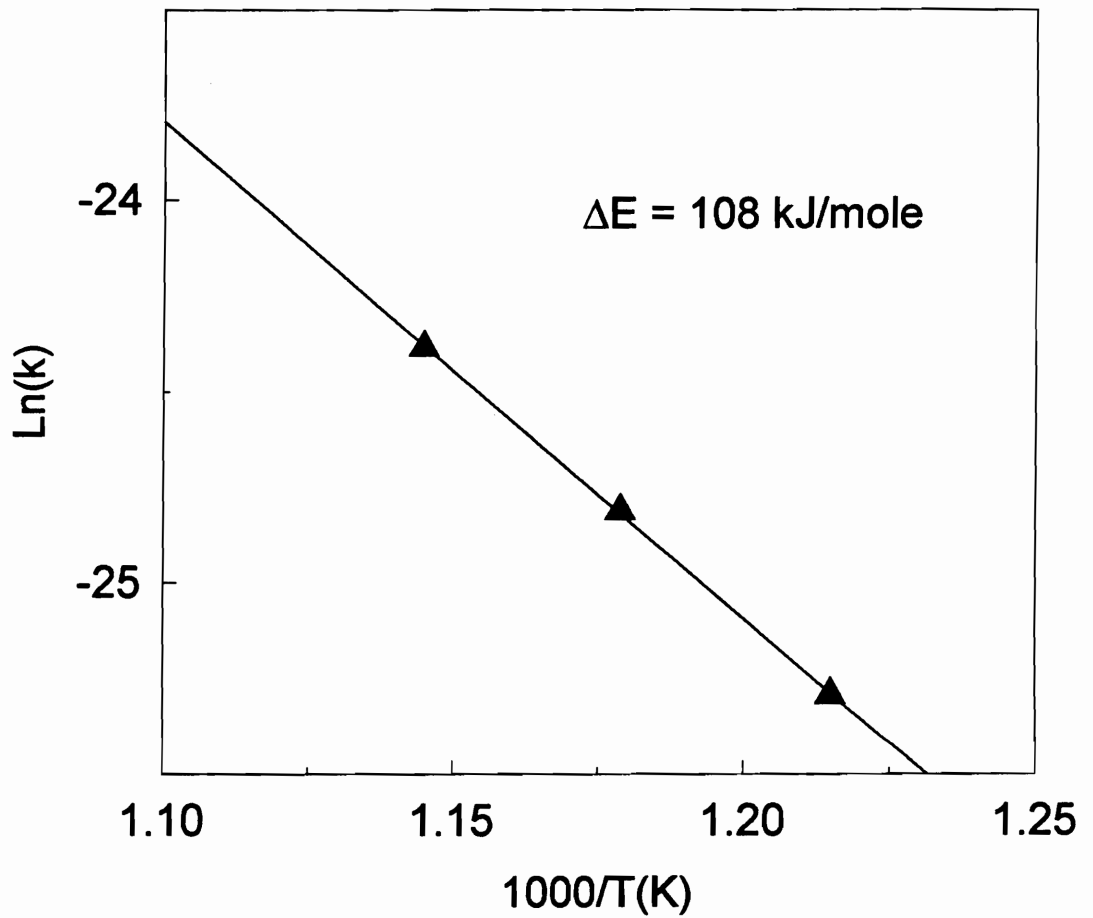

Fig. 11 The Arrhenius behavior of rate constants of $PbTiO_3$ formation.

Table I: Kinetic Data of $PbTiO_3$ Formation

Activation energy(kJ/mole)	Ref.	Process
108, 122	Janson, 1966 [7]	$PbO + TiO_2$ powders
151	Yanson, 1966 [10]	$Pb + TiO_2$ powders
77	Andreeva, 1973 [11]	$Pb(OH)_2 + Ti(OH)_4$
		$PbCO_3 + Ti(OH)_4$
81, 69	Dvernyakova, 1985 [12]	$TiO_2 \cdot nH_2O + PbCO_3 \cdot nH_2O$
108	**this work, 1993**	**PbO/TiO_2 thin films**

cm^2/sec at 575°C. The chemical diffusion constants at this temperature were estimated to be $1x10^{-12}$ cm^2/sec for PbO [13] and $7.4x10^{-16} cm^2/sec$ for TiO_2 [13]. Our experimental value is approximately an order magnitude lower than that for PbO and two order higher than that for TiO_2. This could suggest that transport of Ti^{4+} ions through the product layer is the rate-determining step. Furthermore it is believed that the participating components mainly diffuse through grain boundaries. It is then reasonable to write the grain-boundary diffusion constant as,

$$D_{gb} = 3x10^{-7}exp(-108{,}000/kT)\ cm^2/sec. \tag{12}$$

It is well known that the effect of compressive stress on atomic or molecular diffusion in a constrained solid is to reduce the diffusivity because of the enhancement of steric hindrance in the lattice [14]. Therefore one can expect a lower grain boundary diffusion constant for stress-free $PbTiO_3$ formation.

From the above equation (12), one can extrapolate the rate constant of the $PbTiO_3$ formation at 500°C. The amount of reaction between PbO and TiO_2 films annealed at 500°C for 0.1 minute was calculated to be 2%. This is self-consistent with the assumptions.

2.6 Summary

A novel in-situ stress measurement technique has been successfully developed to study the formation kinetics of multi-component thin films such as $PbTiO_3$.

Using the multilayer approach, film composition can be simply controlled by the thickness of the individual layers. the formation of the $PbTiO_3$ layer at the interface of PbO/TiO_2 altered the total stress of the multilayers. By monitoring stress changes in the multilayers, the in–situ formation kinetics of $PbTiO_3$ films was successfully examined and quantitatively documented. The activation energy of $PbTiO_3$ formation was estimated to be 108 KJ/mole which is in excellent agreement with the literature value. It is believed that the formation of $PbTiO_3$ phase was dominated by grain boundary diffusion mechanism because of the very fine grain size in the films. The grain boundary diffusivity responsible for this reaction was also deduced.

2.7 References

1. M. Okuyama and Y. Hamakawa, Int. J. Engng. Sci., 29(3), 391 (1991)

2. E. R. Myers and A. I. Kingon, "Ferroelectric Thin Films," Materials Research Society Symposium Proceedings, Vol. 200, Materials Research Society, Pittsburgh, PA, 1990

3. J. C. Braveman, W. D. Nix, D. M. Barnett, and D. A. Smith, "Thin Film Stresses and Mechanical Properties," Materials Research Society Symposium Proceedings, Vol. 130, Materials Research Society, Pittsburgh, PA, 1989

4. C. A. Apblett and P. J. Ficalora, Materials Research Society Symposium Proceedings, Vol. 239, p.99, 1992

5. R. L. Holman, Ferroelectrics, 14, 675 (1976)

6. G. C. Stoney, Proc. Royal Society London, A82, 172 (1909)

7. G. Janson, E. Z. Friedenfelds, I. Skomorokha, and O. S. Maksimova, Uch, Zap. Riehsk. Politekh. Inst. 16, 387 (1965)

8. W. D. Kingery, H. K. Bowen, and D. R. Uhlmann, "Introduction to Ceramics," 2nd Ed., 1976, p. 595,

9. G. Shirane and S. Hoshino, J. Phys. Soc. Jpn., 6, 265 (1951)

10. G. D. Yanson, E. N. Bindar, O.S. Maksimova and E. Zh. Freidenfel'd, Zh. Neorgan. Materialy. 2, 1563 (1966)

11. V. I. Andreeva, T. F. Limar, N. G. Kisel, D. S. Domenko, Yu. N. Velichko, Kinet. Katal., 24(5), 1144 (1973)

12. A. A. Dvernyakova, V. I. Stetsenko, M. V. Sidorenko, Ukr. Khim. Zh., 51(11) 1136 (1985)

13. S. Mrowec, "Defects and Diffusion in Solids: An Introduction,' Elsevier

Scientific Publishing Company, Amsterdam, Netherland, 1980

14. S. Ikegami, I. Ueda, and T. Nagata, J. Acoust. Soc. Am., 50, 1060 (1971)

Chapter 3

A NOVEL TECHNIQUE FOR INVESTIGATING MULTICOMPONENT OXIDE FILMS: II, STRESS RELAXATION

3.1 Abstract

Stress relaxation in $PbTiO_3$ films was investigated by the in–situ stress measurement technique. A simple viscous flow model was successfully employed to interpret the kinetics and behavior of stress relaxation of $PbTiO_3$ thin films. The activation energy responsible for stress relaxation was estimated to be 190 kJ/mole, which was accounted for by lattice diffusion of vacancies. A Nabarro–Herring creep model was successfully exploited to correlate the relationships among the viscosity, lattice diffusion coefficient and grain size of the $PbTiO_3$ films. The estimation of the lattice diffusion coefficient of vacancy motion during relaxation was obtained. Also, the observed time required for complete relaxation was found to be in accord with theoretical values. Hillock formation resulted from grain boundary sliding was believed to contribute to stress relaxation in its early stage. Thereafter, grain growth resulted from lattice diffusion played a major role in stress relaxation.

3.2 Introduction

Unlike bulk materials, thin films condensed onto substrates are in an extremely non–equilibrium state characterized by a high level of stress. This

non–equilibrium is caused by a number of factors associated with both preparation techniques and physicochemical properties of substrates and film materials. Stress can be introduced in a thin film due to differential thermal expansion between the film and its substrate, due to lattice misfit with substrate, or due to chemical reaction within the film or with its substrate.

The tendency of a thin film towards equilibrium brings about relaxation of the internal stress in the film. Stress relaxation in thin films can take place during their thermal treatment. The relaxation in thin films often causes the formation of hillocks, whiskers, voids and cracks, and in certain cases the film breaks down into separate islands and peels off the substrate [1]. Of course, this leads to changes in performance of the thin film devices. Accordingly, in order to understand and therefore control the effect of stress on the performance of thin film devices, it is of great importance to investigate the mechanisms of stress relaxation in the materials of interest.

Deformation mechanisms [2] such as defectless flow, dislocation gilde, dislocation creep, diffusional creep, grain boundary sliding, and other mechanisms have been proposed to explain the stress relaxation in a number of thin films including metals [3], alloys [4], silicides [5], simple oxides [6]. At present it has been generally accepted that stress relaxation in most thin films is the result of plastic deformation by diffusional creep [7]. However, it is essential to notice that relaxation mechanisms in thin films are greatly influenced by many factors such as film stress level, temperature, film thickness and grain size. Thin films often contain extremely high concentrations of excess vacancies which are built in during

deposition. The stress level may be considerably affected by the flow of vacancies to the film surface and by structural defects [8]. It has also been suggested that in thin film grain growth, the removal of grain boundaries — and hence the reduction of the excess volume in the grain boundaries — will induce stress in the film when it is constrained by the substrate.

Little has been done, to the best of our knowledge, on stress relaxation of multicomponent oxide thin films [9]. In this paper, an in–situ stress measurement technique was employed to investigate the kinetics and mechanisms of stress relaxation in $PbTiO_3$ thin films. It is assumed that the stress relaxation of thin films can be described by the creep phenomena in bulk materials. An attempt was made to correlate stress relaxation with creep behavior using a simple viscous flow model and diffusional creep mechanisms. Using this technique, the diffusion coefficient responsible for the relaxation mechanism was estimated. Furthermore, the kinetics of stress relaxation was also found to be in excellent agreement with experimental and theoretical values.

3.3 Analysis

In order to understand the stress–relaxation phenomena of $PbTiO_3$ films at elevated temperatures, consider a viscous flow model as depicted in Fig. 1. For simplicity, only uniaxial compressive stresses are assumed to act on a slab of $PbTiO_3$, which is free to flow vertically (Fig. 1a). The $PbTiO_3$ film is modeled as a Maxwell element whose overall mechanical response reflects a series combination of

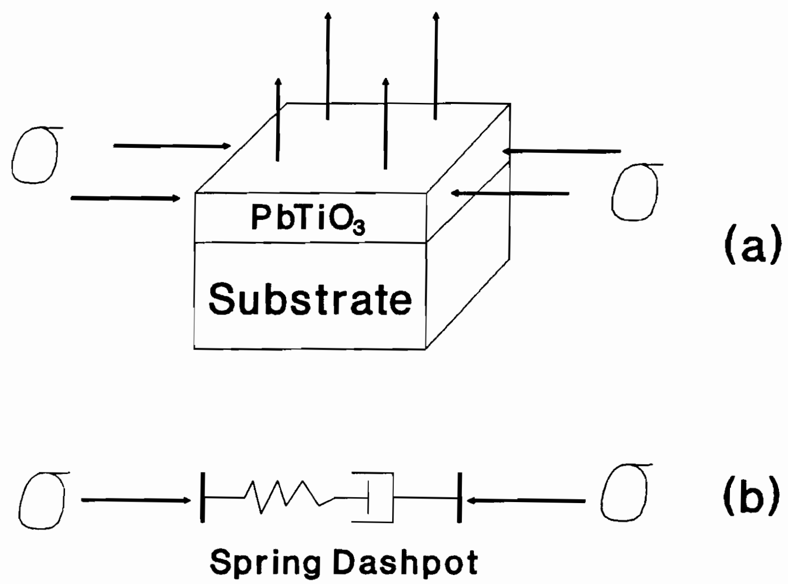

Fig. 1 The viscous flow model for stress relaxation.

an elastic string and a viscous dashpot (Fig. 1b), which incorporates the various relaxation mechanisms of the film. Upon loading, the spring instantaneously deforms elastically, With time, the elastic strain, ϵ_e, is accommodated by the development of a plastic strain, ϵ_p, which is in a time–dependent viscous fashion, but the total strain, ϵ_t, remains constant. Since the net stress, σ, acting on the film is dictated by the current level of the elastic strain:

$$\sigma = E\epsilon_e/(1-\nu) \tag{1}$$

where E is Young's modulus and ν is Poisson's ratio, as the time proceeds, film stresses relax.

The same compressive stress stress, σ, concurrently acts on both the spring and dashpot so that

$$\epsilon_e = \sigma/E \text{ and } \dot{\epsilon}_p = \sigma/\eta \tag{2}$$

where $\dot{\epsilon}_p = d\epsilon_p/dt$ and η is viscosity. For ϵ_t is constant, $\dot{\epsilon}_e = -\dot{\epsilon}_p$ or $(1/E)d\sigma/dt = -\sigma/\eta$. Upon integration, we obtain

$$\sigma = \sigma_o\exp(-Et/\eta) = \sigma_o\exp(-t/\tau) \tag{3}$$

where time constant $\tau = \eta/E$. The initial stress in the film, σ_o, therefore relaxes by decaying exponentially with time. In fact σ_o is equivalent to the σ_{ab} which indicates the stress level upon the completion of $PbTiO_3$ formation. Therefore, in

connection with the stress curve developed during $PbTiO_3$ formation, we can obtain a full schematic of the stress–time curve as shown in Fig. 2, assuming time constant $\tau = 50$ minutes.

3.4 Experimental Procedure

The detail of experiment was presented in chapter 2.

3.5 Results and Discussion

Fig. 3 shows the typical stress–time plots of $PbTiO_3$ thin films for four different temperatures. These plots were found to be very similar to the schematic in Fig. 2. However, the cusp in Fig. 2 was not seen in Fig. 3. The absence of the cusps in Fig. 3 could be attributed to the initial stress relaxation as the multilayer approached the completion of $PbTiO_3$ formation.

Take the absolute value of the data in the region of relaxation and replot them in a semi–log scale of stress against time, as shown in Fig. 4. The data showed very good linearity except for the data of 625°C. The deviation of data from the straight line could be likely caused by the change in relaxation mechanism. From the slopes of the straight lines in Fig. 4 the viscosity, η, can be obtained as shown in Fig. 5, by taking the Young's modulus of $PbTiO_3$ films to be 13.1×10^{11} dyne/cm^2 [10]. Since the viscosity decreases with increasing temperature and is governed by the following formula

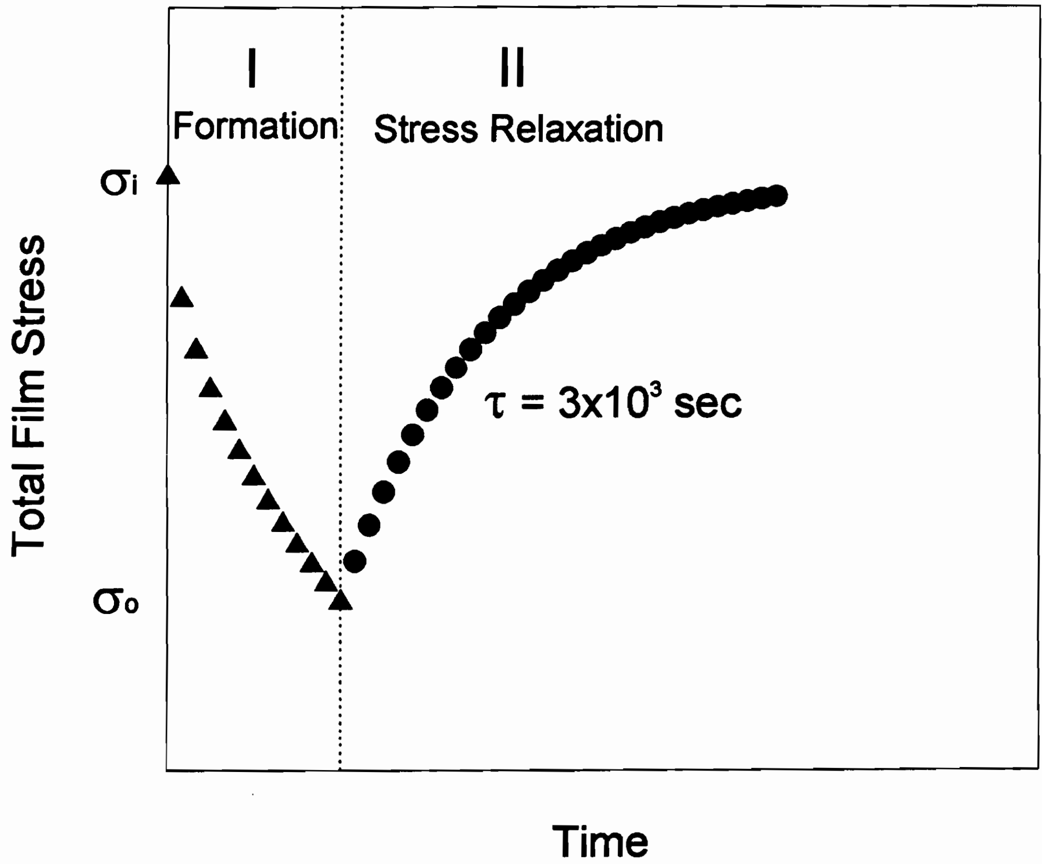

Fig. 2 A modeled stress-time curve.

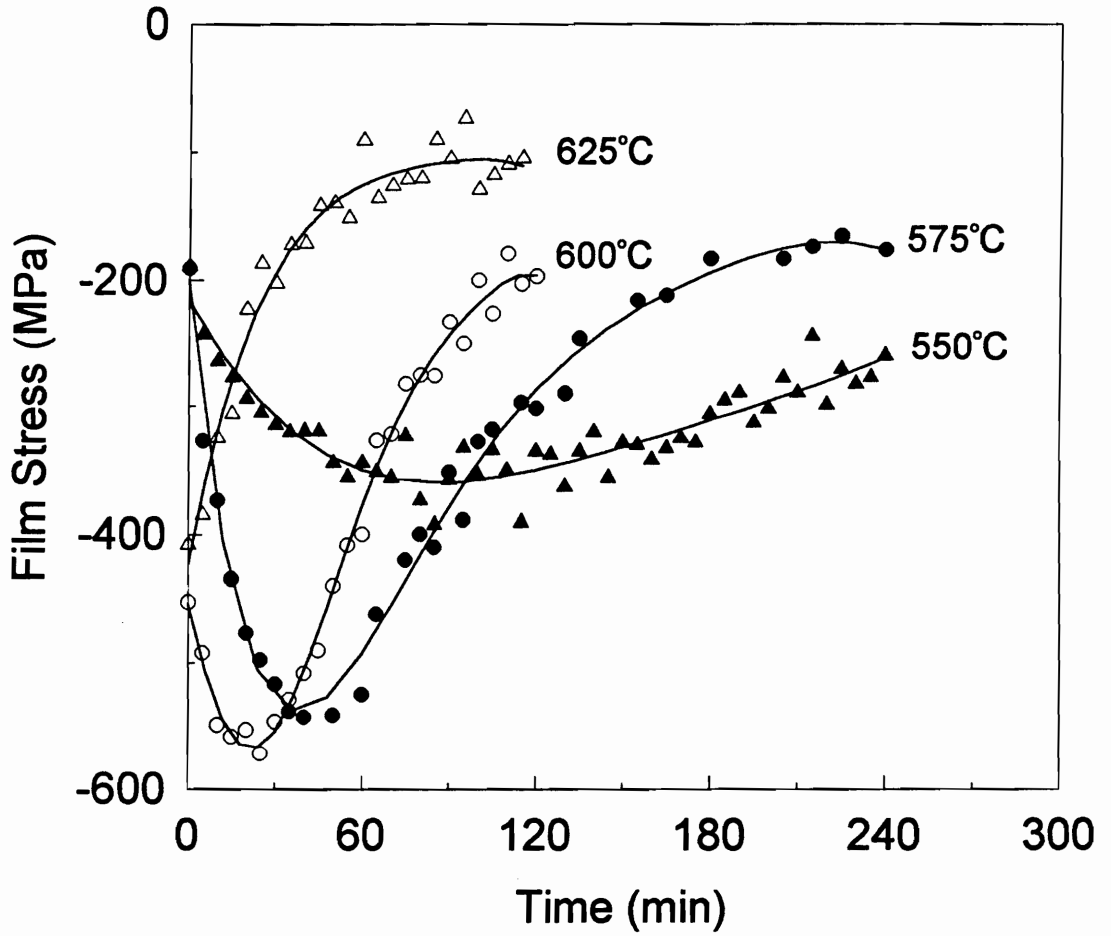

Fig. 3 Experimental stress-time plots for $PbTiO_3$ thin films.

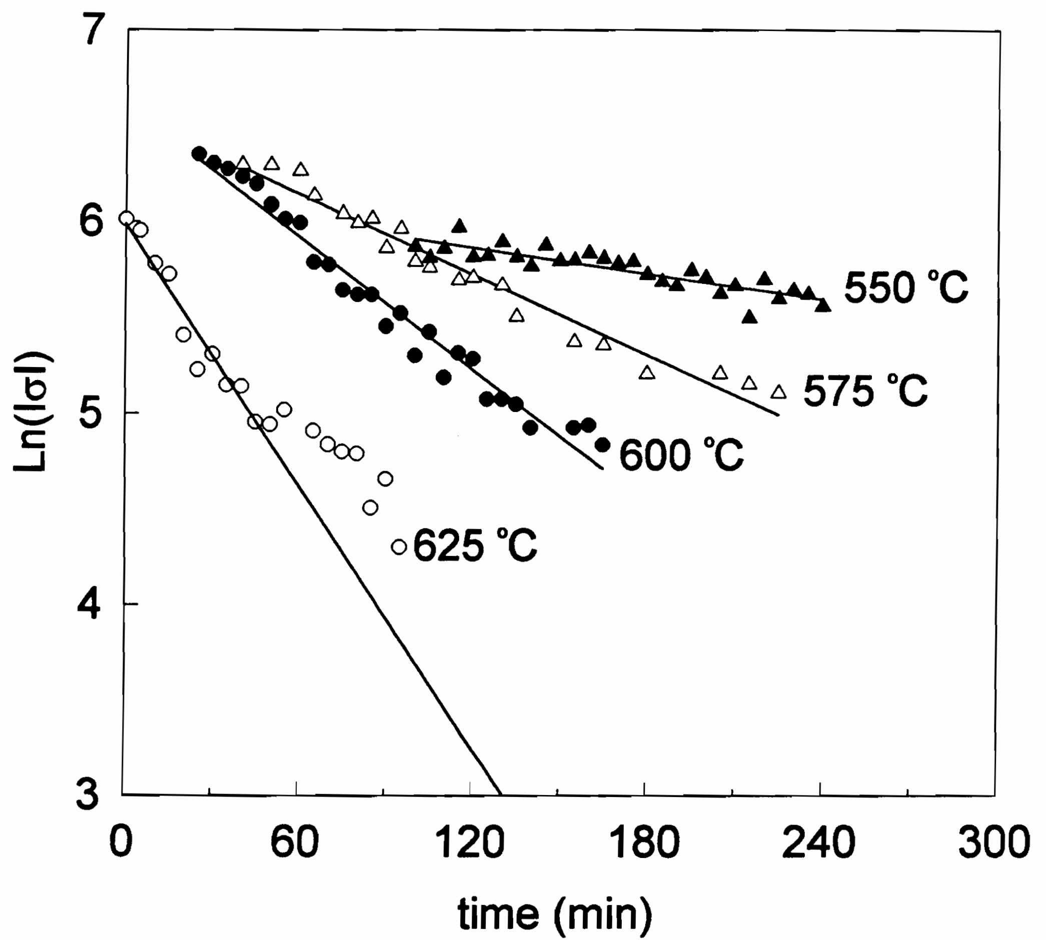

Fig. 4 Ln(lσl) as a function of time.

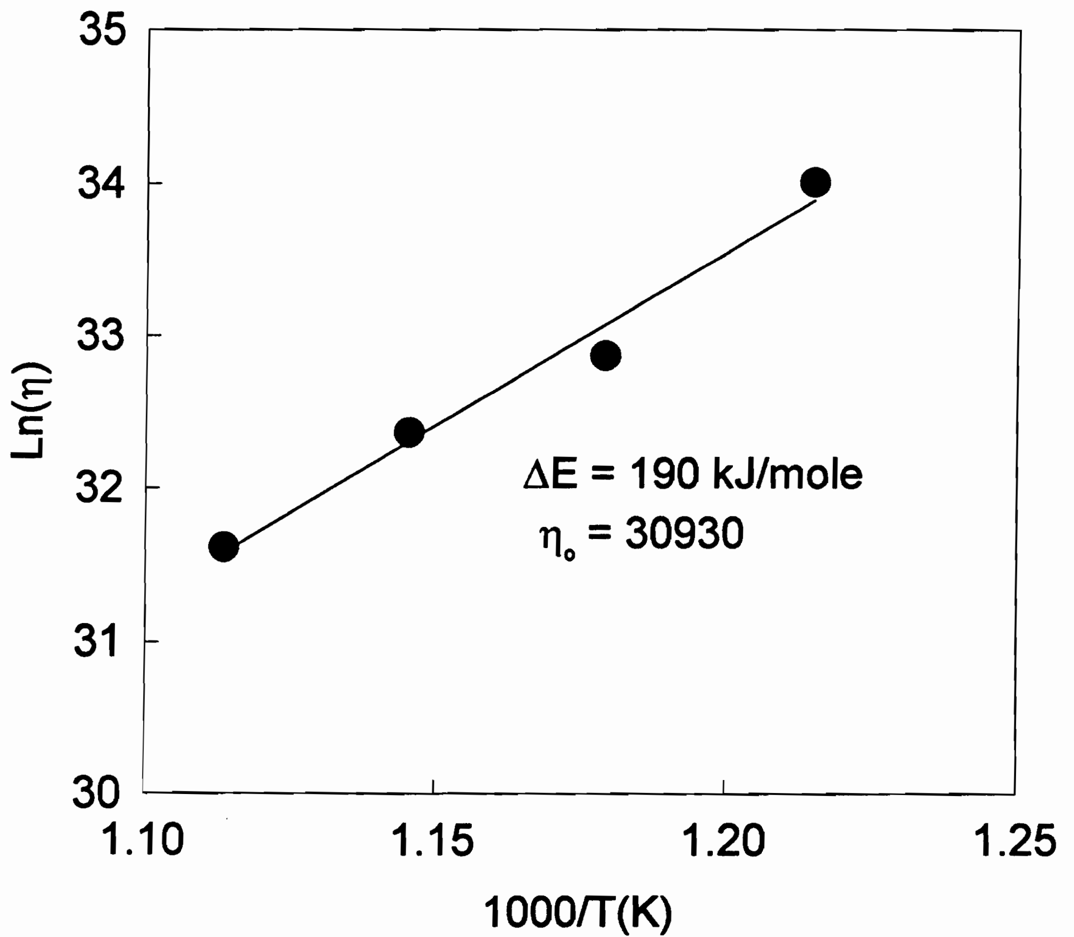

Fig. 5 The Arrhenius behavior of viscosity of $PbTiO_3$ films.

$$\eta = \eta_0 \exp(\Delta E/kT). \quad (4)$$

The activation energy of the stress relaxation can be estimated to be 190 kJ/mole. This value is 1.76 times greater than the activation energy for $PbTiO_3$ formation in which the mechanism was believed to be grain boundary diffusion.

3.5.1 Mechanism of Stress Relaxation

Although it has been accepted that mainly diffusional creep causes relaxation in thin films, in general, several concurrent processes are expected to contribute to the relaxation of a film. The mechanisms which dominate stress relaxation in thin films depend on the stress level, film thickness, and temperature [11]. If we assume the grains in thin films are circular disks, to a first approximation, with radius, r, and thickness, h. We have the following relationship between the surface area (including grain boundary and interface area) and volume:

$$S_V = \frac{1}{2} \frac{2\pi r \cdot h + 2\pi r^2}{\pi r^2 \cdot h} = \frac{1}{r} + \frac{1}{h} = \frac{2}{d} + \frac{1}{h} \quad (5)$$

where d is the average grain diameter, i.e. average grain size. The factor 1/2 was introduced in the expression above because each surface is shared between two grains. From the dimension of film thickness and average grain size, we can have the following relationships,

$$S_V = 1/h, \; d >> h,$$

$$S_V = 3/h \text{ or } 3/d,\ d \simeq h,$$

$$S_V = 2/d,\ d << h.$$

It is believed that predominant mechanism is lattice diffusion when $d >> h$, whereas grain boundary diffusion when $d << h$. When $d \simeq h$, which is our case, it is likely that lattice diffusion dominates the mechanism of stress relaxation in the temperature range around 0.55Tm. However, we believe that grain boundary diffusion could be essential in the early stage of stress relaxation in which the grain size was still very small.

In the original formulation of Coble and Nabarro–Herring creep, atoms and vacancies are assumed to flow between neighboring grain boundaries subjected to different normal stress, when the film is loaded in a nonbiaxial fashion, For an equibiaxially compressed film as shown in Fig. 6, the atoms should flow between the grain boundaries and the free surface rather than between neighboring boundaries. However, possible paths along which atoms can diffuse to relax stresses are the grain boundaries and the grains.

3.5.2 Stress Relaxation by Diffusional Creep Mechanism

Diffusional creep or Nabarro–Herring creep occurs by the movement of point defects (usually vacancies) under a concentration gradient generated by the applied stress [12]. In thin films under biaxial stress this concentration gradient is present

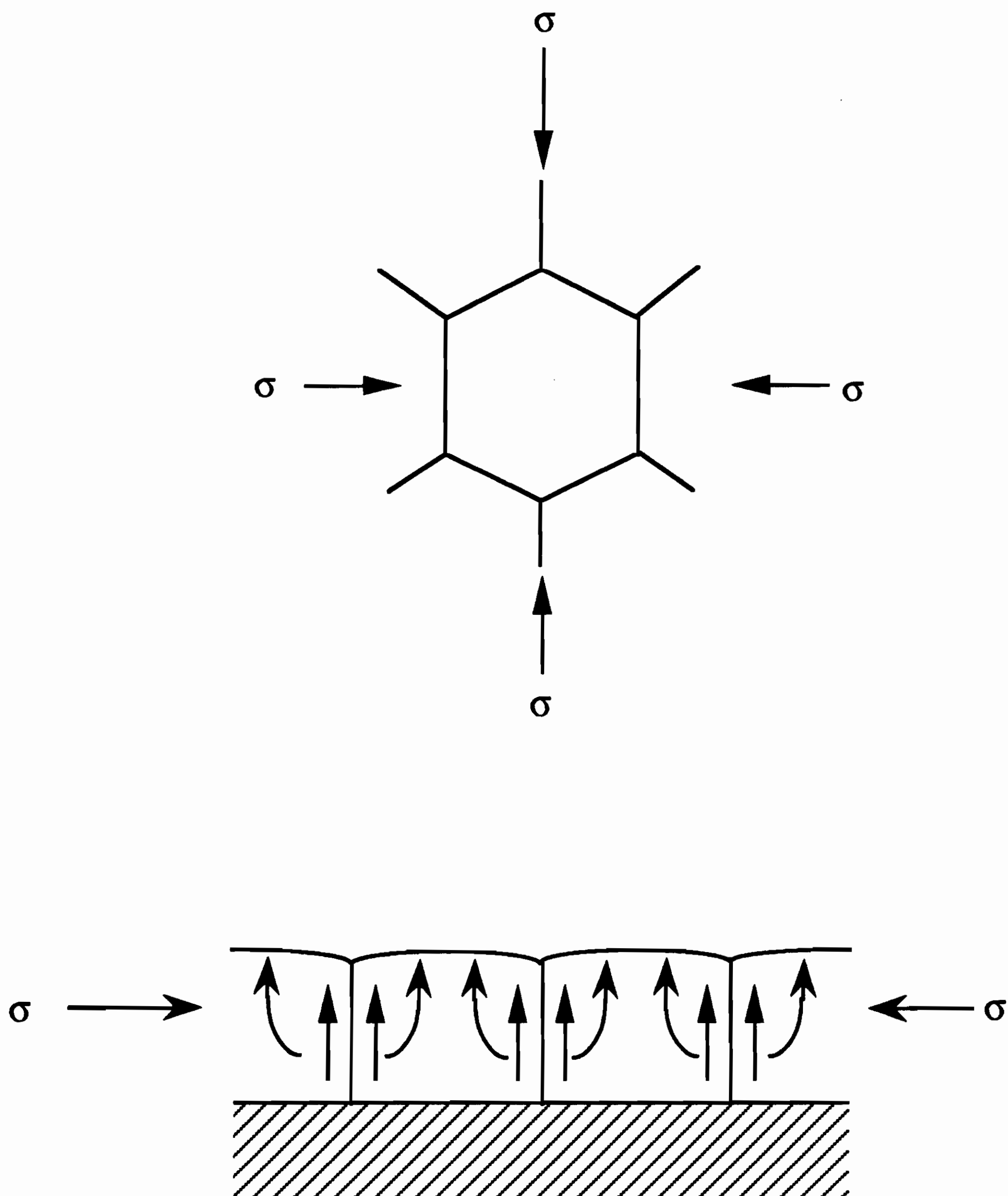

Fig. 6 Schematic illustrations of possible paths along which atoms diffuse to relax stresses.

between grain boundaries parallel and perpendicular to the direction of film stresses. The simplified analysis of diffusional creep in thin films under uniaxial stress has been previously carried out. The viscous flow model was successfully employed to interpret the annealing kinetics of the films. The viscous flow model has been widely used in the stress relaxation of metallic glass [13]. In a crystal, assumed that lattice diffusion dominated stress relaxation in $PbTiO_3$ thin films, viscous flow also occurs through the movement of vacancies. This is Nabarro–Herring creep, in which the viscosity is given by

$$\eta = \frac{kTd^2}{4\Omega D_l} \tag{6}$$

where Ω is the atomic volume, d is the average grain size, k is the Boltzmann constant, η is the viscosity, T is the absolute temperature, and D_l is the lattice diffusion constant. The viscosity can be derived from Fig. 5 as η = 30930exp(–190,000/kT). Since the mechanisms are the same both for lattice diffusion and for viscous flow, lattice diffusion constants could be deduced as $D_l = D_{lo}\exp(-190{,}000/kT)$, where D_{lo} is the pre–exponential factor. Equation (6) can be used to correlate the viscosity and lattice diffusion constant of $PbTiO_3$ films with their grain size. Taking $\Omega = 12.6 \times 10^{-24} cm^3$, the average grain size, d, of $PbTiO_3$ films was measured to be 0.2μ for the $PbTiO_3$ film annealed at 600°C and D_{lo} was calculated to be approximately 3×10^{-5}. This value is two order of magnitude greater than the pre–exponential factor for the grain boundary diffusion constant as shown previously. It is found that this magnitude of difference is comparable to that for alloys [14]. From this analysis, the estimation of lattice diffusion through vacancies was calculated as

$$D_l = 3x10^{-5}\exp(-190{,}000/kT)\ cm^2/sec. \qquad (7)$$

3.5.3 Estimation of Relaxation Time

During annealing film morphology such as grain size can grow with time, therefore vacancy flow or ionic flow can predominantly take different paths for different regimes of relaxation. It is difficult to precisely evaluate the relative contributions of diffusional flow by lattice diffusion and grain boundary diffusion in predicting kinetic behavior of stress relaxation. The present experimental observations and previous discussions suggest that both processes probably contribute to stress relaxation in the $PbTiO_3$ films.

Assuming that the sum of the elastic (ϵ_e) and plastic (ϵ_p) strains remain constant and that film stresses, as observed in the stress–time plots in Fig. 3, cease to relax when the stress–time plots are leveling off, it can be shown that, for diffusional creep [15] (when $\epsilon_p = K\sigma$, where K is a factor characteristic of different creep mechanism), the time, t, required for essentially complete stress relaxation is given by the relation

$$t = \frac{\beta(1 - \nu)}{KE}, \qquad (8)$$

where $\beta = 2.3$, ν is the Poisson's ratio, and E is the Young's modulus. If grain boundaries act as vacancy sinks and grain growth is due to diffusional creep with lattice diffusion predominating [15, 16],

$$K \simeq 10\left(\frac{D_l}{dh}\right)\left(\frac{\Omega}{kT}\right), \qquad (9)$$

where D_l is lattice diffusion constant, Ω is atomic volume, h is film thickness, d is the average grain size, k is the Boltzmann constant, and T is absolute temperature. Taking $D_l = 3 \times 10^{-5} \exp(-190{,}000/kT)$, $d = 0.2 \times 10^{-4}$cm, $\Omega = 12.6 \times 10^{-24}$cm^3, $\nu = 0.2$, and $E = 13.1 \times 10^{11}$ dyne/cm^2, the time, t_v, required for complete stress relaxation is calculated and listed in Table I. For comparison, the time constants, τ $(= \eta/E)$, required for the initial film stress to fall to 1/e of its initial value were also calculated and listed in Table I. The calculated times of relaxation agree with the experimentally observed values. For instance, at 625°C, the stress–time curve started leveling off when the annealing time reached 50 minutes, as shown in Fig. 3. For the other temperatures the data are also in excellent agreement with the experimental value. It follows that diffusional flow of vacancy by lattice diffusion is the mechanism for stress relaxation in $PbTiO_3$ films.

One may argue that stress relaxation is likely dominated by grain boundary diffusion only. If this is the case, K would be given by

$$K \simeq 10\left(\frac{D_{gb}a}{dh^2}\right)\left(\frac{\Omega}{kT}\right) \qquad (10)$$

where a is grain boundary width and D_{gb} is given by $3 \times 10^{-7} \exp(-108{,}000/kT)$ [17]. t_{gb}'s could be calculated and listed in Table I. It was found that t_{gb} is smaller than the experimental values and even smaller than τ. This indicated that stress relaxation was not likely dominated by grain boundary diffusion. It was also found that t_{gb} is approximately two order smaller than t_v for Pb [18] and Cu [11] thin

Table I: The Time Required For Complete Stress Relaxation of $PbTiO_3$ films.

Temp.($^\circ$C)	625	600	575	550
t_v (min.)	52	104	219	482
t_{gb} (min.)	53	78	117	181
τ (min.)	41	87	144	446

films, when the temperature is around 0.5Tm. From this, we can realize that the grain boundary diffusion obtained from formation kinetics may not be used as that for stress relaxation.

Since $PbTiO_3$ thin films were exposed to elevated temperatures, they displayed a number of interesting time-dependent deformation processes characterized by the thermally activated motion of ions and defects. As a result, changes in the film morphology occurred and stress levels reduced.

3.5.4 Morphology Development During Stress Relaxation

Fig. 7 depicts the effects of grain orientation and mean grain size on film stresses. Several points were selected from the stress-time plots (Fig. 7a) and their microstructures were examined. It was found that recrystallization in films played a major role in stress relaxation. Recrystallization concurrent with deformation is believed to occur by two different mechanisms which result in rather different microstructures. The first mechanism is identified by the rotation of the misorientation of the small grains or sub-cell microstructure, and eventually the sub-boundaries are indistinguishable from high angle grain boundaries. This mechanism could account for the change of the I_{100}:I_{001} ratio associated with film stress levels (Fig. 7b). The second mechanism is characterized by the migration of pre-existing high angle grain boundaries, i.e. grain growth. This mechanism could contribute to the reduction of stress levels as well (Fig. 7c). Fig. 8 shows a typical microstructure of $PbTiO_3$ films annealed at 625°C for 30 minutes. From Fig. 8, it

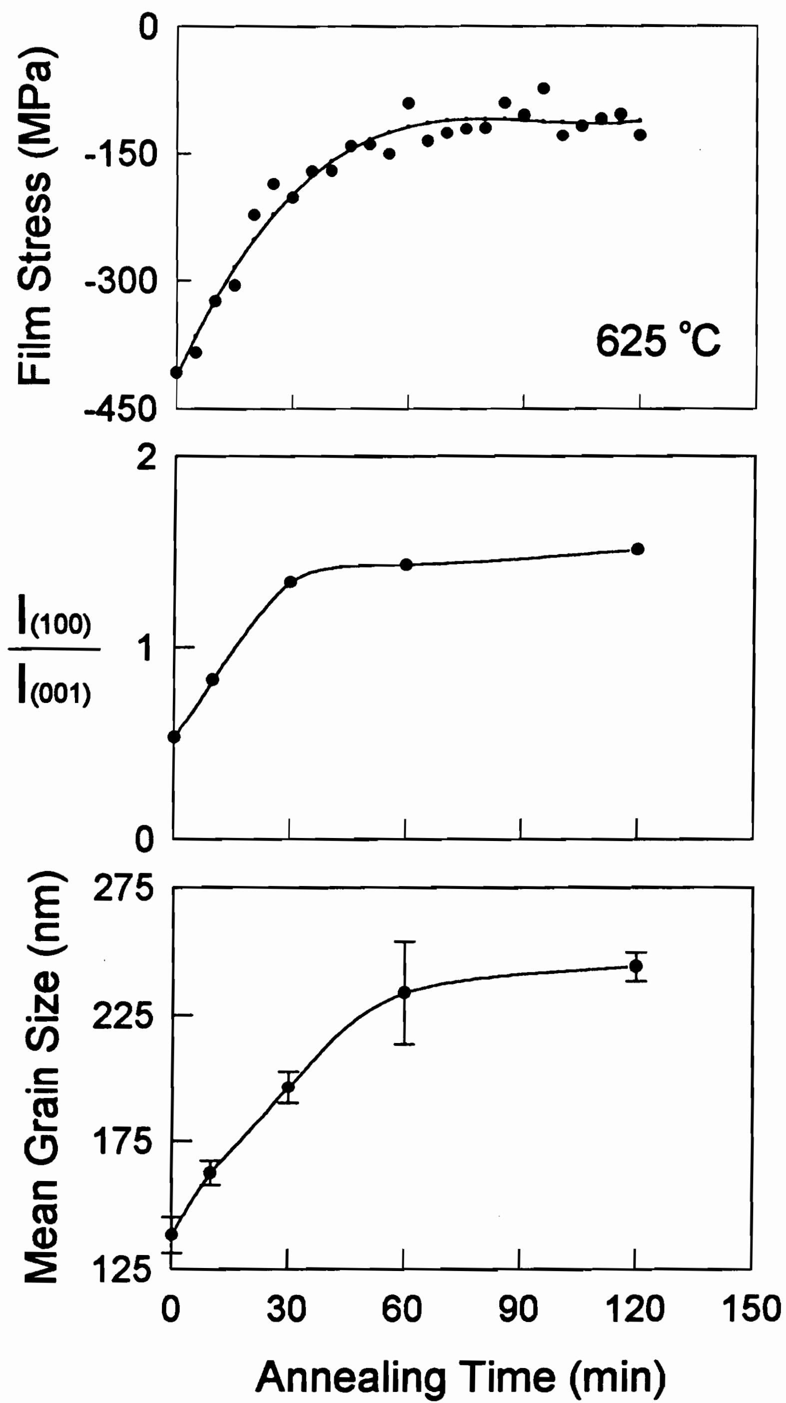

Fig. 7 Effects of both orientation and grain size on film stress.

is clear that grain growth took place by consuming smaller grains. Since reorientation of small grains is a part of the grain growth process, grain growth can be considered to be the predominating mechanism.

3.5.5 Hillock Formation by Grain Boundary Sliding

From previous discussion, it is understood that lattice diffusion is the dominant role in stress relaxation. However, from morphological observations we believe that grain boundary is of great importance in the early stage of stress relaxation. Fig. 9 illustrates hillock formation in $PbTiO_3$ thin films annealed at 600°C for 30 minutes. Hillocks were also found in the films annealed at other temperatures. It is noticed that the number density of hillocks remained relatively constant as the anneal time increased. This behavior suggested that hillocks only formed in the beginning of relaxation at which the grain size was still very small. At this stage, vacancy diffusion mainly via grain boundaries could cause grain boundary sliding (as shown in Fig. 10) which usually happens at grain boundary junctions [19]. For some instance it is possible for a grain to be squeezed and to form a protrusion in the films. As relaxation proceeded, the grain size increased, the effect of grain boundary sliding diminished, and lattice diffusion mechanism conquered.

Hillock formation has been found in some other thin film systems such as lead [20], gold [21], copper [22], tin [23], silver [24], aluminum [25], and $TiSi_2$ [26]. Hillocks were caused by localized surface growth at high temperature which resulted from the compressive stress in the films [12]. One can sometimes see [25] a groove

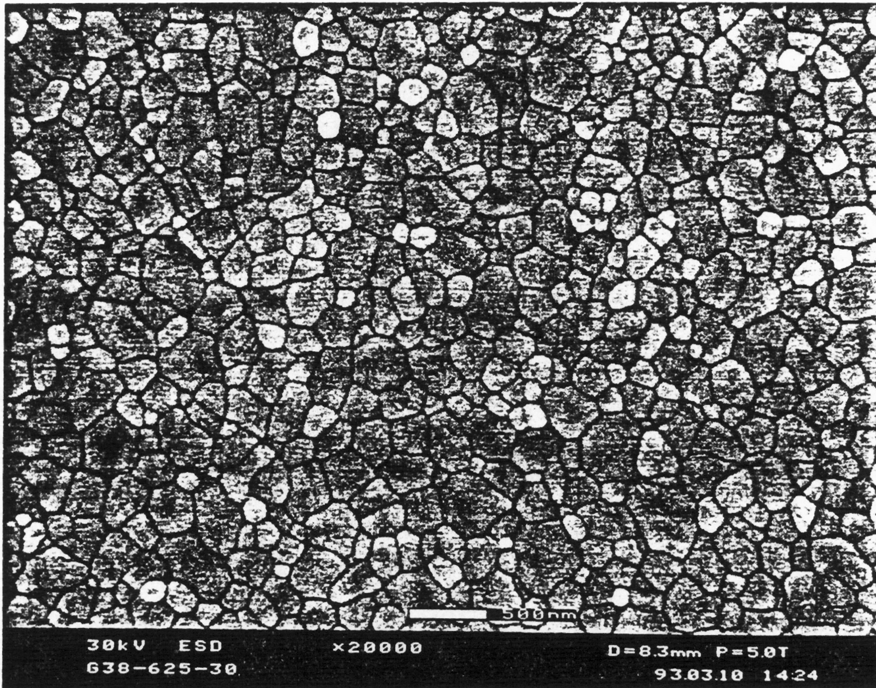

Fig. 8 SEM microstructure of a $PbTiO_3$ film annealed at 625°C for 30 minutes.

Fig. 9 Hillock formation in a $PbTiO_3$ film annealed at 600°C for 30 minutes.

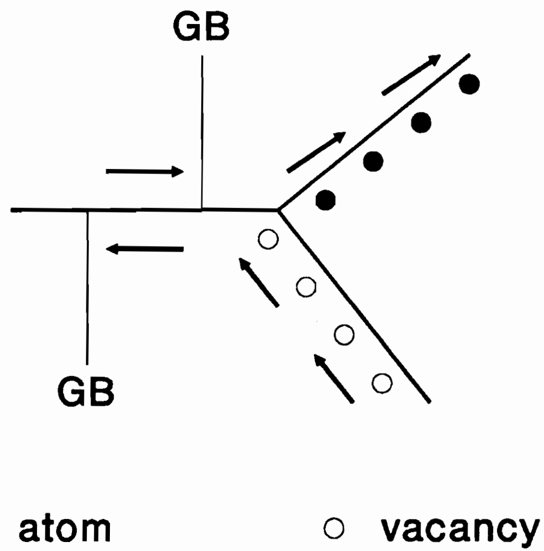

Fig. 10 Grain boundary sliding by diffusion along grain boundaries around the triple edge.

surrounding a hillock in Al films which formed during cooling. However, this phenomenon was not significant in $PbTiO_3$ films. Hillocks may result not only from uniformly distributed strains but also from localized electro–migration effects [27].

3.6 Summary

Stress relaxation in $PbTiO_3$ films was investigated by the in–situ stress measurement technique. A simple viscous flow model was successfully employed to interpret the behavior of stress relaxation in the $PbTiO_3$ thin films. Using this model the estimation of the effective viscosity (η) of $PbTiO_3$ films was made possible. The activation energy responsible for stress relaxation was estimated to be 190 KJ/mole. The relaxation of film stresses was dominated by the lattice diffusion through vacancy movement.

In order to microscopically understand stress relaxation in the $PbTiO_3$ thin films, the Nabarro–Herring creep model was employed to correlate the viscosity (η), lattice diffusion coefficient (D_l), and grain size of the films. From this Nabarro–Herring model the lattice diffusion coefficient of the vacancy motion was estimated to be $3x10^{-5}exp(-190,000/kT)$. Using these data the time required for complete relaxation of the $PbTiO_3$ thin films was calculated and compared with the experimental values. It was found the experimental values, observed from stress–time plots, matched very well with the calculated values. Therefore, it follows that this stress relaxation process is dominated by the lattice diffusion of the vacancies. Hillock formation caused by grain boundary sliding could partially relax

the film stress in its early stage. Thereafter, grain growth resulted from lattice diffusion mainly accounted for the stress relaxation.

3.7 References

1. V. M. Koleshko and V. F. Belitsky, Massoperenosv Tonkikh Plenkakh, Naukai Teknika, Minsk, 1980.

2. V. M. Koleshko and V. F. Belitsky and I. V. Kiryushin, Thin Solid Films, 142, 199 (1986).

3. P. Chaudhari, IBM J. Res. Dev., 13, 197 (1969).

4. C. A. Apblett and P. J. Ficalora, Materials Research Society Symposium Proceeding, Vol. 239, 99 (1992).

5. P. Gas, V. Deline, F. M. d'Heurle, A. Michel, and G. Scilla, J. Appl. Phys. 60, 163 (1986)

6. P. M. Valov, J. Solid State Chem., 1, 215 (1970).

7. D. S. Herman, M. A. Schuster and R. M. Gerber, J. Vac. Sci. Technol., 9, 515 (1972).

8. J. R. Lloyd and S. Nakahara, J. Electrochem. Soc.,125, 2037 (1978).

9. Y. Oishi and K. Ando, J. Chem. Phys., 63, 376 (1975).

10. S. Ikegami, I. Ueda, and T. Nagata, J. Acoust. Soc. Am., 50, 1060 (1971)

11. H. J. Frost and M. F. Ashby, "Deformation–Mechanism Maps," Pergamon Press, 1982

12. M. F. Doerner and W. D. Nix, CRC Critical Reviews in Solid State and Materials Sciences, 14(3), 225 (1988)

13. A. H. Cottrel, "The Mechanical Properties of Matter," Wiley, New York, 1964

14. R. E. Reed–Hill, "Physical Metallurgy Principles," 3rd ed., PWS–KENT, Boston, MA, 1991

15 J. Weertman, Trans. Amer. Soc. Metals, 61, 681 (1968)

Chapter 4

A NOVEL TECHNIQUE FOR INVESTIGATING MULTICOMPONENT OXIDE FILMS: III: EFFECTS OF ION BOMBARDMENT

4.1 Abstract

For the first time, the effects of ion bombardment on multicomponent oxides, such as $PbTiO_3$, and multilayer systems were extensively studied by in–situ stress measurement technique. Energetic ion bombardment has been found to accelerate $PbTiO_3$ formation. Both annealing temperature and time needed for completion of reaction were reduced. Whereas, the apparent activation energy responsible for stress relaxation was 310 kJ/mole for IAD films, which is 120 kJ/mole higher than that for non–IAD films. This was attributed to stress reduction in $PbTiO_3$ thin films resulting from ion bombardment. In addition, effects of ion bombardment on the stress of as–deposited multilayers, on the stress development in multilayer during annealing, and on the structure–property–processing interrelationships were also investigated.

4.2 Introduction

Effects of ion bombardment on simple (one or two element system) and single layer thin film systems have been reviewed and well documented [1]. Examples of these effects include grain size [2], preferred crystalline orientation [3], increased (or

decreased) packing density [4], lattice expansion and contraction [5], surface topological effects [5], enhanced surface or bulk diffusion [6], nucleation density [7] in the early stages of film growth and other related effects such as film stoichiometry [8] and the modification of thin film stresses [9]. However, ion beam effects in multicomponent oxides and/or multilayers have not been studied and this has been the major concern of this study.

Recently we have successfully formed multicomponent oxide, such as $PbTiO_3$, thin films using PbO/TiO_2 multilayer approach [10]. The formation of the $PbTiO_3$ phase has been studied using an in–situ method by monitoring changes of stresses in the multilayers [11]. The formation kinetics and stress relaxation of the $PbTiO_3$ films have been documented [12].

In this paper, we will study the effects of ion bombardment on the formation kinetics and stress relaxation of $PbTiO_3$ films. In addition, we will also discuss the effects of ion bombardment on the initial stress of as–deposited multilayers, the stress development of the multilayers during annealing, and the structure–property–processing relationships.

4.3 Basics of IAD

Ion–assisted deposition (IAD) is a deposition process, as shown in Fig. 1, in which a growing film produced from an evaporation source (usually electron beam) is bombarded by an ion beam produced by a low–energy (50 eV – 1 keV) ion source. IAD also offers independent control over fluxes of ions and evaporated atoms, ion

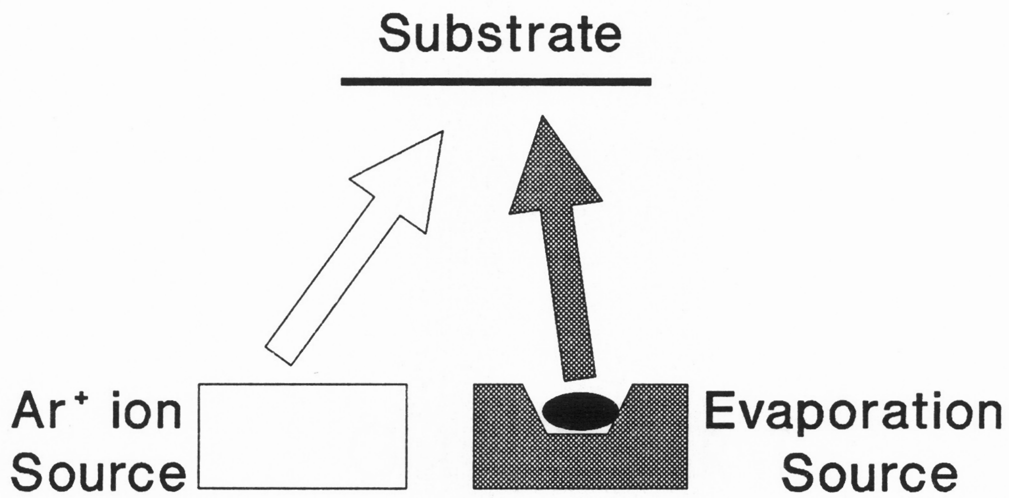

Fig. 1 Schematic of IAD deposition.

energy, nature of ion species and their charge state, and incident direction (and divergence), background pressure, and composition, and if necessary the substrate temperature.

For this low energy range in IAD, four most important physical processes have been identified [13] : (1) desorption or sputtering of impurities from the substrate surface by ion impact, (2) penetration and entrapment of coating and support gas in the growing film, (3) sputtering of the substrate and eventually the coating as film growth progresses, and (4) The generation of defects in the substrate and growing film. In addition, the energetic bombardment can also enhance the migration of the deposited atoms along the substrate surface. Furthermore, ion of low energies may influence film nucleation and growth and enhance chemical reactivity.

Using IAD to deposit multilayers, several phenomena can be expected such as entrapment of the incident ions, e.g. argon, in the multilayer, densification of the individual layers, implantation and intermixing between film and substrate and between film and film, and creation of activated centers for nucleus formation of $PbTiO_3$ phase. Accordingly, the multilayers are never in true thermodynamic equilibrium, therefore, kinetics of film growth can be altered and in turn can dramatically affect the properties of the growing film. In this study, we only concentrate on the property of thin film stress.

In general, compressive stress were found when the growing film was bombarded by atoms or ions with energies of tens or hundreds of electronnvolts by a mechanism known as "ion peening" [9]. The energetic ions or atoms are forced into

preciously unoccupied interstitial sites owing to their high kinetic energy of as a result of impacting with other high–velocity particles [14] and this leads to an expansion of the film outward from the substrate. However the film is not free to expand in the plane of the film and, therefore, the entrapped atoms and/or ions cause macroscopic compressive stress.

4.4 Experimental Procedure

4.4.1 System

The experimental arrangement for ion–assisted deposition system was discussed in detail in a previous study [10]. A conventional cryopumped electron beam evaporation system was modified by the addition of a 3–cm broad beam Kaufman ion gun with dual defocused graphite grid optics. The gun was used to provide a beam of low–energy (30–1500 eV) Ar^+ ions incident on the substrate surface at an angle of 30° from substrate normal. 2–inch sapphire substrates with [1102] direction were placed 34 cm above the electron beam evaporation source.

The substrates were cleaned by a series of organic solutions and deionized water followed by drying in N_2 gas. Prior to deposition, the substrates were further cleaned by low energy ion bombardment for 2 minutes. High purity, vapor deposition grade oxides (99.999% PbO and 99.995% TiO) were used as the evaporation sources. The oxides were conditioned prior to evaporation to prevent from splattering.

4.4.2 Preparation

Prior to deposition, the system was pumped down to $4x10^{-7}$ Torr, rising to approximately 10^{-6} Torr for conventional evaporation operation. The chamber pressure was brought up to $8x10^{-5}$ Torr by introducing high purity (99.999%) Ar gas for ion–assisted deposition operation. All the deposition were performed at ambient substrate temperature. The deposition rate of both oxides were kept constant at 0.3 nm/sec for TiO and 0.5 nm/sec for PbO, for which the molecules of both oxides could have the same arrival rate onto the substrate. Total film thickness was kept constant at 300 nm, 100 nm for TiO layer and 200nm for PbO layer, in which the loss of PbO layer was taken into account. The deposition scheme was shown in Fig. 2, in which the number of ions and atoms arriving on the substrate are plotted as functions of the processing time. The substrate was subjected to sputtering cleaning for two minutes by the bombardment of 600 eV ion beams. Then the beam energy was turned down to designated energy and deposition started. Oxide multilayer was deposited under the concurrent bombardment of Ar^{+} ion irradiation with several different ion beam energy (100, 200, and 300 eV) and ion flux density ranging from 30 to 160 $\mu A/cm^2$.

4.4.3 Characterization

Film stress measurements as functions of temperature (550° to 600°C) and time (120 to 240 minutes) were performed for the PbO/TiO oxide multilayers. The heating rate was 5 °C/min. The value of film stresses was characterized by the curvature method. The in–situ stress measurement technique was developed and

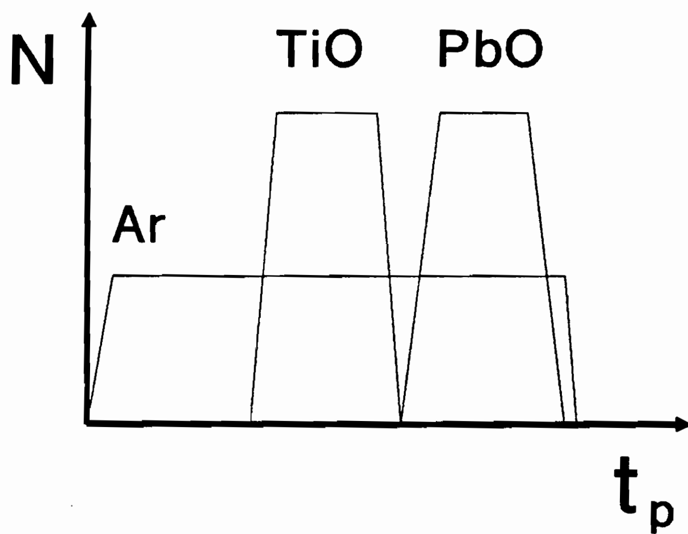

N : number of ions and atoms arriving at the target
t_p : process time

Fig. 2 Sequence of multilayer deposition.

was thoroughly described in our companion paper [12]. Selected as–deposited films were also subjected to post–deposition annealing in a conventional box furnace using the same annealing profile. The development of $PbTiO_3$ phase and texture in the films was identified by x–ray diffraction analysis. The evolution of film morphology, such as grain size, was examined by scanning electron microscopy.

4.5 Results and Discussion

4.5.1 Effect of ion bombardment on stress of as–deposited multilayers

Fig. 3 shows the effect of ion bombardment on the stress of as–deposited TiO/PbO multilayers as a function of ion flux density for ion energy of 300 eV. Since the multilayer was prepared at ambient temperature, the observed film stress was the intrinsic stress. It was found that the intrinsic stress decreased with increasing ion flux density. In another words, compressive stress were developed when the growing multilayer was bombarded by the energetic ions. The argon ions and depositing atoms were forced into previously unoccupied interstitial sites owing to their high kinetic energy or as a result of impacting with other high–velocity paricles [14]. It is also likely that the generation of compressive stress was partially attributed to the incorporation of the incident Ar^+ ions in the growing films.

It was also found that the film stress in the as–deposited multilayer approached to a constant value when the ion flux density was above 100 $\mu A/cm^2$. This implied that as the ion flux density reached a certain critical value, film stress

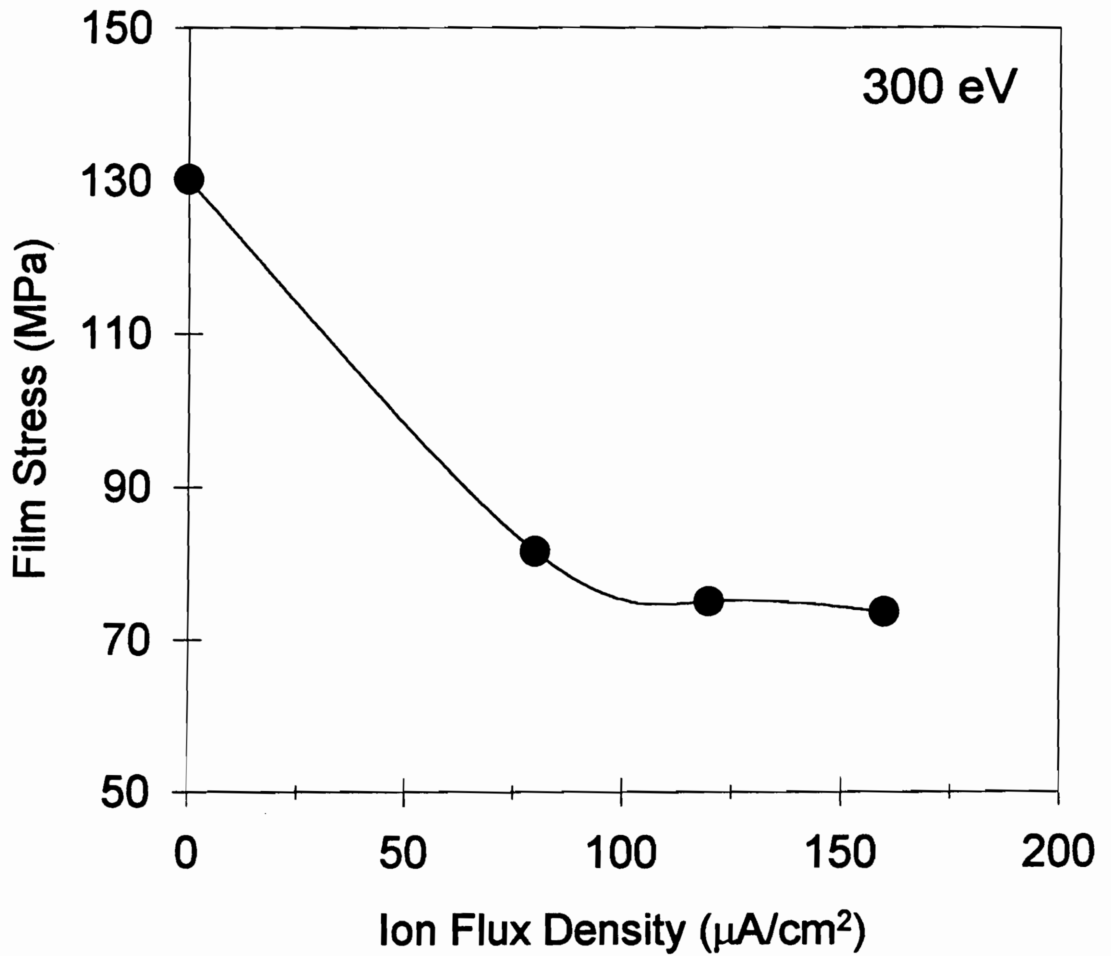

Fig. 3 Film stress of as-deposited multilayer as a function of ion flux density.

could not be further changed. Similar stress behavior as in Fig. 3 was also found in the IAD–deposited chromium films [15]. For chromium films, the critical ratio value indicated the condition at which film stress changed from tensile to compressive. However, compressive stresses were never found in the as–deposited TiO/PbO multilayers in this study.

It is believed that changes in IAD thin films can be not only related to ion flux density, but also related to ion energy. Fig. 4a shows the effect of ion bombardment on the film stress as a function of normalized ion beam energy in eV/atom, which is simply the product of the relative ion/atom flux and the average ion energy. The normalized ion beam energy indicates the average kinetic energy carried by each individual deposited atoms. The tensile stress of the as–deposited multilayers initially decreaes and later slightly increased as the normalized ion beam energy increased. The minimum was found at normalized ion beam energy of approximately 6.6 eV. With increased normalized ion energy, the tensile stress slightly increased. Similar stress behavior as in Fig. 4a was also found in IAD–deposited copper films on silicon substrates. [16]

By comparing the stress of the IAD–deposited films with that of the evaporated films, the generated compressive film stress can be plotted as a function of normalized ion beam energy, as shown in Fig. 4b. The generated compressive stress showed a maximum at around 6.6 eV. Davis [17] considered a steady state in which film stress formation by knock–on implantation of film atoms is balanced by thermal spike excited migration of implanted atoms, and also showed film stress, σ, is proportional to

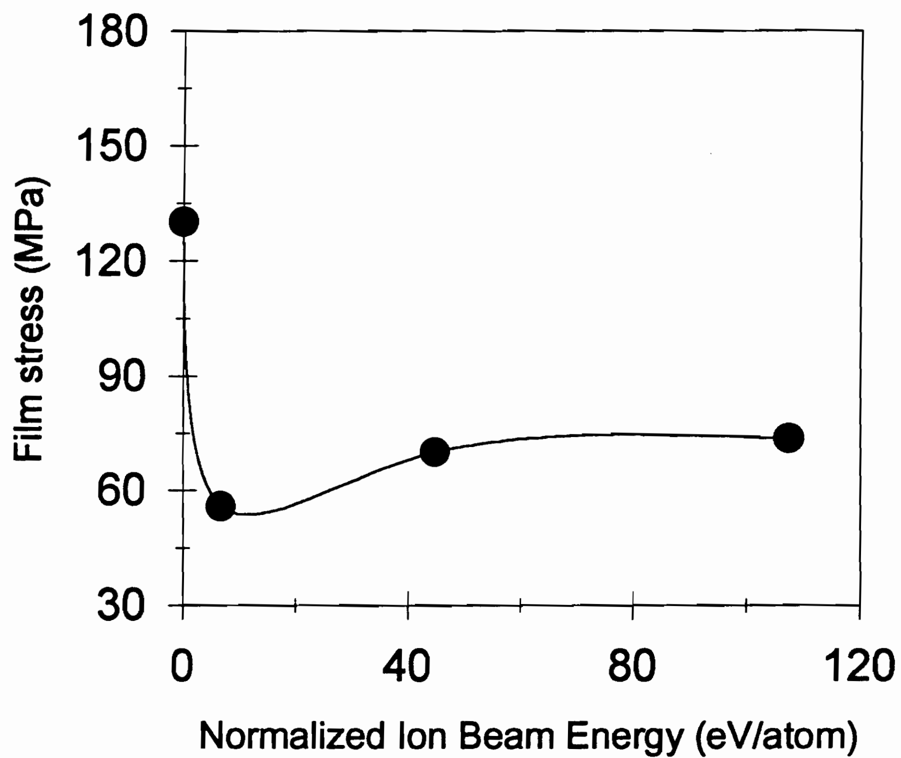

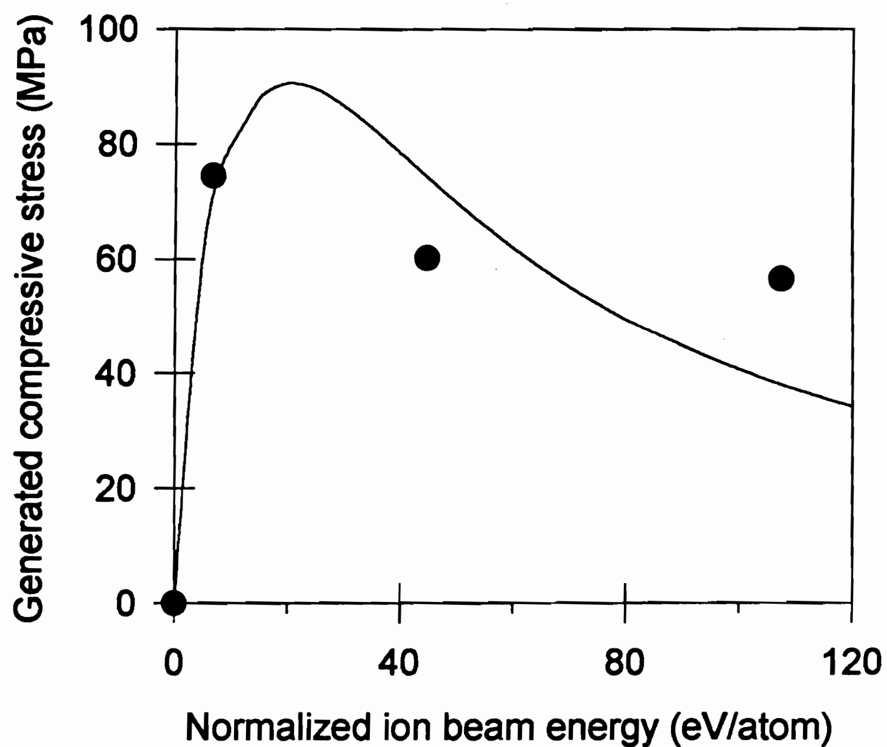

Fig. 4 Film stress of as-deposited multilayer as a function of normalized ion beam energy.

$$\frac{Y}{(1-\nu)} \frac{E^{1/2}}{M/I + kE^{5/3}} \qquad (1)$$

where E is the ion energy, M the net depositing flux, I the ion flux, $Y/(1-\nu)$ the biaxial modulus of the film, $k = 0.016\rho E_0^{-5/3}$, ρ is a material–dependent parameter which is of order 1, E_0 is the excitation energy of the film material.

Replacing E by E_n, the normalized ion beam energy, the generated compressive stress as shown in Fig. 4b can be curve fitted by the following equation

$$\sigma = \frac{Y}{(1-\nu)} \frac{c E_n^{1/2}}{a + bE_n^{5/3}} \qquad (2)$$

where $a = (M/I)^{1/2}$, $b = k(M/I)^{7/6}$, and c is a proportional constant. Assuming $E_0 = 4$ eV and $\rho = 1$ and take the average I/M ratio to be 0.4, the theoretical curve can be obtained and plotted in Fig. 4b.

Although the experimental data is limited, a relatively good fit was obtained. The behavior is similar to that obtained in literature [18]. The initial rapid rise and later reduction in stress at larger normalized ion beam energies are modeled. Davis [17] has explained that this phenomena is caused by a balance between knock–on implantation and thermal spike relaxation processes. At lower energy level, the implantation process was predominant and relaxation process was insignificant. Whereas, at higher energy level, the generated compressive stress was partially relaxed by the thermal spikes. The extent of relaxation was found to be dependent on the normalized ion beam energy level.

4.5.2 Effect of ion bombardment on stress development in multilayers

Fig. 5 depicts a typical stress–temperature plot for PbO/TiO multilayer on sapphire substrate which was subjected to annealing in air at 575 °C for 4 hours with a heating rate of 5 °C/min. This multilayer was deposited under concurrent Ar^+ ion bombardment with ion energy of 100 eV and ion flux density of 100 $\mu A/cm^2$. For better understanding, Fig. 5 was divided into four regions.

As the temperature increased, film stress did not change much as shown in region I'. Compressive film stress started building up while the curve entered region II' at around 200°C. The development of compressive stress was found to be faster when the curve entered region III' at around 340°C and reached a minimum at around 420°C, then tensile stress started to build up and reached a local maximum at around 500°C. The stress development in region II' and III' could be attributed to the oxidation of both oxide layers. The incorporation of oxygen into the multilayers from the atmosphere could result in increased film volume, generating compressive stress. In region II' the buildup of compressive stress was found to be less than that in region III'. This could be attributed to the compensation of the release of trapped argon atoms in the films. The process of releasing argon atoms observed in region II' was found to be through at around 340°C. This value was found to be close to 300°C for tungsten films [19], although it could depend on materials. Accordingly, for region III' only oxygen intake could dominate the oxidation process in the films. For region III' and IV', the stress–temperature curve entirely fell into the compressive state. Compressive stress continued developing in the films when the temperature was above around 500°C and reached a local

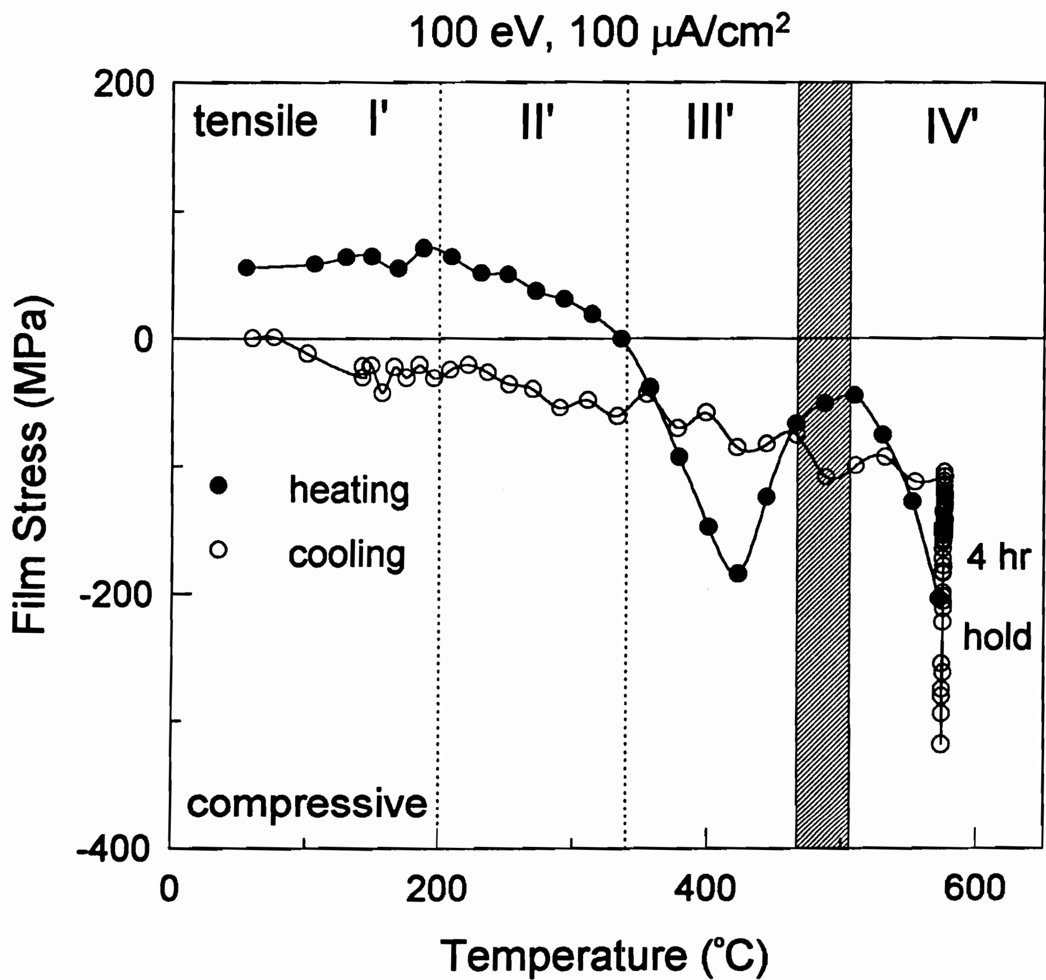

Fig. 5 Typical stress-temperature plot of an IAD-$PbTiO_3$ film annealed at 575°C for 4 hours.

minimum in the isothermal region, and then tensile stress started building up. Region IV was attributed to the formation of $PbTiO_3$ phase in the film and stress relaxation. The location of the boundary between region III' and IV' was uncertain, because of the existence of the intermixed layer between oxide layers. Therefore, it is uncertain where the formation of $PbTiO_3$ phase started in the stress–temperature plot.

Compared to electron beam evaporation, ion–assisted deposition process provides a much more complicated picture in multilayers. Oxide multilayer prepared by evaporation could form a sharp interface in between layers, as shown in Fig. 6a, and oxygen deficiency in each layer if decomposition occurs. In IAD process, with energetic particle bombardment during deposition, several phenomena could alter the nature of the multilayers: (1) sputtering and preferential sputtering which causes off–stoichiometry, such as oxygen deficiency in the films, (2) recoil and ion implantation which cause the intermixing between layers, as shown in Fig. 6b, and (3) ion trapping which causes the incorporation of impurity ions such as Ar in the films. The existence of the intermixed layer and therefore the uncertain boundary between region III' and IV' were caused by the second phenomenon.

For comparison, the data during heating stage was replotted with another plot [12] in which the multilayer was prepared without ion bombardment, as shown in Fig. 7. Fig. 7 displays the effect of ion bombardment on the stress development in multilayers. It can be seen that region II in Fig. 7(a) expanded toward lower temperature when the growing films was bombarded by energetic Ar^+ ions. Besides, region II also turned into region II' and III' due to the difference in the inflow of

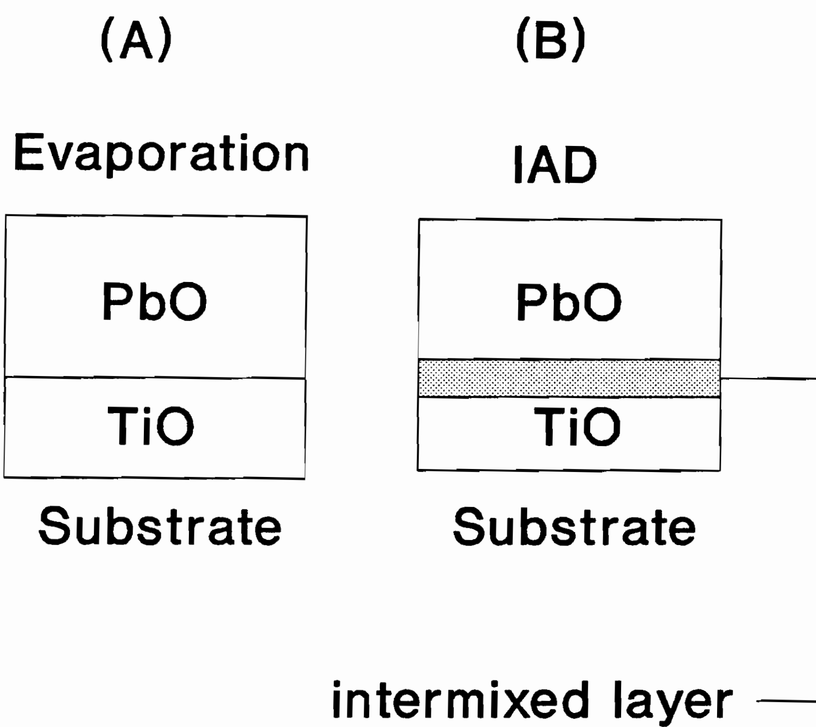

Fig. 6 Effect of ion bombardment on multilayer formation

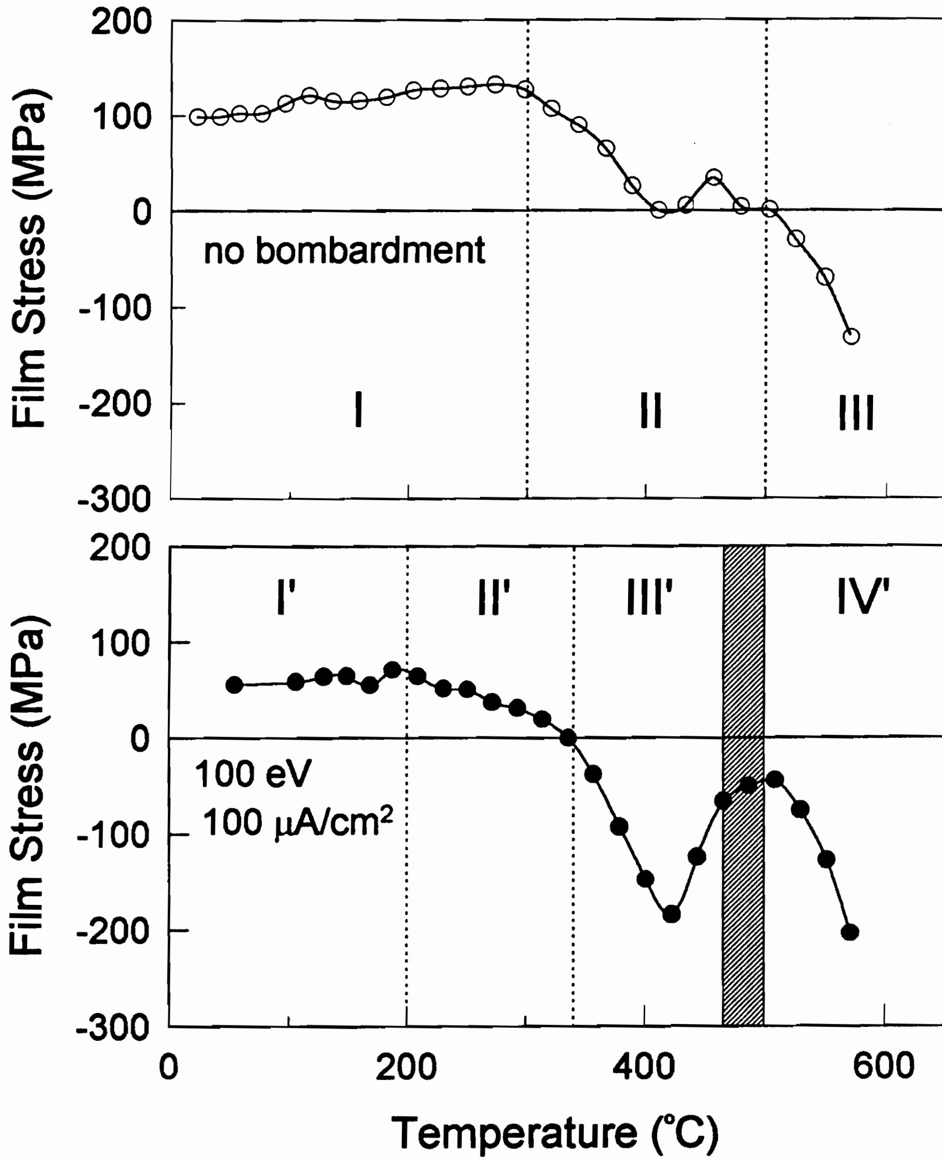

Fig. 7 Heating stage of the stress-temperature plots.

oxygen and outflow of argon atoms in the films. Although the release of argon atoms came to an end when the temperature entered region III', there is, however, likely some argon residue left in the films. This argument can be supported by the fact [19] in which residual argon atoms were always found in the IAD tungsten films even at substrate temperature as high as 750° C. The boundary between III' and IV' in Fig. 7(b) is not as certain as that between II and III in Fig. 7(a), because the thickness of the intermixed layer was not able to be accurately determined, which is believed to affect film stress as the temperature reaches approximately 500° C. The formation of $PbTiO_3$ layer might have occurred prior to 500° C.

Film stress during cooling showed good linearity against temperature only. Therefore thermal stress could be readily obtained. From the slope of the cooling region in Fig. 5, thermal expansion coefficients of $PbTiO_3$ films could be derived. It was found that the thermal expansion coefficient of $PbTiO_3$ films were dependent on the processing parameters such as ion energy and ion flux density. These phenomena will be discussed in a later section.

The isothermal region in region IV' for several different annealing temperatures was replotted in Fig. 8. It is clear that in Region IV' stress developments involve two kinetic process, $PbTiO_3$ formation and stress relaxation. There two processes will be individually reported in the following sections.

4.5.3 $PbTiO_3$ formation

The development of compressive stress in the early stage of the stress–time

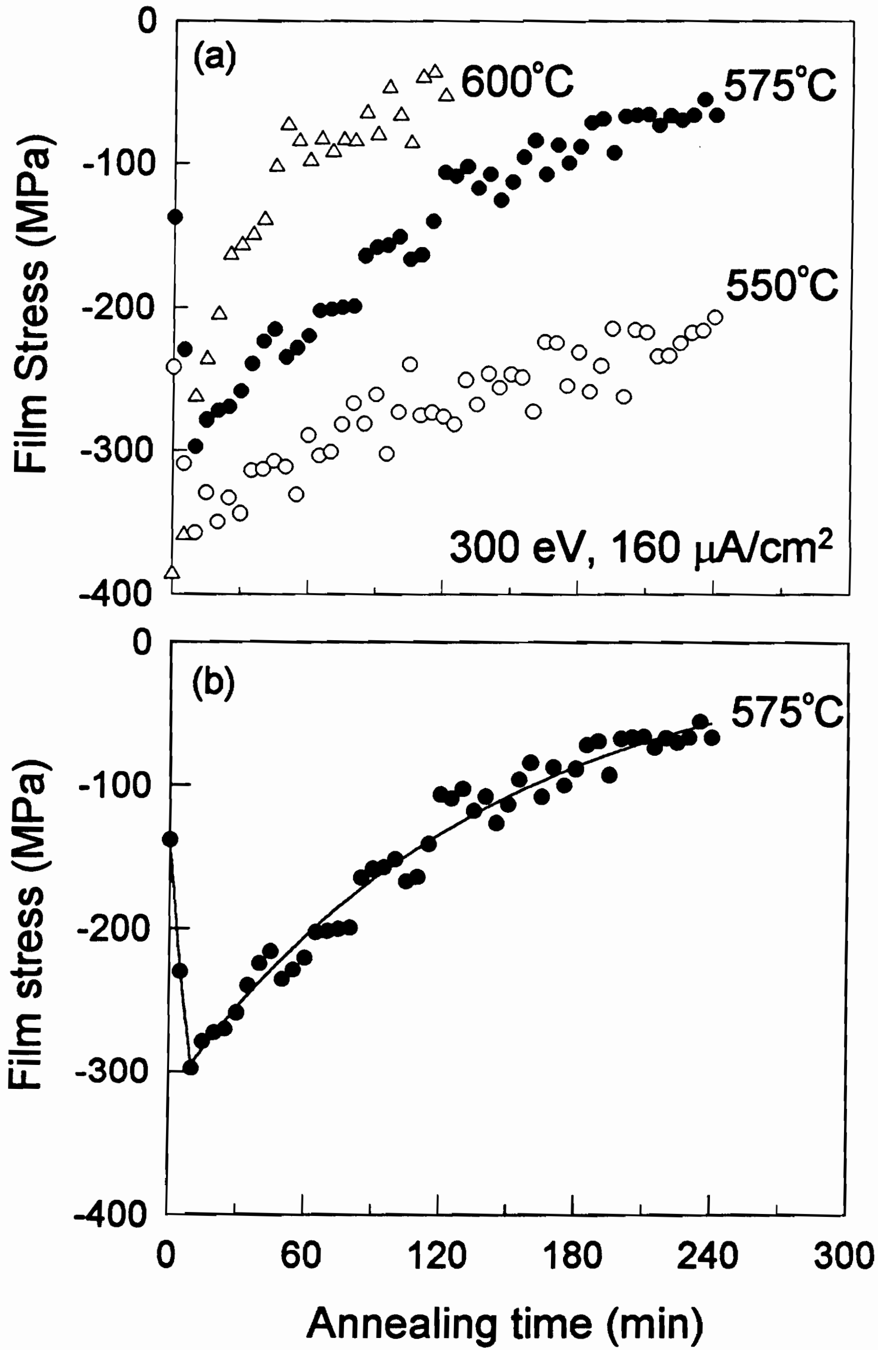

Fig. 8 Typical stress-time plots for $PbTiO_3$ films.

plots (Fig. 8) was attributed to the growth of the $PbTiO_3$ layer [12]. During the growth process, absorption of vacancies from a free surface by the product layer can bring about a compressive stress because of "swelling" of the deposit. As the growth process completed, film stress reached an extreme, that is the local minima in the plots as shown in Fig. 8. These phenomena was verified in our previous study [12] and also confirmed by x–ray diffraction analysis in this work. After the completion of $PbTiO_3$ formation, stress relaxation became the dominant role in stress development and also tensile stress was generated eventually.

The in–situ stress measurement technique has been successfully developed to characterize the kinetics of compound formation in multilayer when the reaction is relatively fast [12]. In the IAD–deposited thin film systems, the reaction between layers was found even faster and completed at lower temperature. For instance, using the same heating rate, 5°C/min, the $PbTiO_3$ formation completed at or before the temperature reached 600°C for IAD films, whereas 600°C and 20 minutes for non–IAD films [12]. For annealing temperature of 550°C, the reaction completed at around 20 minutes for IAD films, whereas approximately 100 minutes for non–IAD films [12]. Both the kinetics and activation energy responsible for the reaction are very difficult to determine, because of the uncertain boundary between region III' and IV' due to the existence of the intermixed layer. This boundary is of great importance in defining the initial stress value, σ_i, which indicates the start of reaction during annealing. Besides, the thickness of the intermixed layer not only can shift the location of σ_i, but also can change the value of σ_i.

Although the kinetics of reaction is hard to investigate for IAD films, the

effect of ion bombardment on $PbTiO_3$ formation can still be studied by other aspects such as t_C, the time needed to complete $PbTiO_3$ formation at a given temperature. Fig. 9 shows the the effect of normalized ion beam energy, eV/atom, on t_C, where the annealing was performed at 575° C. t_C dropped from 40 minutes for non–IAD films to 20 minutes for IAD films with normalized ion energy of 6.6 eV. It was also found that t_C remained at 20 as normalized ion beam energy increased. The value of 6.6 eV is in the order of bond energy of average materials. This result therefore suggested that the formation kinetics of $PbTiO_3$ formation was altered by the bombardment of energetic Ar^+ ions. The transfer of energy from ions to atoms overcame the activation energy of the reaction. The formation of the $PbTiO_3$ phase was also accelerated by the ion bombardment. However, the reaction could not be further promoted by ion bombardment with excessive energy. The excessive energy was expected to transform into thermal energy and to be absorbed by the films and the substrate.

Fig. 10 depicts the effect of ion bombardment on t_C as a function of ion flux density for 300 eV ion beams. The error bars in Fig. 10 indicate the time interval of stress measurement. t_C decreased as ion flux density increased. This phenomena could be attributed to the increase of nucleation density in the intermixed layer between PbO and TiO_2 layers. In general the effect of ion irradiation is to create activation sites that stimulate nucleation [20]. It was also found [21] that increasing ion flux density could increase the nucleation density during film growth. Accordingly, the kinetics of the $PbTiO_3$ formation could be aided by the increase of nucleation sites in the intermixed layers caused by increasing ion flux density. Fig. 11 shows the stress of $PbTiO_3$ films upon completion at 575° C. It was found that

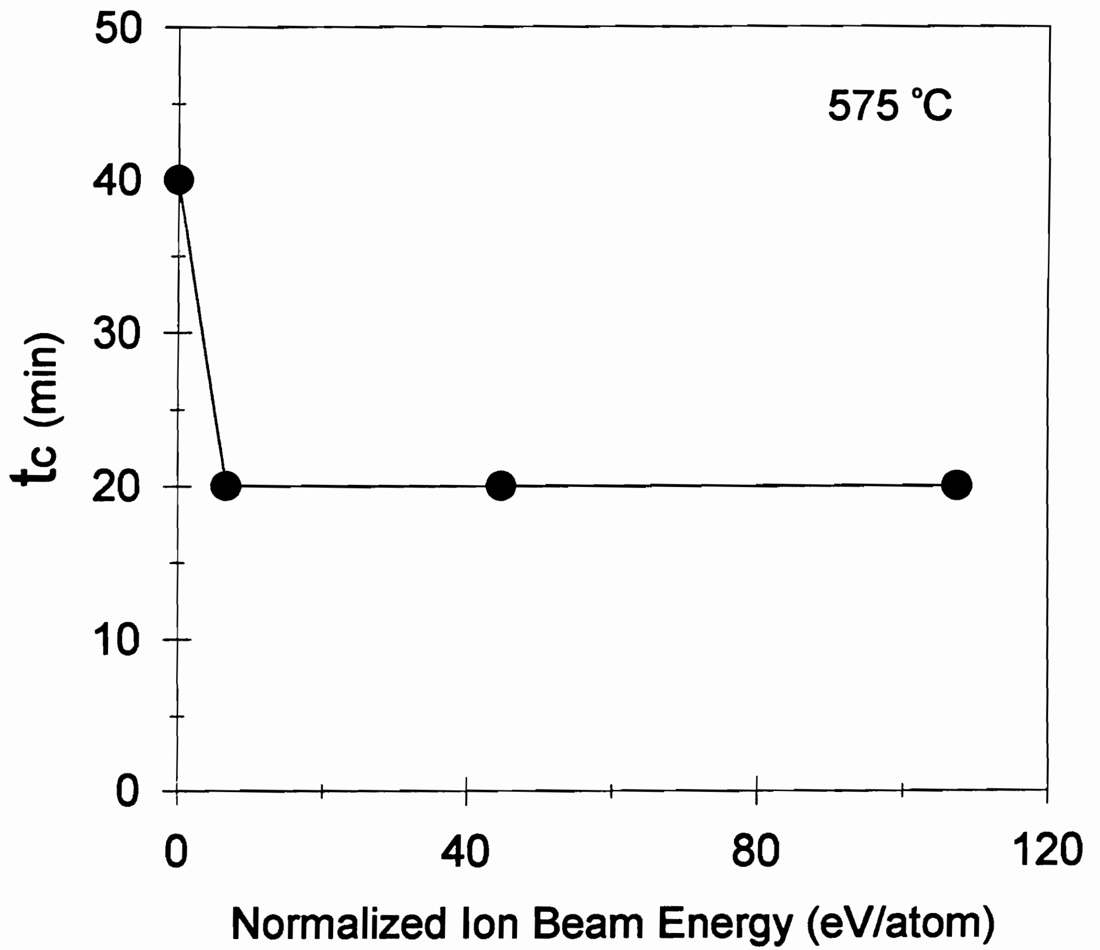

Fig. 9 t_c as a function of normalized ion beam energy.

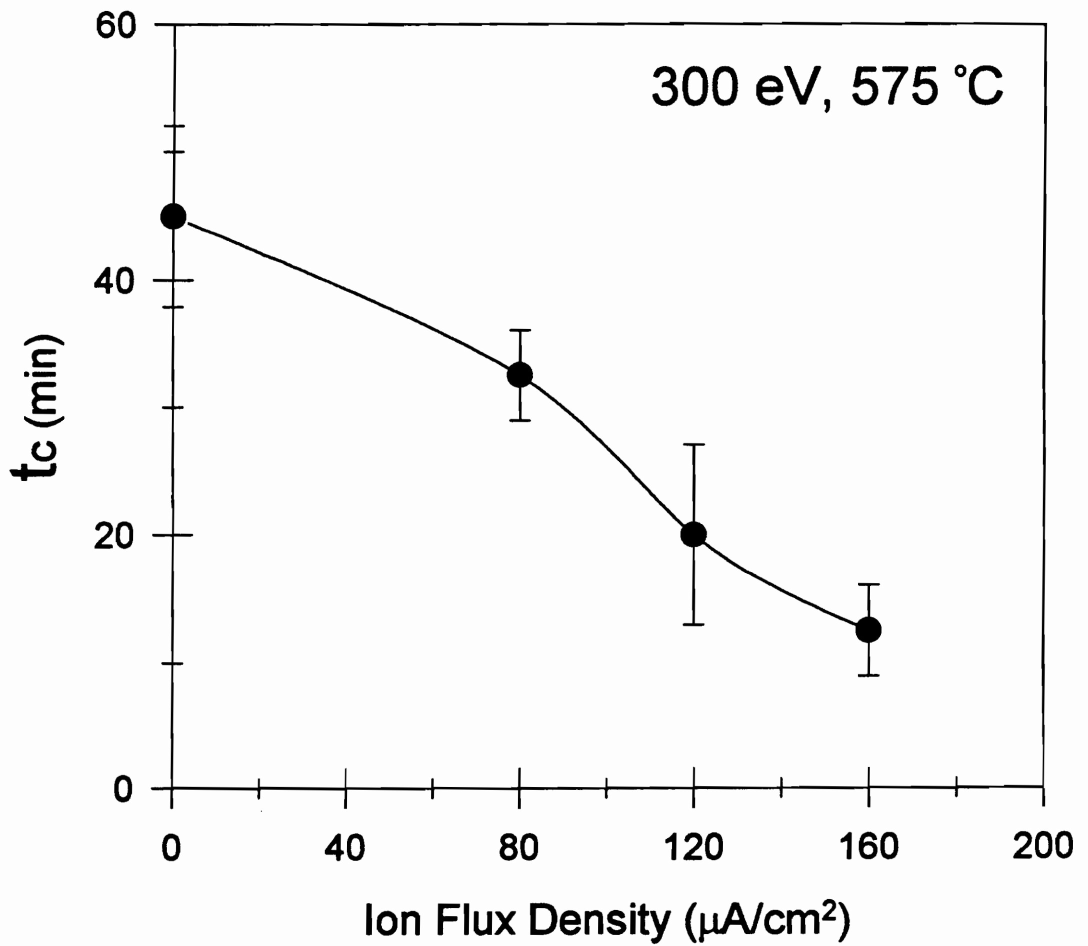

Fig. 10 t_c as a function of ion flux density.

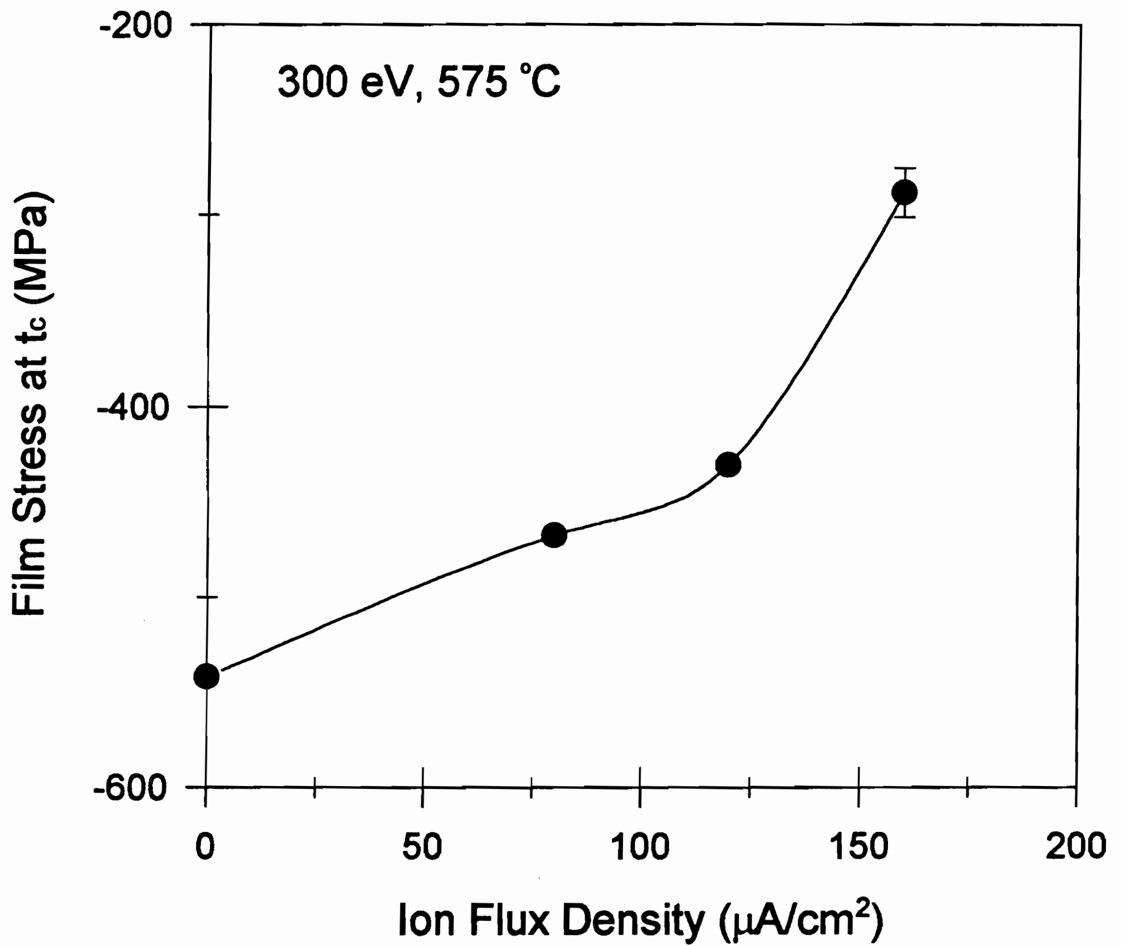

Fig. 11 Film stress at t_c as a function of ion flux density.

the compressive stress of $PbTiO_3$ films upon formation was reduced due to ion bombardment and decreased with increasing ion flux density at 300 eV.

4.5.4 Stress Relaxation

From our previous study [12] stress relaxation behavior of $PbTiO_3$ thin films (deposited without ion bombardment) was successfully described by a viscous flow model and obeyed a exponential relation against time,

$$\sigma = \sigma_0 \exp(-Et/\eta), \tag{3}$$

where E and η are the Young's modulus and viscosity of the films, respectively, and σ_0 is the pre–exponential factor.

Using the above relation, we intend to study the stress relaxation behavior of the $PbTiO_3$ films deposited with Ar^+ ion bombardment of 300 eV and 160 $\mu A/cm^2$. Take the absolute value of the data in the region of relaxation, as shown in Fig. 8, and replot them in a semi–log scale of stress against time, as shown in Fig. 12. The data showed very good linearity except for the data of 600° C. The deviation of data from the straight line could be likely caused by the change in relaxation mechanism.. From the slopes of the straight lines in Fig. 12 the viscosity, η, can be obtained as shown in Fig. 13, by taking the Young's modulus of $PbTiO_3$ films to be 13.1×10^{11} dyne/cm^2 [22]. The values of viscosity were found to obey a Arrhenius relationship,

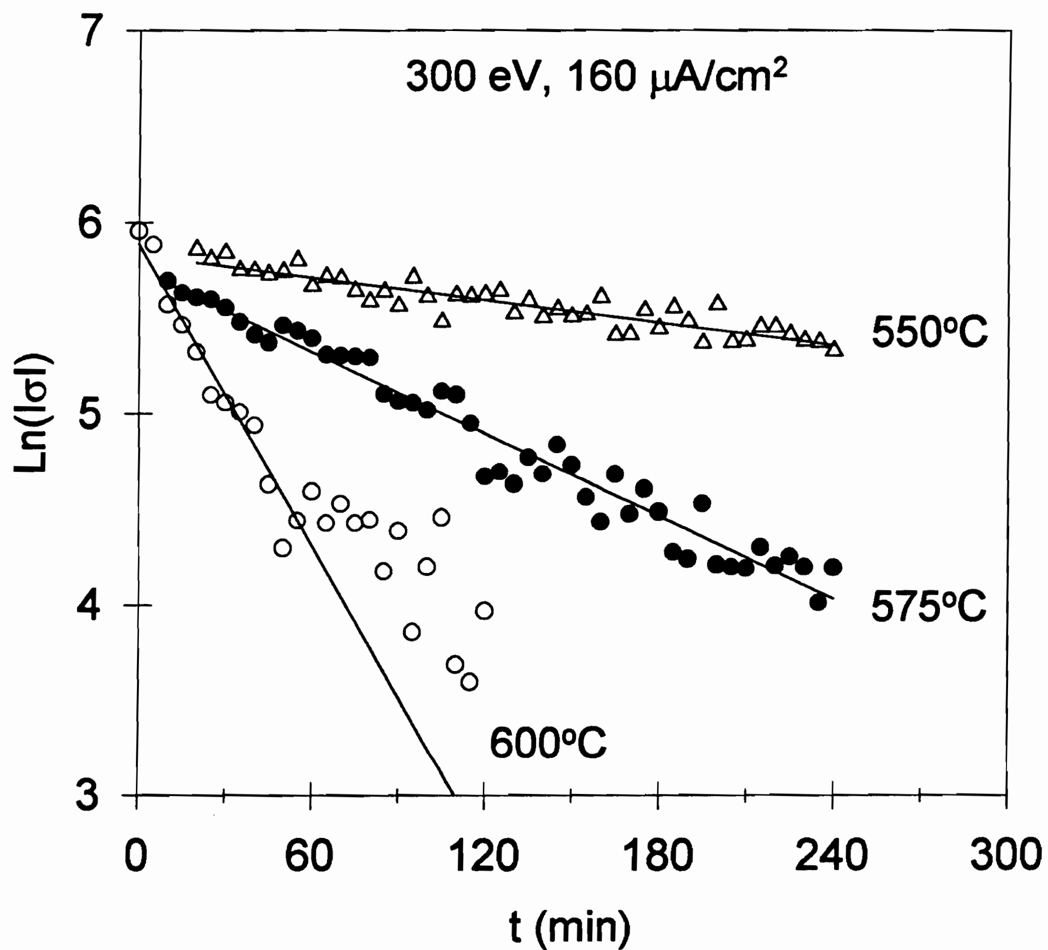

Fig. 12 Ln(IσI) as a function of time.

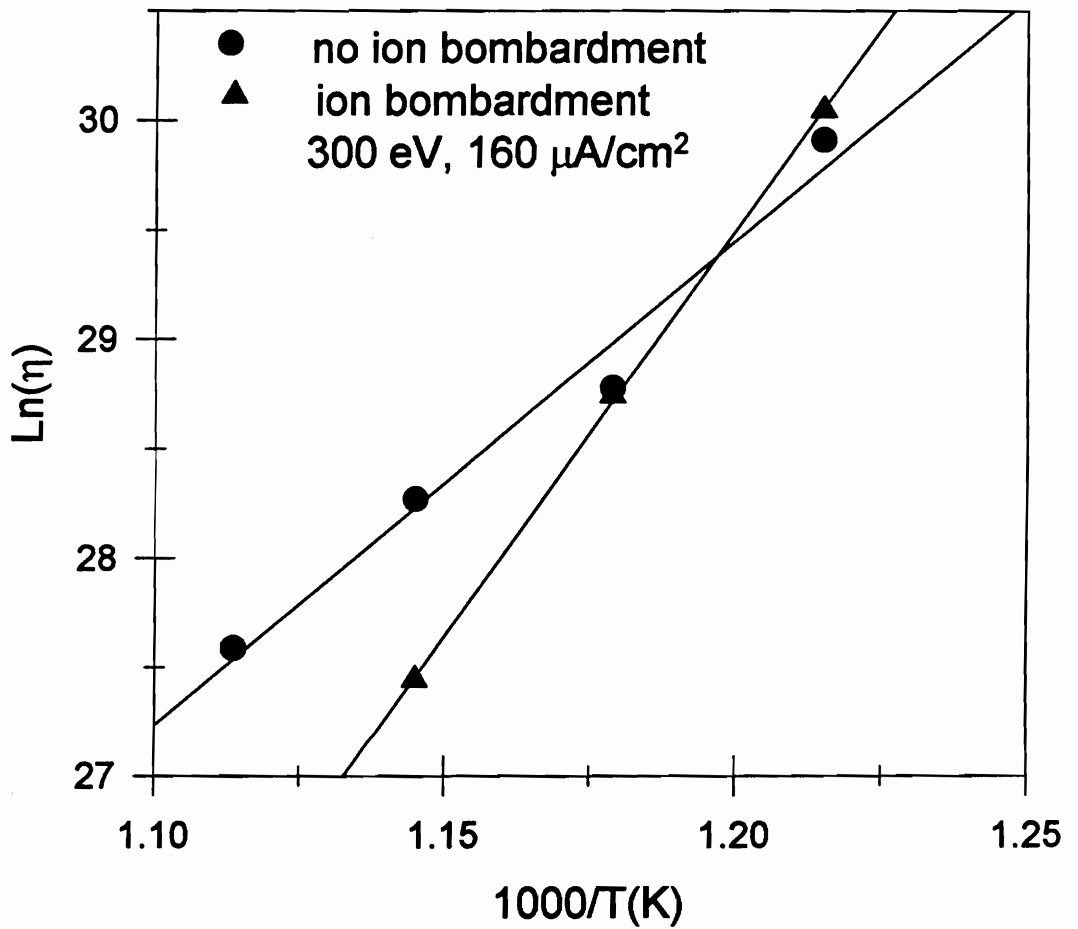

Fig. 13 The Arrhenius behavior of viscosity of $PbTiO_3$ films.

$$\eta = \eta_0 \exp(\Delta E/kT) \quad (4)$$

The activation energy of the stress relaxation can be estimated to be 310 kJ/mole. This value is much larger than the value of 190 kJ/mole for non–IAD $PbTiO_3$ films.

Fig. 14 depicts the effects of grain and mean grain size on film stresses. Several points were selected from the stress–time plot (Fig. 14a) and their microstructures were examined. It was found that stress relaxation in $PbTiO_3$ film was dominated by two mechanisms [12]: the rotation of the misorientation of the small grains or sub–cell microstructure, and grain growth. The former mechanism could account for the change of the I_{100}:I_{001} ratio associated with film stress levels (Fig. 14b). The latter mechanism could contribute to the reduction of stress levels as well (Fig. 14c). However, the average grain size was found to be smaller than that for non–IAD films. It was occasionally found some single–grain hillocks in the films. The number density of hillocks in the IAD films was found significantly lower than that in non–IAD films.

From the aforementioned results, one can relized that the stress relaxation in IAD films also obeyed the viscous flow model, and the dominant mechanism associated with stress relaxation was still grain growth. The difference in activation energy can be converted into the stress difference of the difference in film stress prior to relaxation. The difference was 160 MPa which is resonably close to the experimental value. Therefore, energetical ion bombardment could result in the reduction in film stresses. Accordingly, the rate of stress relaxation was also decreased.

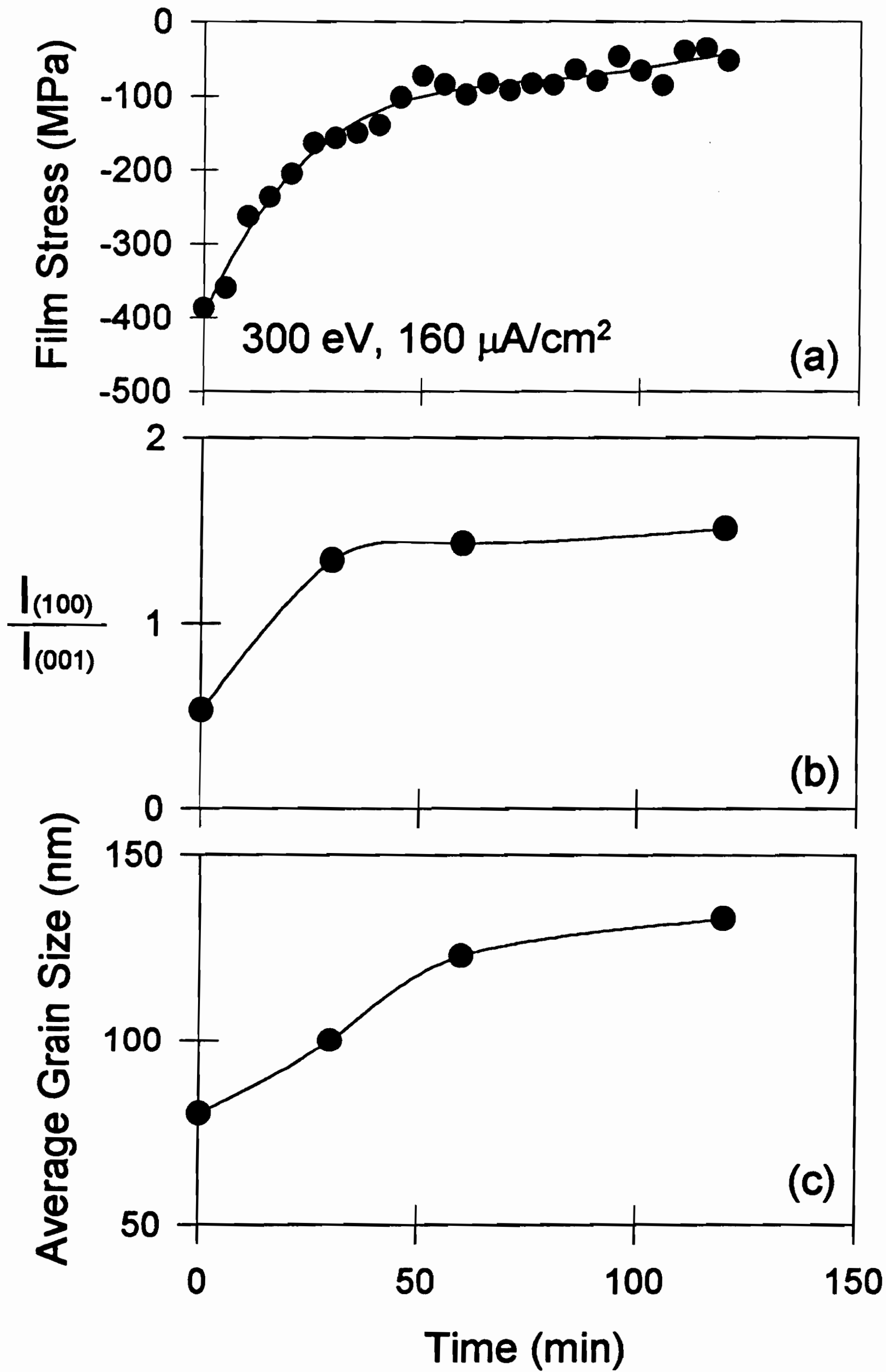

Fig. 14 Effects of both orientation and grain size on film stress.

Fig. 15 depicts the effect of ion bombardment on stress relaxation. It was found that for the same ion beam energy, the stress level of the $PbTiO_3$ films may be different, the stress relaxation behavior of $PbTiO_3$ films, however, was not affected by increasing ion flux density.

4.5.5 Structure–Property–Processing interrelationships

4.5.5.1 Property–process relations

The cooling portion of the stress–temperature plot in Fig. 5 depicts the development of thermal stress (σ_{th}) in the films, and it also shows very good linearity. Thermal stress generated during cooling can be obtained from the slope of the curve which is defined as followed

$$\text{slope} = \frac{d\sigma_{th}}{dT} = \frac{E_f}{(1 - \nu_f)}(\alpha_s - \alpha_f) \qquad (5)$$

where $E_f/(1 - \nu_f)$ is the biaxial modulus of the films and $(\alpha_s - \alpha_f)$ is the difference in the coefficient of thermal expansion (CTE) between substrate and film. Take the biaxial modulus of the films as a constant, the CTE of the film, α_f, can therefore be readily obtained.

Fig. 16 shows the change of CTE as functions of (a) normalized ion beam energy, eV/atom and (b) ion flux density for 300 eV ion beams. The CTE of thin $PbTiO_3$ films was found to decrease with increasing both normalized ion beam energy and ion flus density for 300 eV, and also approached to the bulk value of

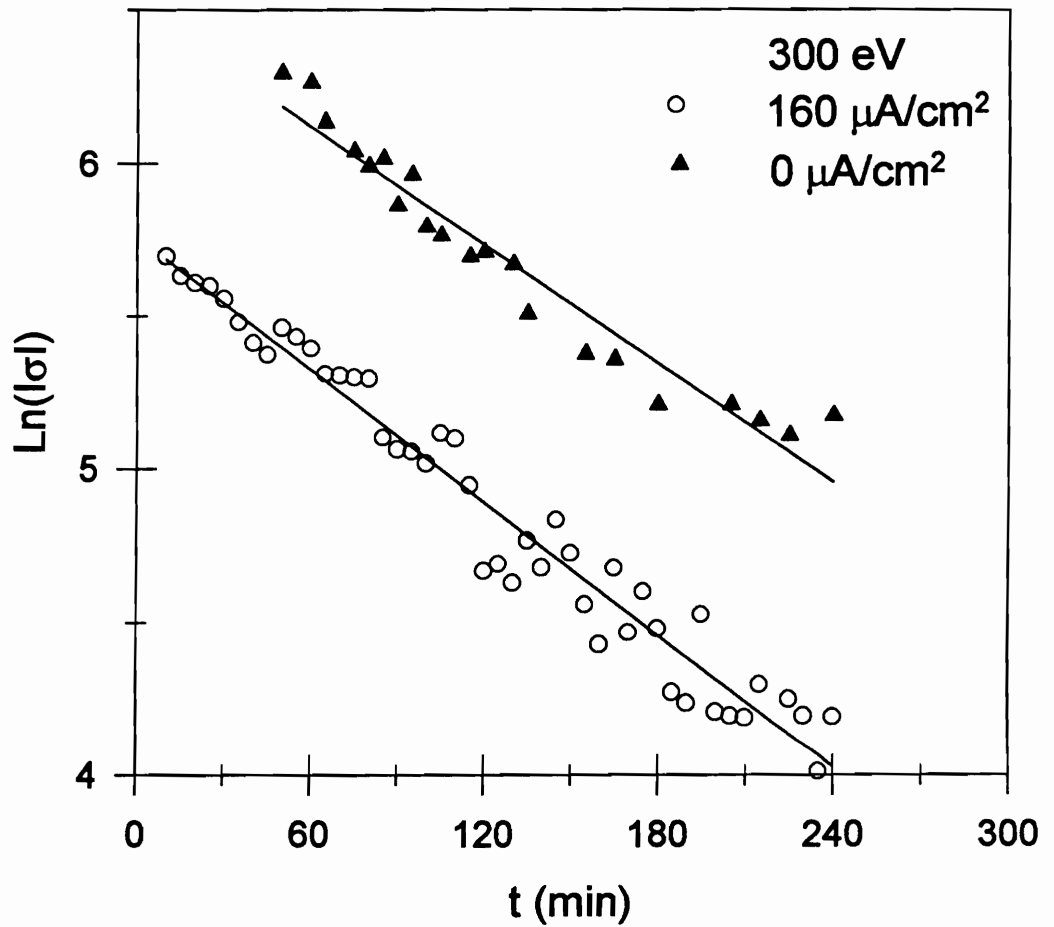

Fig. 15 Effect of ion flux density on stress relaxation behavior.

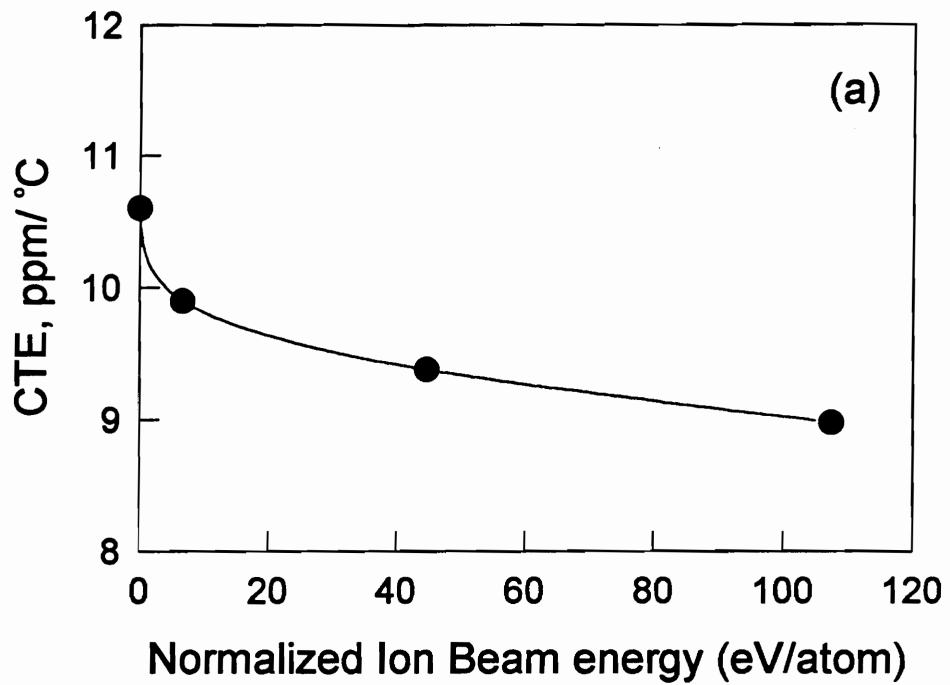

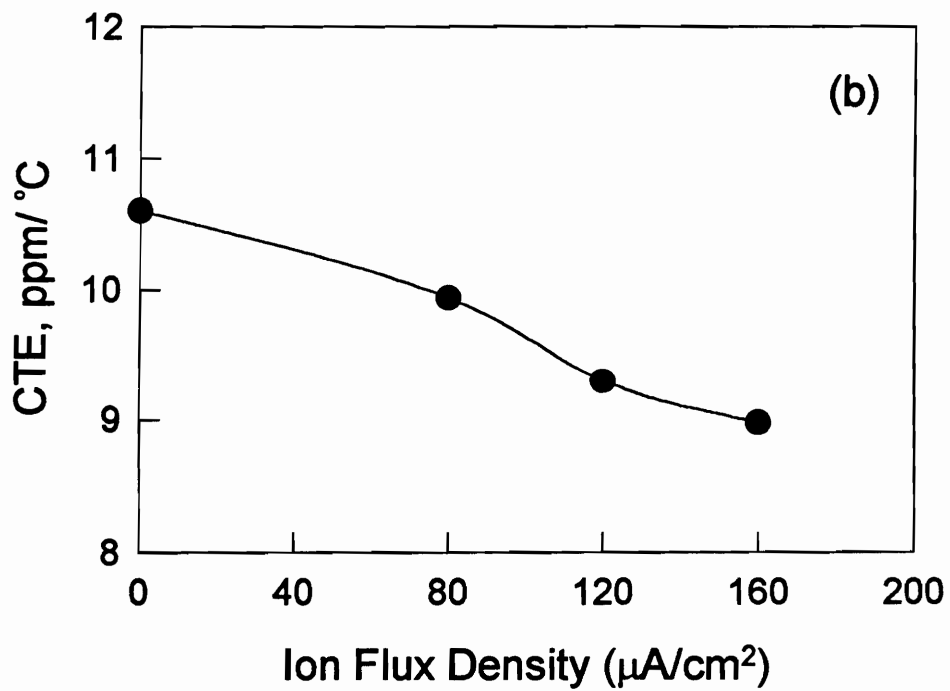

Fig. 16 CTE as a function of (a) normalized ion beam energy (b) ion flux density.

polycrystalline $PbTiO_3$ ceramics [24] compared to the non–IAD films. The reduction of CTE values was attributed to morphological change such grain size. For instance, the mean grain size was approximately 0.2 μm for non–IAD films [12] and 0.1 μm for the IAD film with 300 eV and 160 $\mu A/cm^2$ as shown in Fig. 15. Grain size of the ion bombarded films was also found to decrease with normalized ion beam energy and ion flux density for copper films [16].

4.5.5.2 Property–structure relationships

Fig. 17a shows the change of film stress as a function of grain size. Compressive film stress decreased with increasing grain size. Grain growth has been realized to be the major mechanism in stress relaxation of non–IAD $PbTiO_3$ thin films [12]. For IAD $PbTiO_3$ films, its grain growth associated with stress relaxation has a similar behavior as the non–IAD films except the smaller grain size.

Thin films with compressive stress often show better mechanical strength such as higher hardness and wear resistance [1]. At a first approximation, the strength, S, of a compressive film can be defined as

$$S = S_0 - \sigma \qquad (6)$$

where S_0 is the strength of a stress–free film and σ is the film stress. Since material strength greatly depends on the grain size of the material, and often obey the Hall–Petch relationship [25], $S = S' + kd^{-0.5}$, where S' and k are constants, and d is grain size. It is therefore clear that film strength depends on grain size as

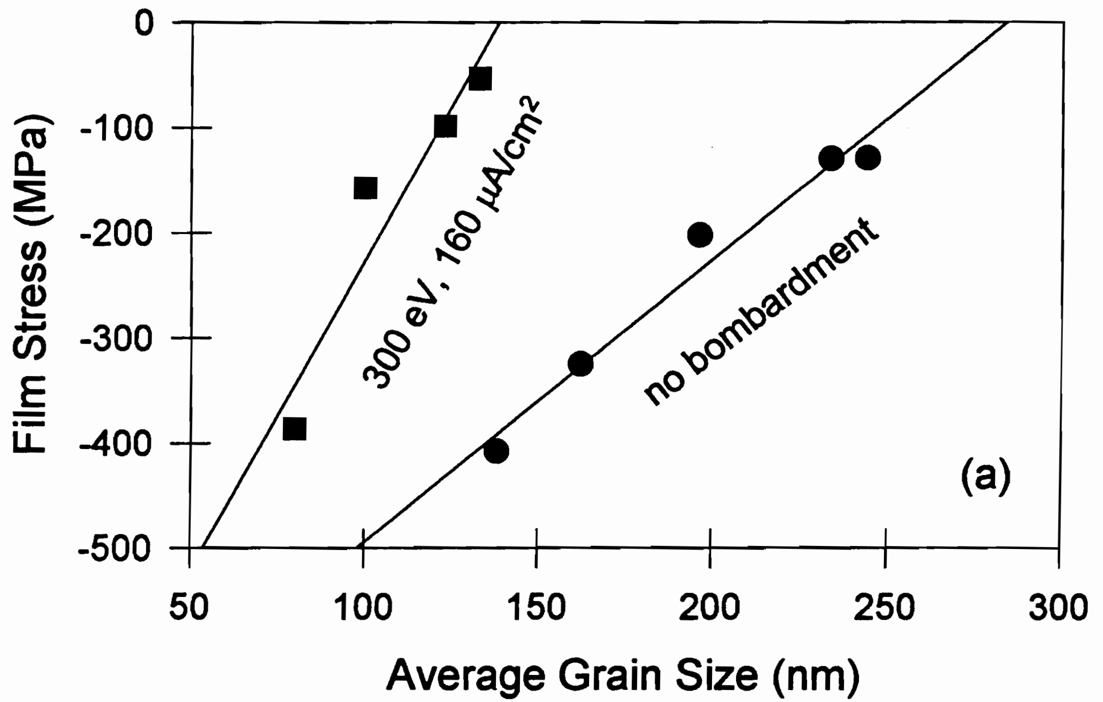

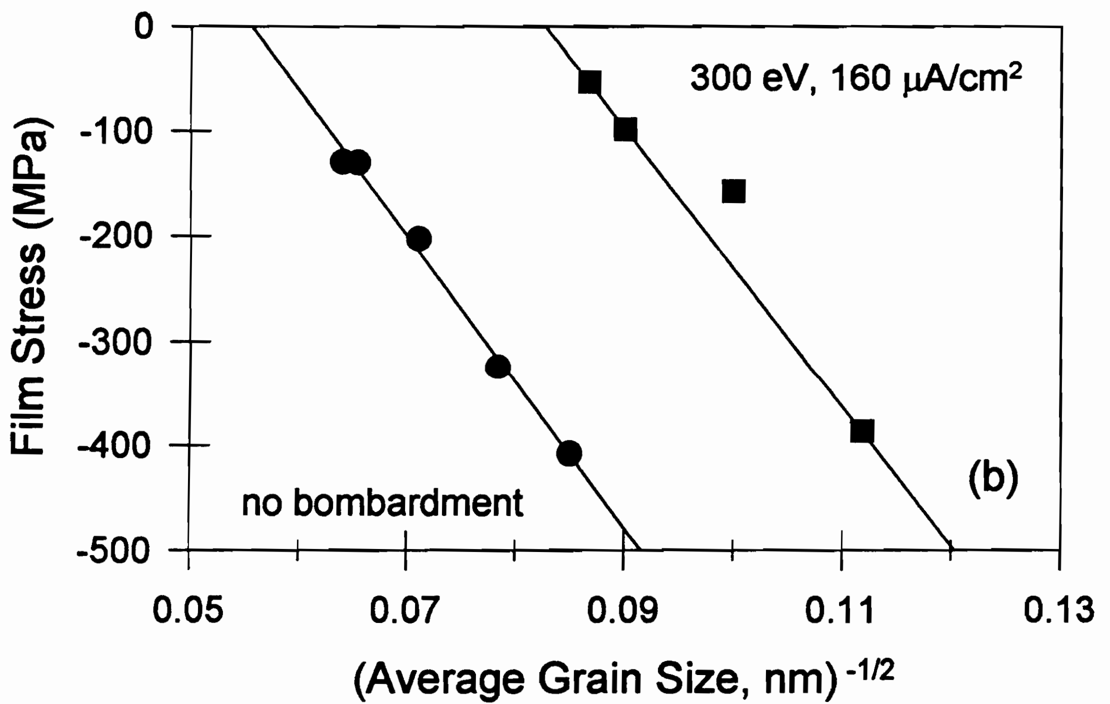

Fig. 17 Film stress as a function of (a) average grain size, d, and (b) $d^{-1/2}$.

$$\sigma = \sigma_0 - kd^{-0.5}. \quad (7)$$

Fig. 17b depicts the film stress as a function of $d^{-0.5}$. It is found that the two straight lines are parallel to each other and that the slope, k, is process–independent. This suggests that the mechanism associated with stress relaxation in $PbTiO_3$ thin films will not change due to the different deposition processes, although the grain size of the films is process–dependent.

4.6 Summary

For the first time, the effects of low energy ion bombardment on multicomponent oxide and multilayer systems were extensively studied by the in–situ stress measurement technique. The multilayer approach was employed to accurately control the composition of the $PbTiO_3$ films. Individual oxide layers, i.e. lead oxide and titanium oxide, were deposited on the sapphire substrate under the concurrent low energy (100 – 300 eV) Ar^+ ion irradiation. The effect of ion bombardment on $PbTiO_3$ formation are summarized.

(1) Film stress of the as–deposited multilayer was tensile and decreased with the increasing ion flux density. It was also found that the initial film stress drastically decreased as the normalized ion beam energy increased and then slightly increased at larger ion energy. The effect of the ion energy on initial film stress was also successfully modeled.

(2) The bombardment of low energy ions during film growth was also found to affect the stress behavior of the multilayer during thermal excursion.

(3) The formation of $PbTiO_3$ phase was accelerated by the ion bombardment, because ion bombardment during deposition could significantly increase the nucleation sites at the interface of the oxide layers and then enhanced the reaction.

(4) The mechanisms of stress relaxation was not affected by ion bombardment. The higher activation energy associated with stress relaxation for the IAD films, compared to that for non–IAD films, was attributed to the difference in film stress value prior to relaxation, resulting from ion bombardment.

(5) The coefficients of thermal expansion of the $PbTiO_3$ films was modified by ion bombardment. The CTE monotonically approached to the bulk value when ion flux density and ion beam energy increased. It was also found that film stress of the $PbTiO_3$ films significantly depends on their mean grain size. Mean grain size of $PbTiO_3$ films decreased when the film was bombarded by low energy ions during deposition.

4.7 References

1. F.A. Smidt, Int. Mater. Rev., 35(2), 61, 1990.

2. T.C. Huang, G. Lim, F. Parmigiani, and E. Kay, J. Vac. Sci. Technol., A3(6), 2161, 1985.

3. P. Ziemann and E. Kay, J. Vac. Sci. Technol., A1, 512, 1983.

4. K.H. Muller, J. Appl. Phys., 59(8), 2803, 1986.

5. E. Kay, F. Parmigiani and W. Parrish, J. Vac. Sci. Technol., A5, 44, 1987.

6. M. Drechsler, M. Junack and R. Meclewski, Surf. Sci., 97, 111, 1980.

7. E. Krikorian and R.J. Sneed, Astrophys. Space Sci., 65, 129, 1979.

8. J.M.E. Harper and R.J. Gambino, J. Vac. Sci. Technol., 16, 1901, 1979.

9. F.M. d'Heurle and J.M.E. Harper, Thin Solid Films, 171, 81, 1989.

10. C.C. Li and S.B. Desu, Ceramic Transactions, Vol. 25: Ferroelectric Films, A. Bhalla and K.M. Nair, eds. The American Ceramic society, 59–71, 1992.

11. S.B. Desu, and C.C. Li, in *Beam Processing of Advanced Materials*, edited by J. Singh and S. M. Copley, pp. 593–606, (1993).

12. C.C. Li and S.B. Desu, submitted to Phil. Mag., 1993.

13. G. Carter and D.G. Armour, Thin Solid Films, 80, 13 1981.

14. O. Knotek, R. Elsing, G. Kramer and F. Jungblut, Surf. Coat. Technol., 46, 265, 1991.

15. D. S. Yee, J. Floro, D.J. Mikalsen, J.J. Cuomo, K.Y. Ahn, and D. A. Smith, J. Vac. Sci. Technol., A3(6), 2121, 1985.

16. R.A. Roy, J.J. Cuomo, and D.S. Yee, J. Vac. Sci. Technol., A6, 1621, 1988.

17. C.A. Davis, Thin Solid Films, 226, 30, 1993.

18. D.R. McKenzie, D.A. Muller, and B.A. Pailthorpe, Phys. Rev. Lett., 67, 773,

1991.

19. R.A. Roy, R. Petkie, and A. Boulding, J. Mater. Res. 6(1), 80, 1991.

20. P.J. Martin, Vacuum, 36(10), 585, 1986.

21. M. Marinov, Thin Solid Films, 46, 267, 1977.

22. S. Ikegami, I. Ueda, and T. Nagata, J. Acoust. Soc. Am., 50, 1060, 1971.

23. J. Baglin, Handbook of Ion Beam Processing Technology, edited by J.J. Cuomo, S.M. Rossnagel, and H.R. Kaufman, p. 279, 1989.

24. G. Shirane and S. Hoshino, J. Phys. Soc. Jpn, 6, 265, 1951.

25. A.G. Guy and J.J. Hren, Elements of Physical Metallurgy, 3rd ed., Addison–Wesley Publishing Company, Massachusetts, p.464, 1974.

Chapter 5

CRYSTALLIZATION–INDUCED STRESS IN $BaMgF_4$ THIN FILMS

5.1 Abstract

Stress change associated with the crystallization of amorphous $BaMgF_4$ films deposited on silicon wafers was studied by using an in–situ stress measurement technique. $BaMgF_4$ thin films with (010) preferred orientation were successfully formed on Si(100) substrates by evaporation under ultrahigh vacuum condition followed by a post–deposition annealing in H_2 atmosphere at a temperature as low as 375° C. The biaxial modulus and thermal expansion coefficient of the BMF films were readily estimated. Film delamination was observed in some cases due to the development of high stresses during thermal excursions.

5.2 Introduction

Compounds of the $BaMF_4$ types (M = Mn, Fe, Co, Ni, Zn, Mg) crystallize in the orthorhombic system with point group symmetry 2mm [1]. The structure consists of MF_6 octahedra sharing corners to form puckered sheets parallel to (010) which are linked by Ba^{2+} ions only. The Ba^{2+} ions are coordinated to eight F^- ions. $BaMgF_4$ is known to be a piezoelectric [2] and luminescent [3] material. It also displays reversible polarization consistent with ferroelectricity. It has postulated that polarization reversal involves a tilt of the MgF_6 octahedra, which is associated

with the displacement of the Ba atoms parallel to the [100] axis. Recently Sinharoy et al [4] has reported that $BaMgF_4$ (BMF) thin films deposited on silicon wafers under clean UHV conditions displayed ferroelectric properties consistent with the behavior previously reported for bulk crystals. This availability of ferroelectric fluoride films now opens exciting possibilities for direct application in monolithic ferroelectric memory field–effect transistor (FEMFET) devices in which the ferroelectric film is deposited directly on the Si or GaAs crystal surface.

With the attempt of integrating $BaMgF_4$ films into the very large integration circuits, the performance of the circuits can often be greatly influenced by the stress state in thin films. Excessive stress developed in films can cause failures such as cracks or film delamination. It is therefore very important to control or minimize the mechanical stresses developed during fabrication. Film stress mainly contains two mechanisms: intrinsic stress originating from the nucleation and growth during film growth, and thermal stress due to the mismatch of thermal expansion coefficients bewteen film and substrate [5].

$BaMgF_4$ thin films prepared by evaporation under ultra high vacuum condition at ambient temperature are often amorphous [4], it is also expected to show high tensile stress state. Upon annealing, the amorphous $BaMgF_4$ films undergo crystallization, and both nucleation and growth proceed in the films, which may cause additional stress. In this study, stress of the $BaMgF_4$ thin films on silicon wafers associated with the development of crystal structure and morphology during annealing was investigated..

5.3 Experimental Procedure

5.3.1 Sample Preparation and Characterization

The fluoride films were grown in a bakeable ultrahigh vacuum (UHV) chamber equipped with a fluoride sublimation source, an ion gun for substrate surface cleaning, and an Auger analyzer for the compositional characterization of the substrate and the film. The experimental set up has been described in detail elsewhere [4]. The base pressure in the baked UHV chamber was less than 1.0×10^{-10} Torr. $BaMgF_4$ films were successfully grown by evaporating BaF_2 (99.995% pure) and MgF_2 (99.99% pure) pressed powders, mixed in equimolar proportions. Si(100) substrates were chemically cleaned using the procedure developed by Ishizaka and Shiraki[6] prior to insertion in the UHV chamber, followed by in situ thermal cleaning at 850°C for 20 min. AES examination revealed no detectable contaminants following this procedure. In this study all the $BaMgF_4$ films were deposited at ambient substrate temperature with film thickness ranging from 60nm to 330nm. Then the films were annealed in Ar atmosphere by directly inserting the samples into a preheated tube furnace. The annealing temperatures range from 350° to 600°C and annealing times range from 5 to 60 minutes . After annealing, the crystal structure of $BaMgF_4$ films were identified by X–ray diffraction analysis. The surface morphology was observed by scanning electron microscopy.

5.3.2 Film Stress Measurement

Film stress measurements as a function of temperature and time were

performed for the $BaMgF_4$ films on 3–inch diameter silicon (100) substrates in H_2 atmosphere. The heating rate was 10° C/min. The sample curvature was calculated from the change in position of a reflected laser beam. The position was measured by a position sensitive detector while the beam was scanned across the sample. The total film stresses, σ_{tot}, were calculated by comparing the substrate curvature before and after film deposition using the Stoney's equation [7], which yields the biaxial total stress, σ_{tot}, in the thin films parallel to the substrate:

$$\sigma_{tot} = \frac{E_s}{6(1-\nu_s)} \frac{t_s^2}{t_f} \frac{1}{R}$$

where E_s, ν_s, and t_s are Young's modulus, Poisson's ratio, and thickness of the substrate, respectively, and t_f is the film thickness. R is an effective radius of curvature of the substrate determined by $R = 1/(1/R_2 - 1/R_1)$, where R_1 and R_2 are the substrate radii of curvature before and after film deposition. This formula is applicable when t_f is far smaller than t_s and the central wafer deflection is much smaller than the diameter of the wafer. Both conditions are met in the present work.

5.4 Results and Discussion

5.4.1 Stress development in $BaMgF_4$ Thin Films

Stress change in the 123 nm $BaMgF_4$ film is summarized in Fig. 1. The horizontal axis is the annealing temperature. The initial stress of the as–deposited

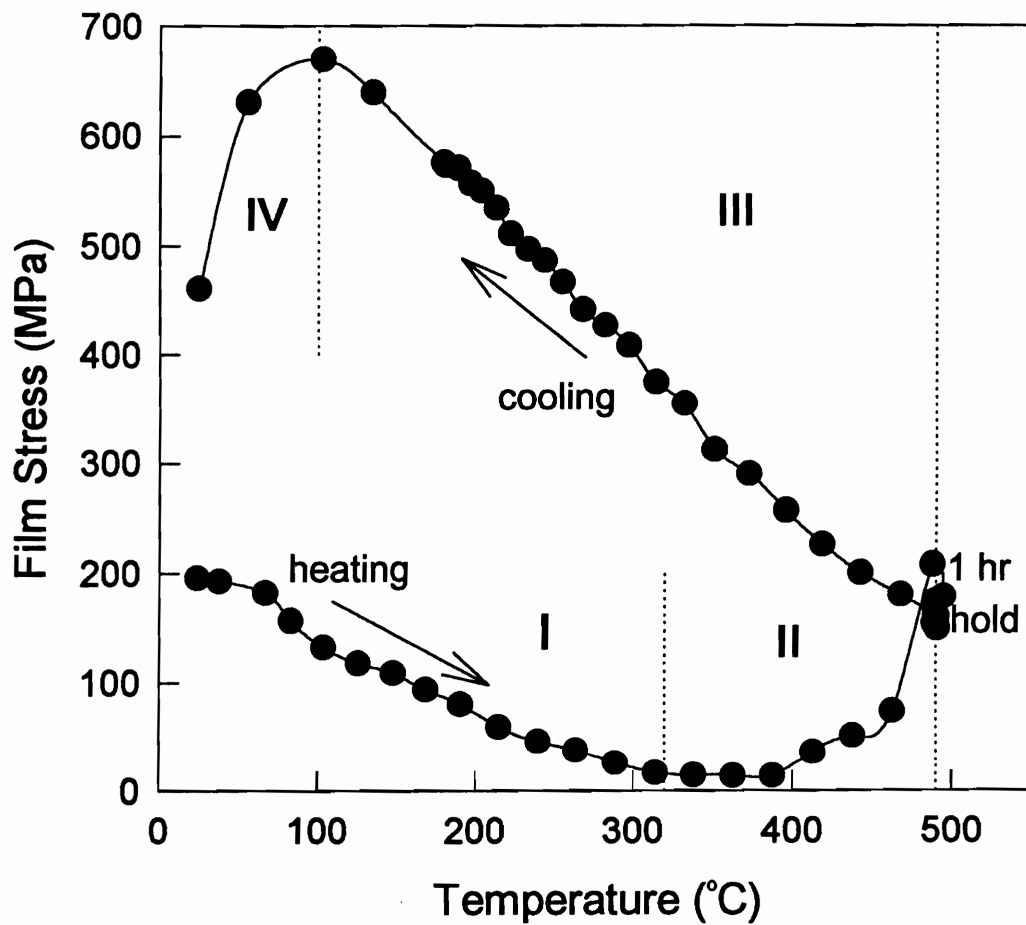

Fig. 1 Stress-temperature plot of the 123 nm $BaMgF_4$ thin film.

amorphous $BaMgF_4$ film was tensile and was about 200 MPa. For better understanding, Fig. 1 was dividied into four regions. Regions I and II represented the heating stage, whereas regions III and IV the cooling stage. During annealing the temperature was also kept at 490° C for an hour.

Upon heating, the tensile stress decreased linearly against annealing temperature as seen in region I, that is to say, compressive stress started building up in the BMF film. This development of compressive stress was attributed to the greater thermal expansion of the BMF film than the substrate. It was found that the tensile film stress reached a minimum at 10 MPa while the curve entered region II at around 320° C and remained constant up to 390° C. Film stress slightly increased at around 390° C, then drastically increased at around 460° C and reached the maximum, 210 MPa, at 490° C. Stress change in region II was associated with the crystallization of the BMF film, for similar behavior was also found in the CVD–WSi_2 film on Si [8] and Si thin films [9]. In the isothermal stage at 490° C film stress slightly relaxed. When the temperature decreased, film stress increased linearly against temperature in region III and reached a local maximum at around 100° C when the curve entered region IV. In region III the BMF film shrank faster than the substrate when the temperature decreased and therefore tensile stress developed. It was found that the slope of the stress–temperature curve in region III is slightly higher than that in region I, which was likely caused by the change in the thermal expansion coefficient after the BMF film crystallized. In region IV film stress quickly relaxed to around 460 MPa at room temperature, and this could be associated with microstructural change in the film.

5.4.2 Formation of $BaMgF_4$ Phase

For further understanding the stress change associated with film crystallization, BMF films with thickness of 60 nm were also annealed in a conventional pre–heated box furnace. The orthorhombic phase in BMF films was first identified at an annealing temperature of 375°C for 60 minutes, as shown in Fig. 2. It was found that the annealed BMF films had an (010) preferred orientation. In the early stage of annealing at 375°C up to 45 minutes, the (040) and (140), instead of (040) and (060), reflections, were first found in the spectrum. For all the BMF films annealed at the temperatures higher than 375°C and prolonged anneal time, for instance at 400°C for 5 minutes, (020), (040), (060), and (0$\underline{10}$0) peaks were found in the XRD spectra along with a tiny (011) peak as shown in Fig. 3.

The annealing behavior of BMF films in the pre–heated box furnace can be correlated with the their stress behavior during thermal excursions as shown in region II of Fig. 1. Crystallization of BMF phase accelerated as the temperature was above 375°C using conventional annealing, for example, the formation of BMF phase could be completed at 400°C for as short as 5 minutes. In Fig. 1, as the temperature increased, crystallization of BMF phase took place at around 390°C, accelerated at around 460°C, and then finished at around 490°C. The difference of temperature at which crystallization accelerated could be accounted for by the differences of film thickness and annealing scheme, especially heating rate. Since crystallization of thin films often results in volumetric shrinkage [10], relatively high tensile stress can be developed in the film. This fact could account for the drastic

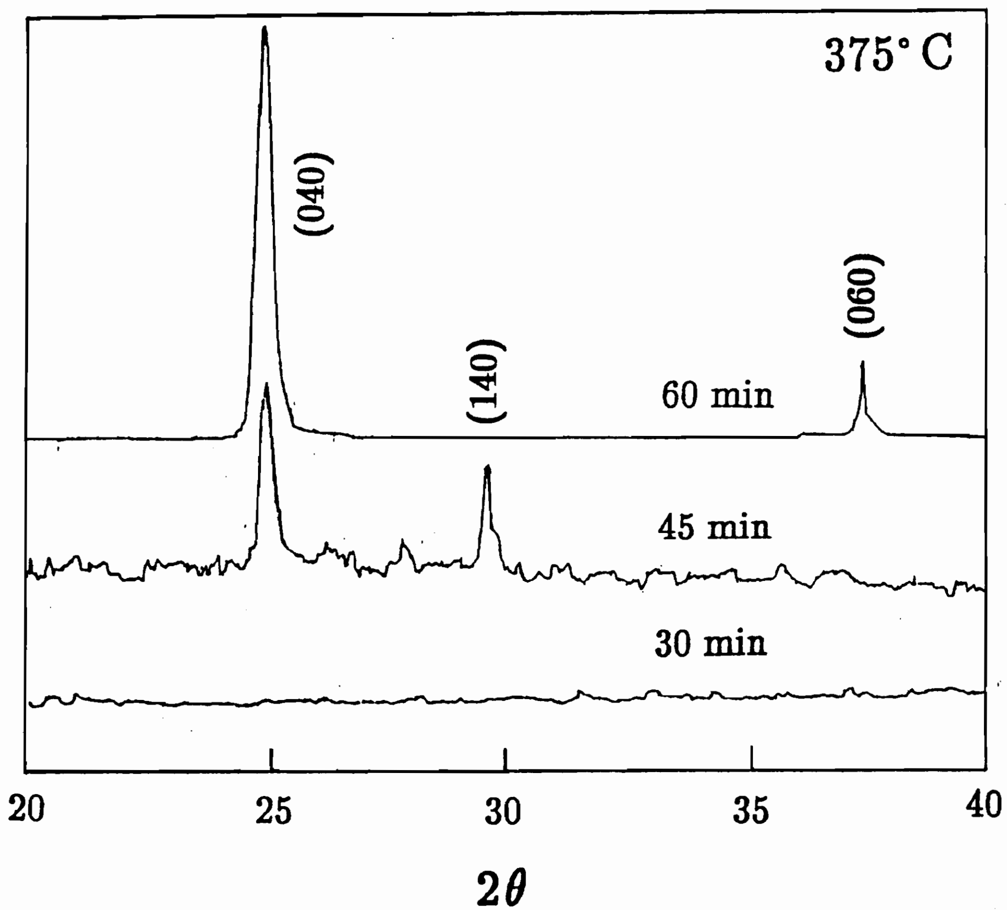

Fig. 2 XRD spectra of BMF thin films annealed at 375°C

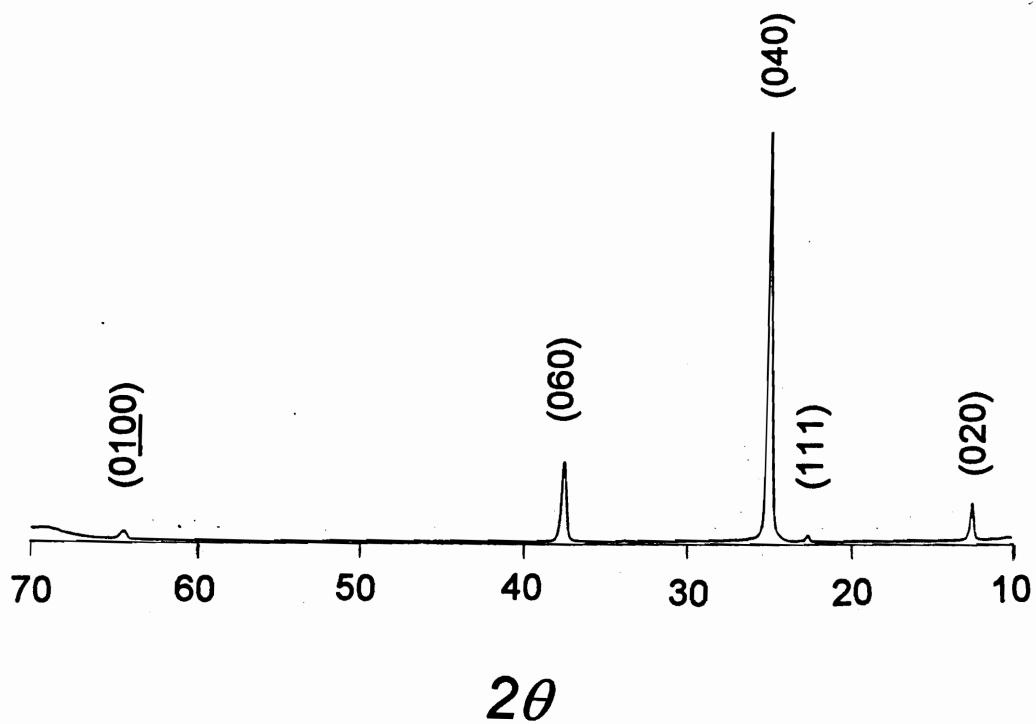

Fig. 3 XRD spectrum of a BMF film annealed at 400°C for 5 minutes.

increase in film stress as shown in region II of Fig. 1.

5.4.3 The mechanics of stress in BMF films

Since the resultant BMF films had a [010] preferred orientation, it is reasonable to assume that a uniaxial strain, ϵ, occurred in the thickness direction during crystallization. It is then possible to calculate the thickness change of the films from the stress surge, σ, in region II of Fig. 1, using the following formula

$$\sigma = M\epsilon,$$

where M is the biaxial elastic modulus of the film.

For a polycrystalline film with strong crystallographic texture, the anisotropy of the elastic properties must be taken into account. For a film in which the (010) plane lies parallel to the plane of the film, the biaxial elastic modulus, M, is isotropic in the plane of the plane of the film and is given by

$$M\,(010) = C_{11} + C_{13} - \frac{C_{12}(C_{12} + C_{23})}{C_{22}}$$

where C_{11} and C_{12} are components of the stiffness matrix (appendix). We note that neither Young's modulus, E, nor Poisson's ratio, ν, alone are isotropic in the (010) plane, but the ratio $E/(1-\nu)$ which forms the biaxial modulus is isotropic in that plane. M(010) was accordingly calculated to be 145 GMa for BMF films.

From region II of Fig. 1 the stress increase associated with crystallization was approximately 200 MPa, the uniaxial strain, ϵ, was calculated to be 0.14%, which is lower than the normal plastic offset of 0.2%. The thickness increase was also calculated to be 0.17 nm. The increase of film thickness also implied lateral shrikage of the film. The possible mechanism of the film shrinkage druing crystallization is the bond angle change of participating atoms between the amorphous and crystallization states. Further study is, however, necessary to clarify the main mechanism of the crystallization–induced stress in BMF films.

In region III of Fig. 1, the slope of the curve is simply the product of the difference in thermal expansion coefficients and the biaxial elastic modulus of the film. The thermal expansion coefficient, α_f, of the BMF films can be readily obtained from the slope. α_f of the crystallized BMF film was calculated as 12.8 ppm/°C, which is very close the literature value.[4] Assume that the amorphous BMF phase has the same biaxial modulus as the crystallized phase. The α_f of the amorphous BMF film could also be calculated as 5.3 ppm/°C, which is much smaller than that for crystallized phase.

5.4.4 Morphology Development in BMF films

Figure 4 illustrates the surface morphology of the crystallized $BaMgF_4$ thin films with 60 nm of thickness on Si(100) wafers annealed at (a) 375°C, 60 min and (b) 500°C, 5 min. It was found that BMF films were specular and featureless at 375°C, 60 min, whereas at 400°C and above (e.g., 500°C in Fig. 4) BMF films showed blister–like features. Furthermore, for some cases the BMF films even

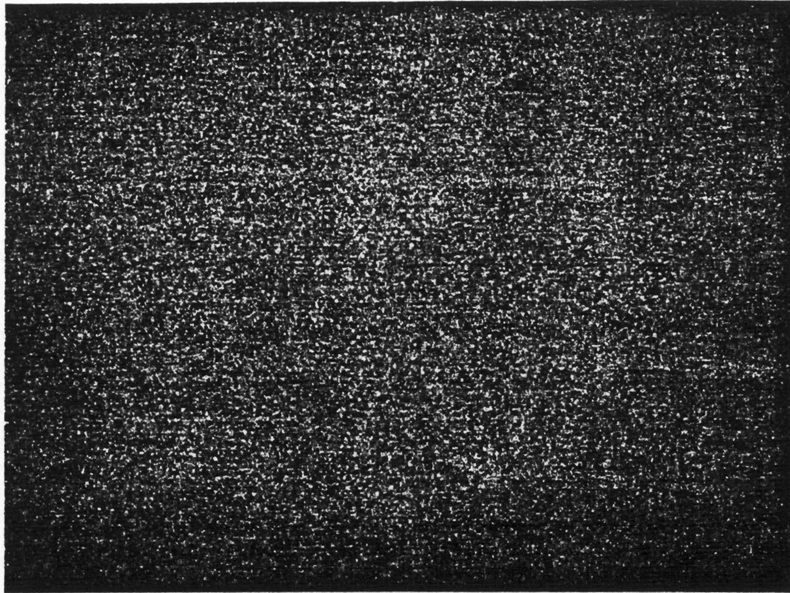

375° C, 60min

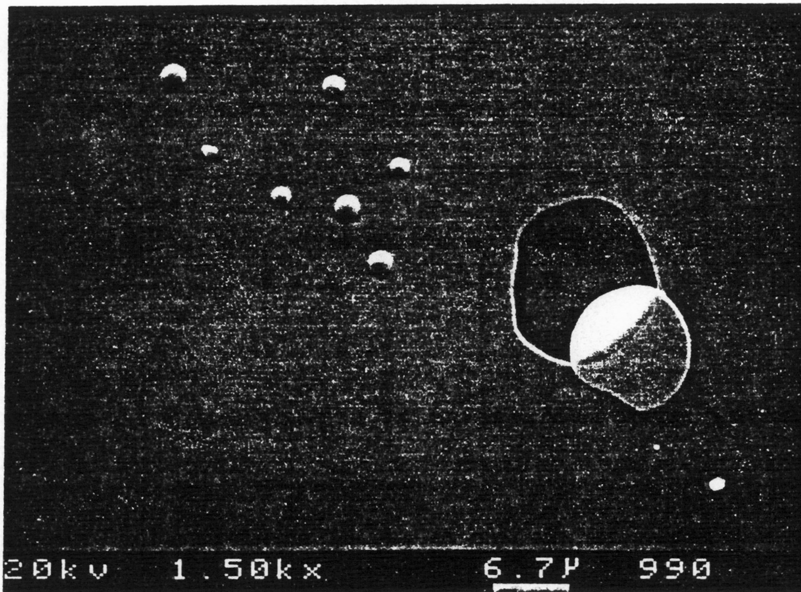

500° C, 5min

Fig. 4 Surface morphology of BMF films on Si(100) substrates.

delaminated from the substrates as shown in Fig. 4. It is likely that, upon cooling, the development of excessive tensile stress could have caused plastic deformation such as blister–like feature in the films (Fig. 4), because the flow strength increases with decreasing temperature. The stress–temperature plots reached a maximum on cooling at around 100°C. This could be attributed to the occurrence of a vast number of blisters being burst open and subsequent relief of the high tensile stress in BMF films as shown in Fig. 4.

5.5 Summary

The stress change associated with crystallization of the amorphous BMF film deposited on silicon wafers was discussed. $BaMgF_4$ thin films with a preferred orientation parallel to (010) were successfully formed on Si(100) wafers by deposition under UHV conditions followed by post–annealing at a temperature as low as 375°C for 60 minutes in Ar atmosphere. It was found that phase transformations and morphology developments in the BMF films could be monitored from its stress–temperature history. The biaxial modulus and thermal expansion coefficients of the BMF film were estimated. Film delamination was observed in the BMF films due to the development of high tensile stresses during the thermal excursions.

5.6 Appendix

The stiffness matrix[4] for the orthorhombic BMF crystal is listed below

$$C_{ij} = \begin{bmatrix} 10.4 & 2.9 & 6.4 & 0 & 0 & 0 \\ 2.9 & 8.1 & 3.6 & 0 & 0 & 0 \\ 6.4 & 3.6 & 13 & 0 & 0 & 0 \\ 0 & 0 & 0 & 3.2 & 0 & 0 \\ 0 & 0 & 0 & 0 & 5.5 & 0 \\ 0 & 0 & 0 & 0 & 0 & 2.5 \end{bmatrix} \text{x } 10^{11} \text{ dyne/cm}^2.$$

5.7 References

1. E. T. Keve, S. C. Abrahams, and J. L. Bernstein, J. Chem. Phys., 51, 4928 (1969).

2. M. Eibschutz and H. J. Guggenheim, Solid State Commun., 6, 737 (1968).

3. P. A. Rodnyi, M. A. Terekhin, and E. N. Mel'chakov, J. Lumines., 47, 281 (1991).

4. S. Sinharoy, H. Buhay, M. H. Francombe, W. J. Takei, N. J. Doyle, J.H. Rieger, D. R. Lampe, and E. Stepke, J. Vac. Sci. Technol. A, 9, 409 (1991).

5. M. F. Doerner and W. D. Nix, CRC Critical Reviews in Solid State and Materials Sciences, 14, 225 (1988).

6. A. Ishizaka and Y. Shiraki, J. Electrochem. Soc., 133, 666 (1986).

7. J. A. Thornton, Semiconductor Materials and Process Technology Handbook, (ed. G. E. McGuire, Noyes, Park Bridge, NJ, 1988), p. 329.

8. P. H. Townsend: Ph.D. Dissertation, Standard Universtity, Standaard CA, 1987

9. H. Miura, H. Ohta, N. Okamoto, and T. Kaga, Appl. Phys. Lett., 60(22), 2746 (1992).

10. L. A. Davis. Metallic Glass, (American Society of Metals, Metal Park, Ohio, 1978), p. 190.

Chapter 6 Summary

A novel in–situ stress measurement technique has been successfully developed to study the formation kinetics of multi–component thin films such as $PbTiO_3$. Using the multilayer approach, film composition can be simply controlled by the thickness of the individual layers. the formation of the $PbTiO_3$ layer at the interface of PbO/TiO_2 altered the total stress of the multilayers. By monitoring stress changes in the multilayers, the in–situ formation kinetics of $PbTiO_3$ films was successfully examined and quantitatively documented. The activation energy of $PbTiO_3$ formation was estimated to be 108 KJ/mole which is in excellent agreement with the literature value. It is believed that the formation of $PbTiO_3$ phase was dominated by grain boundary diffusion mechanism because of the very fine grain size in the films. The grain boundary diffusivity responsible for this reaction was also deduced.

Stress relaxation in $PbTiO_3$ films was investigated by the in–situ stress measurement technique. A simple viscous flow model was successfully employed to interpret the behavior of stress relaxation in the $PbTiO_3$ thin films. Using this model the estimation of the effective viscosity (η) of $PbTiO_3$ films was made possible. The activation energy responsible for stress relaxation was estimated to be 190 KJ/mole. The relaxation of film stresses was dominated by the lattice diffusion through vacancy movement.

In order to microscopically understand stress relaxation in the $PbTiO_3$ thin

films, the Nabarro–Herring creep model was employed to correlate the viscosity (η), lattice diffusion coefficient (D_l), and grain size of the films. From this Nabarro–Herring model the lattice diffusion coefficient of the vacancy motion was estimated to be $3x10^{-5}exp(-190,000/kT)$. Using these data the time required for complete relaxation of the $PbTiO_3$ thin films was calculated and compared with the experimental values. It was found the experimental values, observed from stress–time plots, matched very well with the calculated values. Therefore, it follows that this stress relaxation process is dominated by the lattice diffusion of the vacancies. Hillock formation caused by grain boundary sliding could partially relax the film stress in its early stage. Thereafter, grain growth resulted from lattice diffusion mainly accounted for the stress relaxation.

The effect of low energy ion bombardment on the fabrication of $PbTiO_3$ thin films has been extensively studied by the in–situ stress measurement technique. The multilayer approach was employed to accurately control the composition of the $PbTiO_3$ films. Individual oxide layers, i.e. lead oxide and titanium oxide, were deposited on the sapphire substrate under the concurrent low energy (100 – 300 eV) Ar^+ ion irradiation. The effect of ion bombardment on $PbTiO_3$ formation are summarized.

(1) Film stress of the as–deposited multilayer was tensile and decreased with the increasing ion flux density. It was also found that the initial film stress drastically decreased as the normalized ion beam energy increased and then slightly increased at larger ion energy. The effect of the ion energy on initial film stress was also successfully modeled.

(2) The bombardment of low energy ions during film growth was also found to affect

the stress behavior of the multilayer during thermal excursion.

(3) The formation of $PbTiO_3$ phase was accelerated by the ion bombardment, because ion bombardment during deposition could significantly increase the nucleation sites at the interface of the oxide layers and then stimulate the reaction.

(4) The mechanisms of stress relaxation was not affected by ion bombardment. The higher activation energy associated with stress relaxation for the IAD films, compared to that for non-IAD films, was attributed to the difference in film stress value prior to relaxation, resulting from ion bombardment.

(5) The coefficients of thermal expansion of the $PbTiO_3$ films were modified by ion bombardment. The CTE monotonically approached the bulk value when ion flux density and ion beam energy increased. It was also found that film stress of the $PbTiO_3$ films significantly depends on their mean grain size. The mean grain size of $PbTiO_3$ films decreased when the film was bombarded by low energy ions during deposition.

The stress change associated with crystallization of the amorphous BMF film deposited on silicon wafers was reported. $BaMgF_4$ thin films with a preferred orientation parallel to (010) were successfully formed on Si(100) wafers by deposition under UHV conditions followed by post-annealing at a temperature as low as 375°C for 60 minutes in an Ar atmosphere. It was found that phase transformations and morphology developments in the BMF films could be monitored from its stress-temperature history. The biaxial modulus and thermal expansion coefficients of the BMF film were estimated. Film delamination was observed in the BMF films due to the development of high tensile stresses during the thermal excursions.

Vita

Chen–Chung Li was born on April 25, 1963 in Taipei, Taiwan. He received his B.S. degree from National Cheng Kung University in 1985, and M.S. degree from National Taiwan University (NTU) in 1987. After serving as a research assistant for a year in NTU, he joined Virginia Polytechnic Institute and State University in the Fall of 1988 to pursue his Ph.D. degree and finished in January 1994.